F-BAR protein function in cytokinesis: studies of phosphoregulation and disordered domains

By
MariaSanta C. Mangione

Dissertation
Submitted to the Faculty of the
Graduate School of Vanderbilt University
in partial fulfillment of the requirements
for the degree of

DOCTOR OF PHILOSOPHY
in
Cell and Developmental Biology

September 30, 2019

Nashville, Tennessee

Approved:
Ian G. Macara, Ph.D.
Lauren P. Jackson, Ph.D.
Jason A. MacGurn, Ph.D.
Kathleen L. Gould, Ph.D.

To my grandparents,

Mary Cuba Mangione
Nicholas Bernard Mangione
Joseph Nicholas Zannino, Jr.
Maria Santa Glorioso Zannino

ACKNOWLEDGEMENTS

Thank you to everyone who has taught me, guided me, and supported me during this stage of my training and life: my mentor, Kathy Gould; the members of the lab—Rodrigo Guillen, Chloe Snider, Nathan McDonald, Alaina Willet, Rahul Bhattacharjee, Marcin Wos, Sierra Cullati, Christine Jones, Janel Beckley, Zac Elmore, Tony Rossi, Gabriele Juskeviciute, Emma Stevens, Josh Evers, especially Liping Ren, Jun-Song Chen, and Anna Feoktistova. They taught me and motivated me every day with their enthusiasm for life and science, their kindness and encouragement, and their desire to support everyone in the lab. I am also grateful for the support and professional training that I received from the Vanderbilt MSTP, the Department of Cell and Developmental Biology, and the Biomedical Research Education and Training Office.

Thank you to my friends and family who encouraged me when I doubted myself, celebrated with me (even when I wasn't celebrating), advised me, and motivated me, especially my parents, Lou and Kathy, and my siblings, Lucia and Luigi.

This work was supported by grants from the National Institute of General Medical Studies of the NIH [R01GM101035 (to K.L.G), F31GM119252 (to M.C.M.), T32GM007347 (to the Vanderbilt Medical-Scientist Training Program). Some experiments were performing using the Vanderbilt Cell Imaging Shared Resource (supported by NIH grants CA68485, DK20593, DK58404, DK59637, and EY08126).

TABLE OF CONTENTS

Page

LIST OF TABLES

Table Page

LIST OF FIGURES

Figure Page

LIST OF ABBREVIATIONS

3-BrB-PP1	4-Amino-1-tert-butyl-3-(3-bromobenzyl)pyrazolo[3,4-d]pyrimidine
3MB-PP1	4-Amino-1-tert-butyl-3-(3-methylbenzyl)pyrazolo[3,4-d]pyrimidine
aa	amino acid
BF	brightfield
CDK	cyclin-dependent kinase
CR	cytokinetic ring
ECT	electron cryo-tomography
EM	electron microscopy
EMM	Edinburgh Minimal Media
FOA	5-fluorourotic acid
GST	Glutathione-S-Transferase
fPALM	fluorescence photoactivation localization microscopy
IB	immunoblot
IP	immunoprecipitation
IDR	intrinsically disordered region
MBP	maltose binding protein
mCh	mCherry
mNG	mNeonGreen
MS	mass spectrometry
PM	plasma membrane
pptase	lambda protein phosphatase
SIM	structured illumination microscopy
SIN	septation initiation network
SPB	spindle pole body
TEM	transmission electron microscopy
YES	yeast extract with supplements

CHAPTER 1

INTRODUCTION

Cytokinesis is the final stage in the cell division cycle during which one cell is separated into two daughter cells. Cytokinesis must be temporally and spatially coordinated with genome duplication and segregation so that daughter cells receive a complete and intact genome. In addition to this fundamental principle, many other features of cytokinesis are shared between organisms, including both physical mechanisms and molecular components, which permits the study of model organisms to gain a comprehensive and profound understanding of cytokinesis. The fission yeast *Schizosaccharomyces pombe* is one such organism.

Haploid *S. pombe* are born 3.5 to 4 μm wide by 7 μm long and proceed to grow exclusively at cell ends until they reach a length of 14 μm, at which time they divide symmetrically at the medial plane of the cell (Mitchison, 1957; Mitchison and Nurse, 1985). Their simple, predictable morphology means that progression through the cell cycle can be monitored and any deviations from the standard growth or division pattern are easily detected, such as those resulting from forward or reverse genetic studies. Forward genetic studies led to the discovery of many cell division cycle genes (*cdc*) and revealed significant conservation among cell cycle machinery between yeast and higher eukaryotes (Nurse et al., 1976; Minet et al., 1979; Chang et al., 1996; Balasubramanian et al., 1998).

Like animal cells, *S. pombe* divides using an actin- and myosin-based contractile apparatus called the cytokinetic ring (CR). In the first part of this chapter, I describe the conserved structure of this apparatus and how its form has influenced models of its function. This section highlights shared features of the CR and CR-mediated cytokinesis in organisms as divergent as walled yeast and multi-cellular animals. Next, after establishing *S. pombe* as a relevant model for CR-mediated cytokinesis, I narrate the events of cytokinesis in *S. pombe*, including descriptions of its key players and how it is regulated. Finally, I introduce the F-BAR protein family, whose function in the CR is the focus of this dissertation.

Molecular form and function of the cytokinetic ring

Adapted from:
Mangione, M.C. and Gould, K.L. (2019) *Journal of Cell Science,* 132: jcs226928

Organisms from two of the five eukaryotic supergroups (Burki, 2014), Amoebozoa and Opisthokonta (which includes fungi and animals), assemble an actin cytoskeleton- and myosin motor protein-based contractile ring, or "cytokinetic ring" (CR), to accomplish cytokinesis (Gu and Oliferenko, 2015; Willet et al., 2015c; Balasubramanian, 2016; Srivastava et al., 2016; Bhavsar-Jog and Bi, 2017; Glotzer, 2017; Hardin et al., 2017; Jahan and Yumura, 2017), whereas the other supergroups rely on alternative mechanisms such as other cytoskeletal proteins, motility-based mechanisms, or vesicle trafficking of membrane and cell wall to the division site (Farr and Gull, 2012; Hardin et al., 2017; Smertenko, 2018; Muller, 2019). The elemental steps of CR-

mediated cytokinesis are shared (Figure 1A-B): in response to cell cycle-regulated signaling, F-actin that is assembled through the actin polymerizers formin accumulates at the division plane. The non-muscle myosin-II motor (hereafter called "myosin-II") localizes to the division plane in F-actin-dependent and -independent manners (Wu et al., 2003; Motegi et al., 2004; Dean et al., 2005; Takaine et al., 2014). Myriad additional components also assemble at the division site, including membrane scaffolds (e.g. anillin, septins, and F-BAR domain-containing proteins) and F-actin regulators (e.g. severing

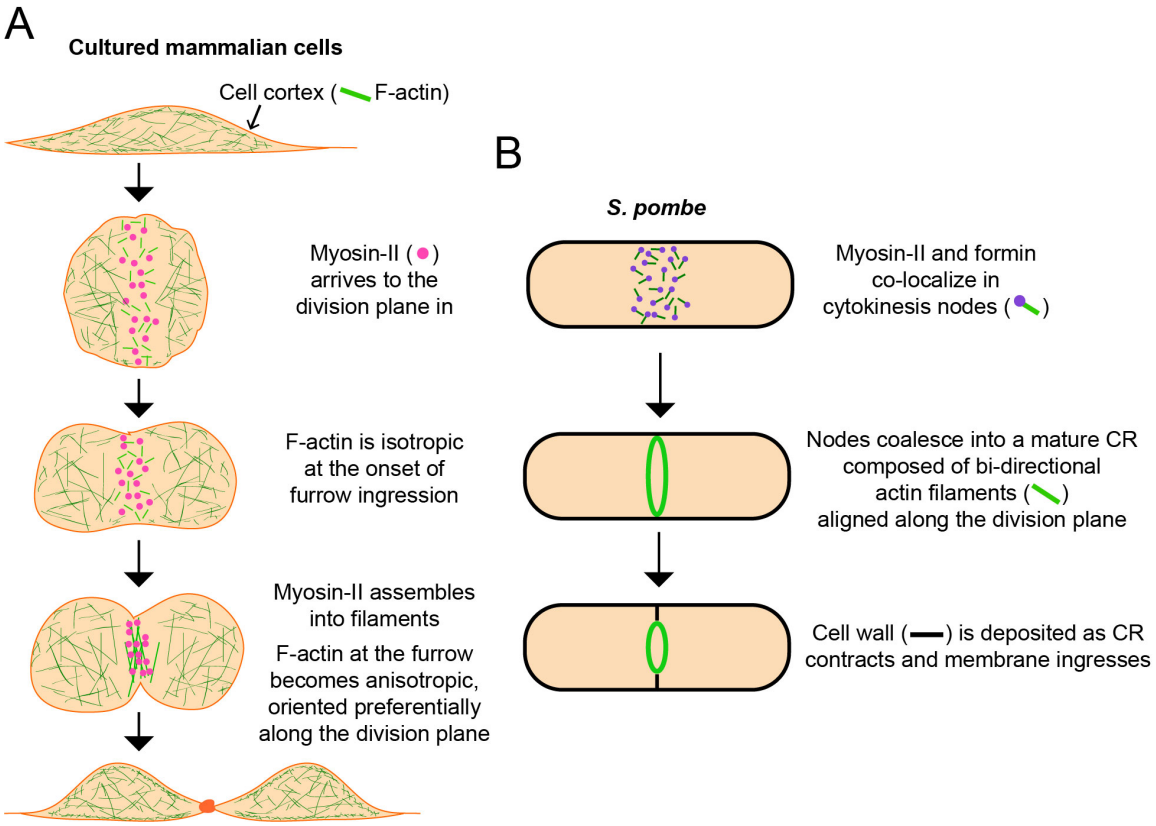

Figure 1. Elemental steps of CR formation and contraction in cultured mammalian cells and *S. pombe*.
Although not depicted, F-actin and myosin-II exhibit similar dynamics in animal embryos (e.g. Caenorhabditis elegans and sea urchin) and amoeboid cells.

proteins, bundlers) (Eggert et al., 2006a). Ultimately, signaling cues trigger myosin-II-mediated contraction of the CR, which simultaneously disassembles as it contracts. Substantial progress has been made towards identifying the molecular participants of CR-mediated cytokinesis through the use of multiple model organisms, including yeast, animal cells, and amoebas (Glotzer, 2017; Pollard and O'Shaughnessy, 2019), but how structural components are integrated into the CR and how it mediates force generation for division remain areas of active research.

Classic electron microscopy (EM) studies in animal cells, amoebas, and yeast revealed that at the division site, F-actin forms a parallel arrangement of bi-directional filaments (Schroeder, 1972; Sanger and Sanger, 1980; Gawlitta and Stockem, 1981; Maupin and Pollard, 1986; Mabuchi et al., 1988; Mabuchi, 1994; Noguchi and Mabuchi, 2001; Kamasaki et al., 2007) (Figure 1A-B). Some EM studies also described CR-adjacent structures that could be myosin-II filaments (Schroeder, 1972; Maupin and Pollard, 1986; Mabuchi, 1994; Kamasaki et al., 2007). However, the arrangement of myosin-II and other CR components relative to F-actin and the plasma membrane has been obscured by the resolution limit of conventional light microscopy (~200 nm) and the difficulty of identifying proteinaceous structures in EM samples. Subsequently, super-resolution fluorescence microscopy (Betzig et al., 2006; Hess et al., 2006; Rust et al., 2006; Gustafsson et al., 2008; Sydor et al., 2015) has been used to examine CR architecture in animal cells and *S. pombe*. In the following sections, I describe these studies and others using improved EM and fluorescence polarization microscopy techniques that have provided high resolution information about F-actin, myosin-II and numerous other CR components. Then, I discuss the various models that have been proposed to explain how the CR mediates plasma membrane ingression at the division site, and explore the contexts in which this may or may not be sufficient for cell division.

F-actin

Classic EM studies of cleavage furrows and CRs revealed F-actin aligned preferentially along the division plane. Electron cryotomography (ECT) of contracting CRs in cryopreserved *S. pombe* (Swulius et al., 2018) and rotary shadow platinum replica transmission EM (TEM) of CRs from the isolated cortices of sea urchin embryos (Henson et al., 2017) confirmed this arrangment. This arrangement was also visible in furrows of HeLa cells stained with phalloidin and imaged using structured illumination microscopy (SIM) (Fenix et al., 2016). Interestingly, even though actin filaments ultimately align roughly parallel to the division plane, studies in *S. pombe* and animal cells indicate that the CR initiates as a network of randomly oriented actin filaments (Fishkind and Wang, 1993; Mabuchi, 1994; Wu et al., 2003; Wu et al., 2006). Fluorescence polarization microscopy determined that in human epithelial cells, F-actin is isotropic at the onset of anaphase and throughout early furrow ingression before re-organizing into bi-directional filaments (approximately 150 seconds after anaphase onset) (Spira et al., 2017) (Figure 1A). This re-organization is myosin-II-dependent. It remains to be seen whether actin reorganization is required for CR contraction or is a consequence of force generation (Spira et al., 2017).

CR-generated force is transmitted to the plasma membrane, which remains closely associated with the CR throughout cytokinesis (Schroeder, 1990). How the CR-plasma membrane association is maintained during contraction is still largely unknown

(Schroeder, 1990; Pollard, 2017). ECT images revealed a gap of approximately 60 nm between the plasma membrane and the actin bundles of contracting CRs in *S. pombe* (Swulius et al., 2018). A gap of approximately 100 nm between the plasma membrane and F-actin was also observed in a fluorescence photoactivation localization microscopy (fPALM) study of fully formed *S. pombe* CRs pre-contraction (McDonald et al., 2017). The modest difference in measured gap size in these two studies could be explained by different sample preparation methods or, more interestingly, by a structural reorganization of the CR during contraction that brings F-actin closer to the membrane. Distinguishing between these two possibilities will require additional studies to obtain the localization and dynamics of other CR components. Importantly, however, two distinct imaging modalities reveal that CR F-actin is not immediately adjacent to the plasma membrane and is linked to the plasma membrane by largely unknown mechanisms.

Myosin-II

In multiple organisms, myosin-II first localizes to the division plane in foci that then reorganize into a ring (Maupin and Pollard, 1986; Noguchi and Mabuchi, 2001; Wu et al., 2003; Maddox et al., 2005; Vavylonis et al., 2008; Zhou and Wang, 2008; Mavrakis et al., 2014) (Figure 1B). Recent SIM and TEM images of sea urchin embryos at sequential stages of furrowing captured fine details of myosin-II rearrangement from a wide band of clusters at the future division site to a linear structure (Henson et al., 2017). As in other organisms, this reorganization is actin-dependent (Henson et al., 2017).

Myosin-II is a double-headed motor (Figure 2A) and *in vitro* studies of myosin-II from animal cells have demonstrated that it can also oligomerize through its C-terminus into bipolar mini-filaments (Verkhovsky and Borisy, 1993; Ricketson et al., 2010; Billington et al., 2013) (Figure 2B). The linearly arranged myosin-II in the CR of sea urchin embryos is presumed to represent myosin-II mini-filaments (Henson et al., 2017). Platinum-replica EM of *Saccharomyces cerevisiae* protoplasts with a CR also identified myosin-II-dependent thick filaments solely at late stages of cytokinesis (Ong et al., 2014). Bipolar myosin-II mini-filaments in the CRs of mammalian cells were demonstrated using SIM, which revealed that the myosin-II mini-filaments are arranged head-to-head, parallel to the plane of division (Beach et al., 2014; Fenix et al., 2016) (Figure 2D). Furthermore, the inhibition of myosin-II motor activity impaired the assembly of myosin-II mini-filaments into larger arrays (i.e. stack formation) (Fenix et al., 2016), supporting the idea that myosin-II undergoes a molecular rearrangement during cytokinesis (Henson et al., 2017).

Unlike animal and amoeboid myosin-II, the two myosin-II heavy chains in *S. pombe*, Myo2 and Myp2, do not form filaments. The nonessential Myp2 is single-headed (Bezanilla and Pollard, 2000) whereas biochemical studies of the essential Myo2 indicate that it functions as a double-headed motor rather than a bipolar mini-filament (Pollard et al., 2017; Friend et al., 2018) (Figure 2A). In mature CRs, the tail of Myp2 localizes approximately 125 nm away from the plasma membrane, whereas the Myo2 C-terminal tail is anchored closer to the plasma membrane (McDonald et al., 2017). Both of the N-terminal motor domains extend into the cytoplasm to co-localize with F-actin (Figure 2C). This Myo2 organization is also present in foci that exist during early CR formation termed “cytokinesis nodes”, as determined by single-molecule high-resolution colocalization microscopy (Laporte et al., 2011) (Figure 1B). Within cytokinesis nodes,

which contain approximately 10 molecules of Myo2, the C-terminal tails of myosin-II have a tighter radial organization compared to the N-terminal motor domains as determined by fPALM (Laplante et al., 2016). This organization led to a proposal that a myosin-II "bouquet", in which N-terminal motor domains are radially arrayed to interact with F-actin, could function as a motor unit comparable to myosin-II mini-filaments (Laplante et al., 2016) (Figure 2C). Despite differences in myosin-II molecular structure, the dynamic rearrangements that occur throughout cytokinesis in fission yeast, budding yeast, and animal cells indicate that myosin-II function is likely highly conserved.

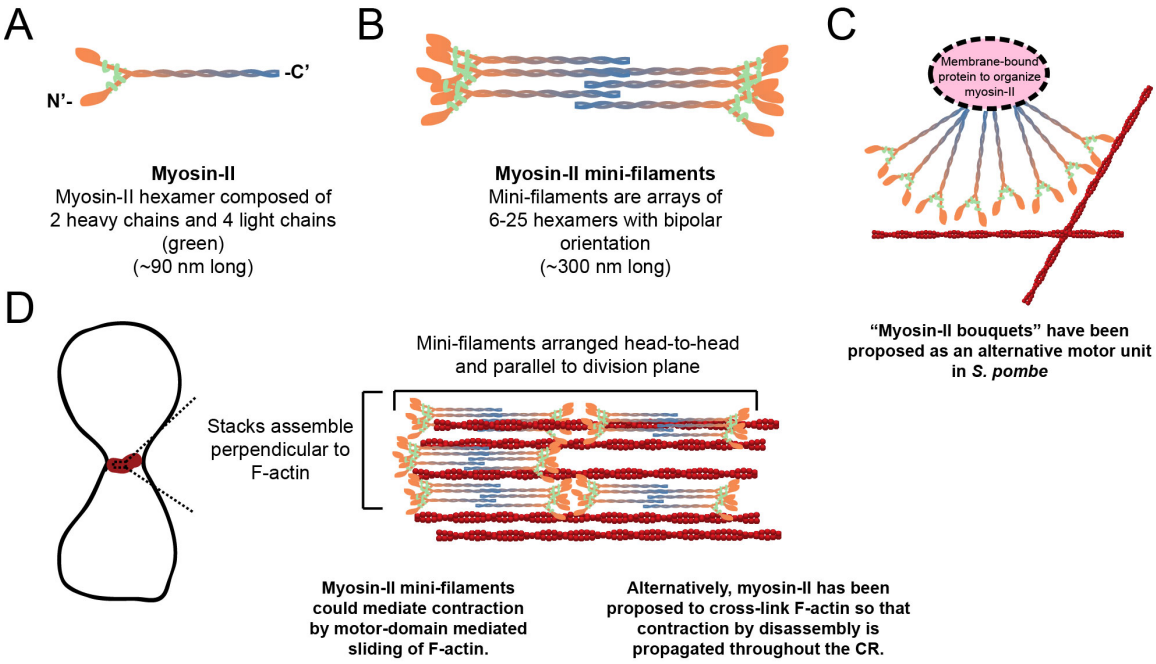

Figure 2. Molecular structure of myosin-II.
(A) Double-headed myosin-II is a hexamer. (B) Animal and amoeboid myosin-II can oligomerize via C-terminal tails into bipolar filaments. (C) Radial arrangement of myosin-II predicted to act as a motor unit in S. pombe, which does not form mini-filaments. Actin is red. (D) Cartoon of myosin-II arrangement in animal cell CRs. Actin is red. Schematics are not drawn to scale.

Other CR proteins

Genetic studies indicate that building and contracting CRs requires many other proteins (Eggert et al., 2006a), some of which are structural components that must be performing key jobs such as linking the CR to the plasma membrane or possibly organizing myosin-II into motor units. However, how these are organized into the whole of the CR is unclear. Other than septins, which form filaments on the plasma membrane and bind components of the CR (Marquardt et al., 2018), most other CR components have not been detected by EM. Super-resolution microscopy can probe their organization at the nanoscale level and two such studies were performed in *S. pombe* (Laplante et al., 2016; McDonald et al., 2017). Our research group used fPALM to measure the distance between 30 CR proteins and the plasma membrane and found that the mature CR appears stratified (McDonald et al., 2017) (Figure 3). Closest to the membrane (on average, 0-80 nm from the membrane) were membrane-bound scaffolds, such as anillin, septins, and F-BAR proteins, and also formin. Just above these proteins — 80 to 160 nm away from the plasma membrane — were most signaling proteins (e.g. kinases, phosphatases, GTPases) and a variety of accessory components scaffolded through SH3 domains, which are critical for ring integrity. Most distal from the membrane was F-actin, the center of which is approximately 200 nm away from the plasma membrane, as well as most direct actin-binding proteins, including the N-terminal motor domain of myosin-II (Figure 3).

The arrangement of proteins within the CR is still unclear; however, some insight was gained by using fPALM to observe proteins within the plane of the CR. CR components in the membrane-proximal layer of pre-contracted CRs cluster, whereas proteins localizing to the middle and distal layers have a more homogenous distribution (McDonald et al., 2017). This is consistent with findings of Laplante et al. who used fPALM in live cells to discover that five cytokinesis node proteins are clustered in contracting CRs (Laplante et al., 2016). These clusters are probably distinct from the cytokinesis nodes present during CR formation given that the essential organizer for cytokinesis nodes, the anillin-like Mid1, leaves the CR during contraction (Wu et al., 2003). Additionally, the four node proteins examined within the plane of the CR remain clustered even in cells with deletion of the *mid1* gene and they have different patterns of clustering in the mature CR (McDonald et al., 2017). Finally, although the estimated size of cytokinesis nodes is within the range of TEM, Swulius et al. did not observe any molecular complexes in contracting CRs (Swulius et al., 2018). Future studies to image additional CR proteins during contraction are needed to determine if molecular complexes exist during contraction, and if yes, their precise composition and the functional implications for contraction. Additionally, whether any of these newly revealed features of the *S. pombe* CR are shared with other model organisms is another area of future investigation.

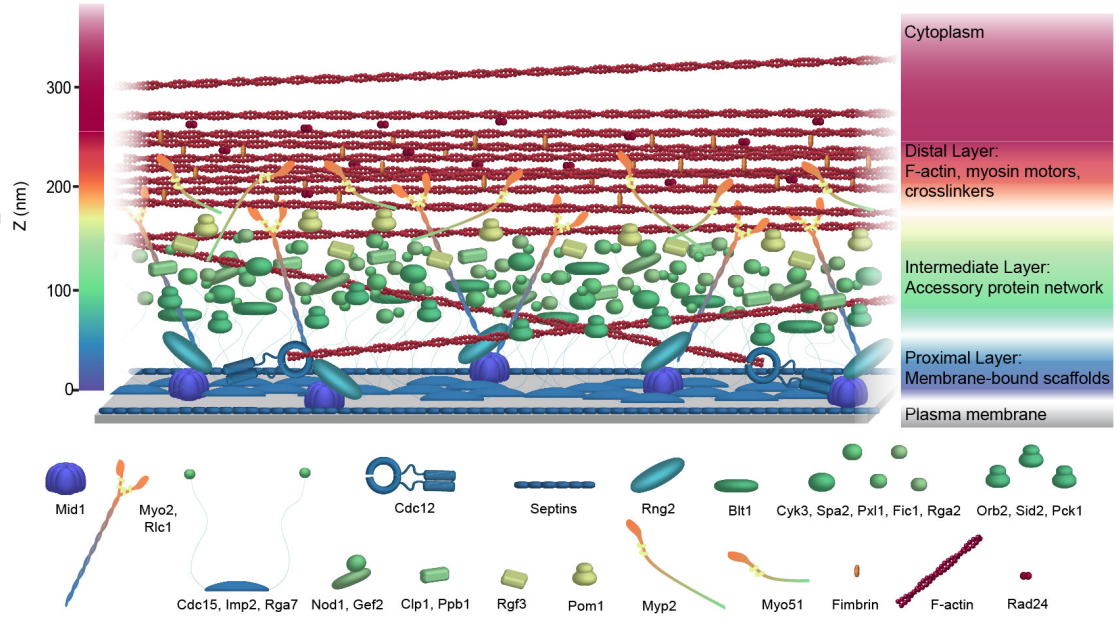

Figure 3. A model for CR arrangement in *S. pombe*.
Scale model of *S. pombe* CR architecture based on experimentally determined distances of CR proteins from the plasma membrane. The model does not incorporate stoichiometry. Panels are reproduced from McDonald et al, 2017 with some text removed. © 2017, McDonald et al. Available at https://elifesciences.org/articles/28865 under the terms of the Creative Commons Attribution License.

Models of CR-mediated furrowing

The organization of proteins within the CR indicates potential modes of CR contraction and net inward force generation during cytokinesis. The identification of myosin-II stacks in the CR of animal cells (Beach et al., 2014; Fenix et al., 2016) is consistent with the classical 'purse-string' theory of contraction, in which myosin-II slides bi-directionally oriented F-actin filaments over one another to reduce CR diameter. Models of contraction in *S. pombe,* which lack myosin-II bipolar filaments, also converge on sliding of bi-directional actin-filaments. These models assume various myosin-II organizations, such as plasma membrane-anchored individual myosin-II motors (Nguyen et al., 2018) or myosin-II "bouquets" (Laplante et al., 2016; Thiyagarajan et al., 2017) (Figure 2C). Myosin-II motors arranged at an angle to each other and bound to different actin filaments would slide the intact filaments past one another. The idea of myosin-II "bouquets" functioning as a motor unit is attractive because of the observed myosin-II clustering (Schroeder, 1990; Stachowiak et al., 2014; Takaine et al., 2015; Wollrab et al., 2016; McDonald et al., 2017) and the proposal that contractile units exist in CRs of multiple organisms (Carvalho et al., 2009; Silva et al., 2016; Thiyagarajan et al., 2017).

However, the finding that furrow ingression initiates while F-actin is still randomly oriented at the division plane (Spira et al., 2017) suggests that an alternative mode of contraction could be at work, at least early in cytokinesis. One proposal is that

rather than sliding almost-parallel actin filaments, myosin-II first contracts a network of isotropic F-actin (Ennomani et al., 2016; Linsmeier et al., 2016; Spira et al., 2017). Over time, F-actin in the furrow becomes preferentially aligned with the plane of division. Still, other models of CR contraction do not rely on filament sliding. Myosin-II might pull on anchored F-actin to the point of breaking such that filament disassembly could drive CR contraction (Harasimov and Schuh, 2018) (Figure 2D). The dispensability of the myosin-II motor domain for cytokinesis in *S. cerevisiae* (Lord et al., 2005; Wloka et al., 2013) and myosin-II motor activity for late stages of *Drosophila melanogaster* cellularization (Xue and Sokac, 2016) led to a related hypothesis wherein disassembly of cross-linked F-actin filaments drives CR contraction (Sun et al., 2010; Mendes Pinto et al., 2012; Mendes Pinto et al., 2013). Determining which of these models is correct, and under which circumstances, will require learning much more about the function and regulation of individual proteins, especially those accessory proteins that have not been extensively studied.

The CR in context

Though the CR generates force, other mechanisms of force generation likely exist given that yeast, amoebas, and animal cells are able to divide in the absence of a robust CR under certain circumstances (Zang et al., 1997; Kanada et al., 2005; Carvalho et al., 2009; Ma et al., 2012; Mendes Pinto et al., 2012; Silva et al., 2016; Davies et al., 2018; Dix et al., 2018). The extracellular matrix of the cell is also a critical factor in cell division. Animal cells and amoebas with a perturbed CR can still divide by "traction-mediated cytokinesis," which relies on force generation by pulling on a substrate as daughter cells separate (Zang et al., 1997; Kanada et al., 2005; Jahan and Yumura, 2017; Taira and Yumura, 2017; Dix et al., 2018). The commonly studied amoeba *Dictyostelium discoideum* can divide in both myosin-II-dependent and -independent manners. In myosin-II null cells, successful cytokinesis depends on adherence to a substratum, which allows daughter cells to exert traction force by migrating away from each other. Although cell rounding is a classic characteristic of mitotic cells, some substrate attachments typically persist (Mitchison, 1992; Taneja et al., 2016; Dix et al., 2018; Lock et al., 2018; Taneja et al., 2019) and eliminating them in non-transformed cells causes cytokinesis failure (Dix et al., 2018). These observations raise the possibility that some proportion of force for cytokinesis during "classical division" is dependent on proper substrate adhesion.

Unlike animal cells and amoebas, fungi have a cell wall, which can be equated with the extracellular matrix. Plasma membrane furrowing must be coordinated with deposition of the "septum," a cell wall structure that physically separates daughter cells. Current models of division propose that the major force for separation comes from cell wall deposition rather than CR contraction. *S. cerevisiae* lacking myosin-II can divide if mutation(s) activating the septum-synthesizing machinery are acquired (Tolliday et al., 2003). In *S. pombe*, biophysical measurements in protoplasts determined that the force generated by the CR is insufficient to overcome turgor pressure (Stachowiak et al., 2014). Thus, the CR may primarily serve as a landmark or mechanical signal guiding septum deposition (Proctor et al., 2012a; Stachowiak et al., 2014; Thiyagarajan et al., 2015; Zhou et al., 2015) rather than a force-generating molecular machine, and this function could

also exist in animal cells and amoebas. The well-studied and extremely tractable *S. pombe* is an excellent system to extend these studies and clarify the functions of the CR.

Dynamics and regulation of CR-mediated cytokinesis *S. pombe*

The ease of genetic manipulation has led to a comprehensive parts list of proteins that participate in cytokinesis and localize to the CR and/or division site (Nurse et al., 1976; Minet et al., 1979; Chang et al., 1996; Matsuyama et al., 2006; Kim et al., 2010; Hayles et al., 2013; Chen et al., 2015; Chen et al., 2016). The study of these proteins has led to substantial, molecular insight into how *S. pombe* coordinate mitosis and cytokinesis and execute the stages of cytokinesis—division site selection, CR assembly and maturation, CR constriction, and septation and cell separation.

Formation

The events of cytokinesis relative to those of mitosis can be monitored by dual imaging of a spindle pole body (SPB) marker and CR marker. The events of cytokinesis occur sequentially with a precise timing, which was first described by Wu et al. (Wu et al., 2003) and has since been confirmed and elaborated by numerous studies (reviewed in (Pollard and Wu, 2010a; Lee et al., 2012)) (Wu et al., 2006; Ge and Balasubramanian, 2008; Hachet and Simanis, 2008; Pinar et al., 2008; Roberts-Galbraith et al., 2010; Almonacid et al., 2011; Arasada and Pollard, 2011; Laporte et al., 2011; Arasada and Pollard, 2014; Goss et al., 2014; Cortes et al., 2015; Laplante et al., 2015; Pu et al., 2015; Ren et al., 2015; Willet et al., 2015a; Li et al., 2016; Snider et al., 2017; Willet et al., 2018). The separation of the SPBs indicates the start of mitotic spindle assembly and marks mitotic onset. Just before SPB separation, the earliest CR proteins arrive at the division site in a broad band of cytokinesis nodes (Wu et al., 2003; Wu et al., 2006; Ye et al., 2012; Guzman-Vendrell et al., 2013; Jourdain et al., 2013; Zhu et al., 2013; Akamatsu et al., 2014). Combined genetic and fluorescence imaging studies have determined the hierarchy of recruitment of node proteins at the CR. The formation of nodes depends on the anillin-like protein Mid1 (Laporte et al., 2011; Padmanabhan et al., 2011; Tao et al., 2014b). Mid1 is sequestered in the nucleus during interphase but upon mitotic onset, Mid1 is released from the nucleus and binds to the overlying plasma membrane in the cell middle (Sohrmann et al., 1996; Paoletti and Chang, 2000). Here it organizes six additional proteins into nodes—the F-BAR protein Cdc15 (Fankhauser et al., 1995; Lippincott and Li, 2000), type II myosin heavy chain Myo2 (Kitayama et al., 1997; May et al., 1997) and its light chains Cdc4 (McCollum et al., 1995) and Rlc1 (Le Goff et al., 2000; Naqvi et al., 2000), the IQGAP protein Rng2, and the formin Cdc12 (Chang et al., 1997; Kovar et al., 2003; Wu et al., 2003; Wu et al., 2006)—but the molecular mechanism by which Mid1 directly recruits node proteins is unknown.

The assembly of node components at the division site is highly regulated by phosphorylation. Mid1 release from the nucleus depends on the Polo-like kinase Plo1. Not only does Plo1 mediate Mid1 release, but it is also important for activating Mid1 so that it can interact with CR proteins (Bahler et al., 1998a; Paoletti and Chang, 2000; Almonacid et al., 2011). Phosphorylation of the heavy chain Myo2 inhibits its interaction with Mid1 and accumulation at the division site until early mitosis (Almonacid et al., 2011). Cdc15 is also regulated by phosphorylation. During interphase, Cdc15 is hyperphosphorylated, but it is dephosphorylated upon mitotic onset, coincident with its

recruitment to the cortex and nodes (Fankhauser et al., 1995; Wachtler et al., 2006; Clifford et al., 2008b; Hachet and Simanis, 2008; Roberts-Galbraith et al., 2010). Cdc15 phosphoablation mutants localize precociously at the cell cortex during interphase and recruit downstream partners (Roberts-Galbraith et al., 2010), including the formin Cdc12 (Carnahan and Gould, 2003; Willet et al., 2015a). In this instance, even though Cdc12 aberrantly localizes to the cortex, it does not form F-actin, indicating that Cdc12 activity is also subject to regulation (Roberts-Galbraith et al., 2010). Indeed, Cdc12 is regulated by cyclin-dependent kinase (CDK) (Willet et al., 2018) and Sid2 (Bohnert et al., 2013), a terminal kinase of the septation initiation network (SIN).

The SIN is a GTPase activated kinase cascade that regulates CR formation, maturation, and constriction and septum formation (reviewed in ((Roberts-Galbraith and Gould, 2008; Johnson et al., 2012; Simanis, 2015)). Association of the bipartite GTPase-activating protein (GAP) Byr4-Cdc16 with the upstream Ras-superfamily GTPase Spg1 inhibits SIN activation during interphase. Upon mitotic entry, Plo1 and CDK (Rachfall et al., 2014) phosphorylate Byr4-Cdc16, liberating Spg1 and activating the downstream kinase cascade. SIN signaling occurs at the SPB, but Sid2 also localizes to the CR during anaphase, where it likely has multiple substrates important for proper CR contraction. SIN signaling is sufficient for CR formation during interphase and required for CR contraction and therefore both activating and inactivating SIN mutants are lethal (Minet et al., 1979).

Concurrently with metaphase and anaphase, nodes coalesce into a coherent ring (Wu et al., 2006), a stage called "formation." A "search-capture-pull-release" model of CR formation has been proposed (Vavylonis et al., 2008) and partially reconstituted *in vitro* (Zimmermann et al., 2017) in which the essential formin Cdc12 that is anchored on the plasma membrane nucleates and elongates linear F-actin in random orientations ('searching'). Actin filaments are then 'captured' by myosin-II from neighboring nodes. Next, myosin-II 'pulls' nodes closer together until their attachment is 'released' by F-actin severing (Vavylonis et al., 2008; Vavylonis and Horan, 2017).

In the absence of Mid1, the CR still forms in the cell middle, but in a less organized manner and later in the cell cycle: during anaphase, actin filaments are nucleated from one-to-many sites on the cortex and CRs often form obliquely at an angle to the long axis resulting in septation defects. This mechanism of CR formation is dependent on the SIN (Sohrmann et al., 1996; Hachet and Simanis, 2008; Huang et al., 2008; Saha and Pollard, 2012; Tao et al., 2014a).

Despite the apparently unrestricted site of CR formation in *mid1*Δ, it was noted that septa are never observed at the hemi-spherical cell tips of *S. pombe,* indicating that a second, inhibitory mechanism exists to regulate CR and/or septum placement (Huang et al., 2007). This mechanism, termed the "tip occlusion pathway," requires microtubules, the microtubule motor complex Tea1 and Tea4, and the DYRK kinase Pom1 (Huang et al., 2007). The Tea1-Tea4 complex transports Pom1 out to cell tips (Bahler and Pringle, 1998). There, Pom1 phosphorylates itself and substrates involved in cell polarity and temporal regulation of cytokinesis (Moseley et al., 2009; Rincon et al., 2014; Kettenbach et al., 2015; Lee et al., 2018). Additionally, Pom1 had already been implicated in regulating division site placement since *pom1*Δ show mis-localized Mid1 and off-center CR and septa (Bahler and Pringle, 1998; Padte et al., 2006; Rincon et al., 2014). *mid1*Δ is synthetic lethal with deletion of *tea1, tea4,* or *pom1* (Bahler and Pringle, 1998; Huang et

al., 2007). Combining *mid1*Δ with temperature-sensitive mutants leads to the formation of tip septa at the restrictive temperature with septa spanning the long-axis of the cell, essentially perpendicularly to the normal division plane (Huang et al., 2007). In summary, division site placement is dictated by both positive and negative signals provided by Mid1 and the tip occlusion pathway, respectively.

Interestingly, combining a hypomorphic allele of the F-BAR protein Cdc15 (*cdc15*-gc1) with *mid1*Δ *tea1*-18 partially rescued tip septation (Huang et al., 2007). Given that Cdc15 is highly phosphorylated (Fankhauser et al., 1995; Wachtler et al., 2006; Clifford et al., 2008b; Hachet and Simanis, 2008; Roberts-Galbraith et al., 2010; Kettenbach et al., 2015; Lee et al., 2018), it was hypothesized that Pom1 provides the inhibitory cue by phosphorylating the CR protein Cdc15, and indeed it has since been confirmed that Cdc15 is a substrate of Pom1 (Kettenbach et al., 2015; Lee et al., 2018). Chapter 4 reports studies to test the hypothesis that phosphorylation of Cdc15 is the main inhibitory signal to prevent tip septation.

Maturation, constriction, septation, and cell separation

The dwells before contraction onset for a period of time called "maturation," during which additional proteins accumulate at the CR. These include the components of a network anchored by the SH3 domains of F-BAR proteins Cdc15 and Imp2 (Roberts-Galbraith et al., 2009; Ren et al., 2015; Davidson et al., 2016; Sethi et al., 2016), such as Pxl1 (Ge and Balasubramanian, 2008; Pinar et al., 2008; Roberts-Galbraith et al., 2009; Cortes et al., 2015; Martin-Garcia et al., 2018), Fic1 (Roberts-Galbraith et al., 2009; Bohnert and Gould, 2012), and Cyk3 (Roberts-Galbraith et al., 2010; Bohnert and Gould, 2012; Pollard et al., 2012). This network is important for maintenance of the CR at the division site (Roberts-Galbraith et al., 2009; Ren et al., 2015; Davidson et al., 2016; Sethi et al., 2016). As previously mentioned, Cdc15 is one of the earliest proteins at the division site and presumably its SH3 domain is available to interact with these proteins. Therefore, there must be additional mechanisms that regulate the arrival of this network. Chapter 3 describes one potential mechanism by which the recruitment of Pxl1 is regulated and begins to explore how this timing impacts cytokinesis.

Contraction onset coincides with maximum spindle length, i.e. when the length between SPBs is greatest. Contraction is visualized as the decreasing length (i.e. circumference) of the CR until it is visible as a single dot. Cell wall material is concomitantly deposited behind the contracting CR, forming a specialized structure called the "septum," which isolates the cytoplasm of the daughter cells. The septum is a trilaminar structure, with an initial primary septum flanked by two secondary septa (Johnson et al., 1973). The cell wall is composed of glucans, which are deposited and remodeled by glucan synthases and glucanase (reviewed in (Willet et al., 2015c; García Cortés et al., 2016; Perez et al., 2016)). The primary septum is deposited by the glucan synthase Bgs1 (Cps1) (Liu et al., 1999) while Bgs4 (Cortes et al., 2005) is primarily responsible for secondary septum deposition. The degradation of the primary septum liberates the two daughter cells and the secondary septa become the cell wall of the new cell ends.

As previously described, biophysical measurements and genetic studies have determined that the force generated by the CR is insufficient to overcome the turgor pressure of the cell (Proctor et al., 2012b; Stachowiak et al., 2014). A temperature-

sensitive allele of Bgs1, *cps1-191*, arrests at the restrictive temperature with fully formed, non-contracted CRs (Liu et al., 1999; Liu et al., 2000; Munoz et al., 2013). Furthermore, cell division can occur even in the absence of a circumferential CR—albeit inefficiently—provided that cell wall deposition initiates (Cortes et al., 2015; Thiyagarajan et al., 2015; Zhou et al., 2015; JC et al., 2018). Therefore, the current model is that cell wall deposition provides the major force for cell division (Proctor et al., 2012b; Stachowiak et al., 2014). Chapter 2 describes the discovery of a novel Cdc15 mutant that has a defective CR but still divides dependent on cell wall deposition. Cdc15 is a member of the F-BAR protein family, which is composed of key membrane-CR scaffolds. In the following section, I introduce F-BAR protein structure and describe what is known about Cdc15.

The F-BAR protein family

F-BAR proteins are members of the Bin/amphiphysin/Rvs167 (BAR) superfamily, which is conserved from yeast to humans (Frost et al., 2007; Frost et al., 2009). These proteins have a Fer/CIP4 homology (FCH)-BAR (F-BAR) domain that is often linked to additional functional domains by an intrinsically disordered linker. This protein structure reflects their function at the interface between membranes and the cytoskeleton in cellular processes such as endocytosis, cell migration and cytokinesis (Lippincott and Li, 2000; Ahmed et al., 2010; Fricke et al., 2010; McDonald and Gould, 2016). In this section, I first describe the structure of F-BAR proteins and then review in detail what is known about the essential cytokinetic F-BAR protein Cdc15 and its paralog Imp2.

Structure of F-BAR proteins

The defining feature of F-BAR proteins is their namesake F-BAR domain. Although these domains have limited sequence similarity, they share a globular structure that is formed when a monomer of three alpha-helices dimerizes to form a crescent membrane-binding interface (Henne et al., 2007). F-BAR domains have shallow, and in some cases flat, curvature. The concave surface of the F-BAR domain forms the membrane-binding interface and consists of multiple positively-charged patches that interact electrostatically with negatively charged phospholipids, such as phosphatidylserine and phosphatidylinositol bis(4,5)phosphate (Tsujita et al., 2006; Shimada et al., 2010; Bai et al., 2012; Goh et al., 2012; Bai and Zheng, 2013; McDonald et al., 2015; McDonald and Gould, 2016; McDonald et al., 2016).

In addition to membrane binding, F-BAR domains interact with each other to form higher-order oligomers. There are multiple modes of oligomerization, such as tip-to-tip, lateral interactions, and tip-to-core (Bai et al., 2012; Bai and Zheng, 2013; McDonald et al., 2015; McDonald et al., 2016), although whether this confers unique functions to F-BAR domains is unknown. This increases the avidity of the F-BAR domain for the plasma membrane and forms a multivalent scaffold upon which the molecular events of various cellular processes (e.g. endocytosis or cytokinesis) are coordinated. Mutations that reduced oligomerization of *S. pombe* Cdc15, human RhoGAP4, and human Fer caused cellular defects (McDonald et al., 2015). This led to the proposal that the primary function of the F-BAR domain is to form a multivalent scaffold with high avidity for the membrane. Thus, the F-BAR domain positions the

protein at the membrane where it can interact with and modulate the cytoskeleton through binding partners.

A small number of F-BAR domains have been shown to directly bind partners (Shoham et al., 2003; Hansen et al., 2011; Senju et al., 2011; Begonja et al., 2015; Garabedian et al., 2018; Liu et al., 2019). However, most F-BAR protein interactions are mediated by accessory domains. These include protein-binding domains such as Src homology 3 (SH3) or mu homology domains (μHD) and signaling domains such as GTPase activating protein (GAP) and tyrosine (Tyr) kinase domains (Roberts-Galbraith and Gould, 2010; McDonald and Gould, 2016). The domains of F-BAR proteins are linked by intrinsically disordered regions (IDRs). IDRs display high intramolecular flexibility and little secondary structure under physiological conditions. Only in the past decade have the functional advantages of disordered proteins been appreciated, such as regulation by post-translational modification and partner binding (Tompa, 2002; Daughdrill et al., 2007; Tompa, 2012; Dunker et al., 2015; Levine et al., 2015; Metskas and Rhoades, 2015; Pappu, 2015; Reed et al., 2015). The IDRs of F-BAR proteins are often sites of phosphorylation (Roberts-Galbraith and Gould, 2010; Roberts-Galbraith et al., 2010; Meitinger et al., 2011; Quan et al., 2012; Merlini et al., 2015). Some IDRs have also been implicated in protein localization and in interactions (Meitinger et al., 2011; Meitinger et al., 2013; Oh et al., 2013) (Hollopeter et al., 2014; Umasankar et al., 2014) (Yamamoto et al., 2018). In Chapter 2, a function for the IDR of *S. pombe* Cdc15 is described.

Function and regulation of S. pombe F-BAR Cdc15

Three F-BAR proteins localize to the CR in *S. pombe*: essential Cdc15 (Fankhauser et al., 1995) and non-essential Imp2 (Demeter and Sazer, 1998) and Rga7 (Arasada and Pollard, 2011; Martin-Garcia et al., 2014). All three have N-terminal F-BAR domains while Cdc15 and Imp2 have C-terminal SH3 domains and Rga7 has a C-terminal RhoGAP domain. Cdc15 is the earliest of these to arrive at the CR (Wu et al., 2003), while Imp2 and Rga7 arrive during maturation (Demeter and Sazer, 1998; Roberts-Galbraith et al., 2009; Martin-Garcia et al., 2014; Ren et al., 2015).

Cdc15 typifies an F-BAR protein serving as a membrane-cytoskeleton scaffold. The F-BAR domain binds phospholipids *in vitro* (McDonald et al., 2015) and oligomerizes in a linear tip-to-tip fashion (Roberts-Galbraith et al., 2010; McDonald et al., 2015). Interfering with the ability of the F-BAR domain to oligomerize destabilizes the CR such that it slides along the cortex during cytokinesis, indicating that F-BAR domain oligomerization is vital for providing a high avidity interaction with the membrane (McDonald et al., 2015). Indeed, super-resolution microscopy localizes the F-BAR domain to within 69 +/- 50 nm of the plasma membrane (McDonald et al., 2017). The F-BAR domain of Cdc15 also directly binds the formin Cdc12 (Carnahan and Gould, 2003; Willet et al., 2015a). Unpublished data from our lab confirms that Cdc15 F-BAR domain can simultaneously interact with membranes and Cdc12 (Chloe Snider), thus positioning it to link the membrane to the F-actin of the CR via its interaction with Cdc12.

The SH3 domain of Cdc15 shares an essential function with the SH3 domain of Imp2 (Roberts-Galbraith et al., 2009; Ren et al., 2015). Both redundantly bind numerous CR components including the C2 domain protein Fic1, the paxillin-like protein Pxl1, and the RhoGEF Rgf3. Cdc15 binding partners themselves bind other proteins, such as Art1

and Pos1, and collectively this network stabilizes the CR and coordinates contraction with septum formation (Ren et al., 2015; Davidson et al., 2016; Sethi et al., 2016). Though cells tolerate deletion of one SH3 domain, the *imp2*Δ*SH3cdc15*Δ*SH3* double mutant is inviable (Roberts-Galbraith et al., 2009). Time-lapse microscopy of the first divisions of *imp2*Δ*SH3cdc15*Δ*SH3* germinating spores expressing the cytokinetic ring marker Rlc1-GFP reveal that the cytokinetic ring begins to form in these cells but then unravels, resulting in multinucleate cells that ultimately die (Roberts-Galbraith et al., 2009).

As previously mentioned, Cdc15 is phosphorylated in a cell cycle-dependent manner: it is hyper-phosphorylated during interphase and dephosphorylated during mitosis (Fankhauser et al., 1995; Wachtler et al., 2006; Hachet and Simanis, 2008; Roberts-Galbraith et al., 2010). Subsequent studies have identified that the majority of Cdc15 phosphorylation occurs in the IDR of Cdc15 (Roberts-Galbraith et al., 2010; Koch et al., 2011; Carpy et al., 2014; Kettenbach et al., 2015; Swaffer et al., 2016; Lee et al., 2018; Swaffer et al., 2018). Studies from our lab demonstrated that Cdc15 phosphorylation regulates its localization in the cell, its ability to bind membranes, oligomerize, and interact with proteins (Roberts-Galbraith et al., 2010). This led to the proposal of a model in which phosphorylation causes a conformational change in the protein that obscures membrane- and protein-binding interfaces (Roberts-Galbraith et al., 2010). However, this model has not been tested. To date, only two kinases have been shown to phosphorylate Cdc15, the DYRK kinase Pom1 and the MARK kinase Kin1 (Kettenbach et al., 2015; Lee et al., 2018).

This thesis describes three independent studies that aim to better understand Cdc15's scaffolding role in the CR. In Chapter 2, a scaffolding function is assigned to the previously unstudied IDR. Chapter 3 reports the regulation of Cdc15's binding partner, Pxl1, providing insight into how it might be contributing to cytokinesis and Cdc15's scaffolding function. Chapter 4 describes the consequences of Cdc15 phosphorylation by Pom1 and also the discovery that two other kinases regulate Cdc15.

CHAPTER 2

THE INTRINSICALLY DISORDERED REGION OF THE CYTOKINETIC F-BAR PROTEIN CDC15 PROVIDES A UNIQUE ESSENTIAL FUNCTION IN MAINTENANCE OF CYTOKINETIC RING INTEGRITY

Abstract

Successful separation of two daughter cells (i.e. cytokinesis) is essential for life. Many eukaryotic cells divide using a contractile apparatus called the cytokinetic ring (CR) that associates dynamically with the plasma membrane (PM) and generates force that contributes to PM ingression between daughter cells. In *Schizosaccharomyces pombe,* important membrane-CR scaffolds include the paralogous F-BAR proteins Cdc15 and Imp2. Their conserved protein structure consists of the archetypal F-BAR domain linked to an SH3 domain by an intrinsically disordered region (IDR). Functions have been assigned to the F-BAR and SH3 domains, and in this study we probed the function of the central IDR. We found that the IDR of Cdc15 is essential for viability and cannot be replaced by that of Imp2, whereas the F-BAR domain of Cdc15 can be swapped with several different F-BAR domains, including that of Imp2. Deleting part of the IDR results in CR defects and abolishes calcineurin phosphatase localization to the CR. Together these results indicate that Cdc15's IDR has a non-redundant essential function that coordinates regulation of CR architecture.

Introduction

Cytokinesis is the final step in the cell division cycle when daughter cells separate. In Amoebozoa and Opisthokonta, cytokinesis employs an actin- and myosin-based proteinaceous apparatus termed the cytokinetic ring (CR) (Mangione and Gould, In press). The CR assembles at the future division plane and eventually constricts coincident with cleavage furrow ingression. Of the many proteins that comprise the CR, membrane-bound scaffolds are crucial for transmitting CR-generated tension to the plasma membrane (PM) and for maintaining CR placement at the division site (Glotzer, 2017). F-BAR proteins are conserved membrane-CR scaffolds that function during cytokinesis as well as other processes involving coordination between the dynamic cytoskeleton and membranes (Lippincott and Li, 2000; Ahmed et al., 2010; Fricke et al., 2010; Roberts-Galbraith and Gould, 2010). The namesake F-BAR domain binds phospholipids and oligomerizes into a multivalent platform that can recruit proteins to membranes through interactions with the F-BAR domain itself or using additional functional domains (McDonald and Gould, 2016).

In the fission yeast *Schizosaccharomyces pombe,* the F-BAR protein Cdc15 is an essential protein that promotes CR stabilization and cell wall deposition (i.e. septation) that occurs coincident with CR constriction (Fankhauser et al., 1995; Wachtler et al., 2006; Huang et al., 2007; Pinar et al., 2008; Roberts-Galbraith et al., 2009; Arasada and Pollard, 2014; Cortes et al., 2015; Ren et al., 2015; Willet et al., 2015b; Sethi et al., 2016; Onwubiko et al., 2019). Cdc15 has an N-terminal F-BAR domain linked by a central intrinsically disordered region (IDR) to a C-terminal SH3 domain. The F-BAR domain directly binds the PM (McDonald et al., 2015) and the essential CR actin nucleator/elongator formin Cdc12 (Carnahan and Gould, 2003; Willet et al., 2015a).

Additionally, the Cdc15 F-BAR domain oligomerizes into a multivalent scaffold with high avidity for the PM at the division site (McDonald et al., 2015). Disrupting the Cdc15-Cdc12 interaction delays CR formation (Willet et al., 2015a), while disrupting Cdc15 F-BAR membrane-binding and oligomerization destabilizes the CR and increases cytokinesis failures (McDonald et al., 2015). Indeed, the F-BAR domain is essential for Cdc15 function and cell viability (McDonald et al., 2015). In contrast, domain-swapping experiments showed that the Cdc15 SH3 domain is redundant with that of its paralog Imp2, which is also a component of the CR (Demeter and Sazer, 1998; Roberts-Galbraith et al., 2009; Ren et al., 2015).

Imp2 shares Cdc15's domain structure: an N-terminal F-BAR domain is linked by an IDR to a C-terminal SH3 domain. However, *imp2* null cells are viable, though they have severe cytokinetic defects (McDonald et al., 2016) and Imp2 dynamics at the CR differ from Cdc15 (Demeter and Sazer, 1998; Ren et al., 2015). The defects of *imp2* null cells are recapitulated by an F-BAR deletion mutant, *imp2(C)* (McDonald et al., 2016); however, replacing the F-BAR of Imp2 with that of Cdc15 or the *Saccharomyces cerevisiae* homolog Hof1 rescues the mutant phenotype (McDonald et al., 2016). These results not only emphasized the importance of membrane binding for F-BAR protein function but also suggested an unexpected plasticity among F-BAR domains to perform this critical function, and pointed to the IDRs of Imp2 and Cdc15 as the key determinants of their functional differences.

IDRs are flexible, unfolded structures for which predicting protein function is difficult. Their flexibility allows them to sample many conformations thus enabling interaction with multiple binding partners (Tompa, 2012). Here, we have extended our comparative analyses of the relative importance of the F-BAR and IDR in the context of Cdc15's essential function in cytokinesis. We found that a variety of F-BAR domains from human and *S. pombe* F-BAR proteins can substitute for the Cdc15 F-BAR. In contrast, the Cdc15 IDR is essential and apparently uniquely so because it cannot be replaced by the Imp2 IDR. Further structure-function analysis of the Cdc15 IDR revealed that cells tolerate removing or exchanging parts of the IDR. However, such mutations are accompanied by cytokinesis defects and one section of the IDR is specifically required to maintain the circularity of the CR during constriction. At least some of the defects caused by deletions within the IDR are explained by failure to recruit the calcineurin phosphatase to the division site. Taken together, our results reveal a remarkable functional plasticity among F-BAR domains and add to the growing appreciation that IDRs make critical contributions in a variety of proteins and biological contexts.

Results

The Cdc15 IDR is essential for viability

We tested the ability of various *cdc15* mutants to support viability by integrating them at one *cdc15* locus of diploid cells to make *cdc15*$^{+}$*/cdc15* mutant heterozygotes. Next, the diploids were sporulated and tetrads dissected to determine if the *cdc15* mutations could support viability when present as the sole *cdc15* allele.

We found that the Cdc15 F-BAR domain alone was not sufficient to support cell viability (Figure 4, A and B). An allele encoding the Cdc15 F-BAR domain juxtaposed to the SH3 domain (*cdc15-*Δ*IDR*) was also unable to support viability, verifying the

necessity of Cdc15's IDR (Figure 4, A and C). Deletion of the SH3 domain was previously determined to be viable (Roberts-Galbraith et al., 2009) and further C-terminal truncation was tolerated to aa 710 but not to aa 700 (Figure 4A). These results, and those from previous studies (McDonald et al., 2015), indicate that the F-BAR domain and part of the IDR are required to perform Cdc15's essential function.

F-BAR domains can be exchanged

We next asked if these features could be replaced by the comparable regions of other F-BAR proteins. We first generated a series of chimeras by fusing various F-BAR domains from human and yeast proteins to the Cdc15 C-terminus and then tested them for viability as previously described. Five of the fifteen chimeras were viable: the fusions with F-BAR domains of human proteins Fer, Gas7, PACSIN2, and PSTPIP1 and *S. pombe* Imp2 (Figure 5A; Table 1). We tagged three with the fluorophore mNeonGreen (mNG) and they indeed localized to the CR (Figure 5B).

In contrast, neither a substitution of the Cdc15 IDR with that of Imp2 (*cdc15-imp2 chimera*) nor a mutant in which the Imp2 IDR was duplicated to match the length of Cdc15's IDR (*cdc15-imp2 extended chimera*) supported viability (Figure 5A). These results indicate that the Cdc15 IDR is essential in a sequence-specific manner.

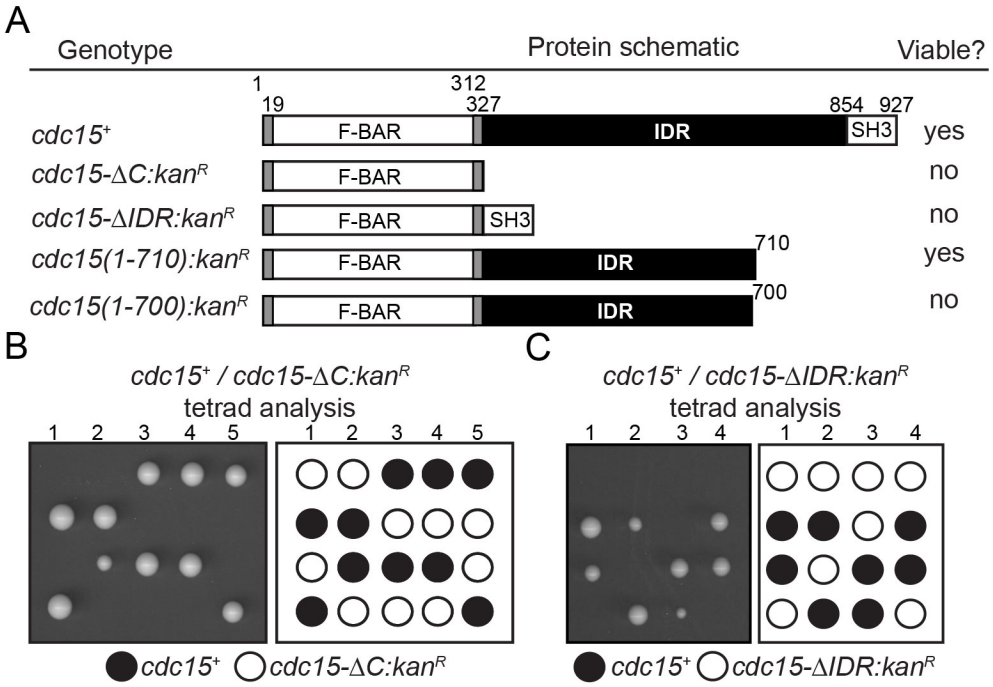

Figure 4. The IDR of Cdc15 is essential.
(A) Table of *cdc15* alleles, schematic of gene product (drawn to scale), and ability to rescue *cdc15* null. Numbers indicate aa position. (B and C) Diploids of the indicated genotype were induced to sporulate and tetrads were dissected on YES plates.

Table 1. F-BAR domains tested for rescuing Cdc15.

Species	Gene	Protein	F-BAR aa	Chimera Viable?
S. cerevisiae	*HOF1*	Formin-binding protein Hof1	1-294	No
S. pombe	*imp2*	Contractile ring protein Imp2	1-320	Yes
H. sapiens	*ARHGAP4*	Rho GTPase-activating protein 4	1-381	No
	FCHO1	F-BAR domain only protein 1	1-303	No
	FCHO2	F-BAR domain only protein 2	1-301	No
	FCHSD1	FCH and double SH3 domains protein 1	1-376	No
	FCHSD2	FCH and double SH3 domains protein 2	1-396	No
	FER	Tyrosine protein kinase Fer	1-287	Yes
	FES	Tyrosine protein kinase Fes	1-288	No
	FNBP1	Formin-binding protein 17 (FBP17)	1-319	No
	GAS7	Growth arrest-specific protein 7	198-476	Yes
	PACSIN1	Protein kinase C and casein kinase substrate in neurons 1	1-306	No
	PACSIN2	Protein kinase C and casein kinase substrate in neurons 2	1-304	Yes
	PSTPIP1	Proline-serine-threonine phosphatase-interacting protein 1	1-290	Yes
	PSTPIP2	Proline-serine-threonine phosphatase-interacting protein 2	1-312	No

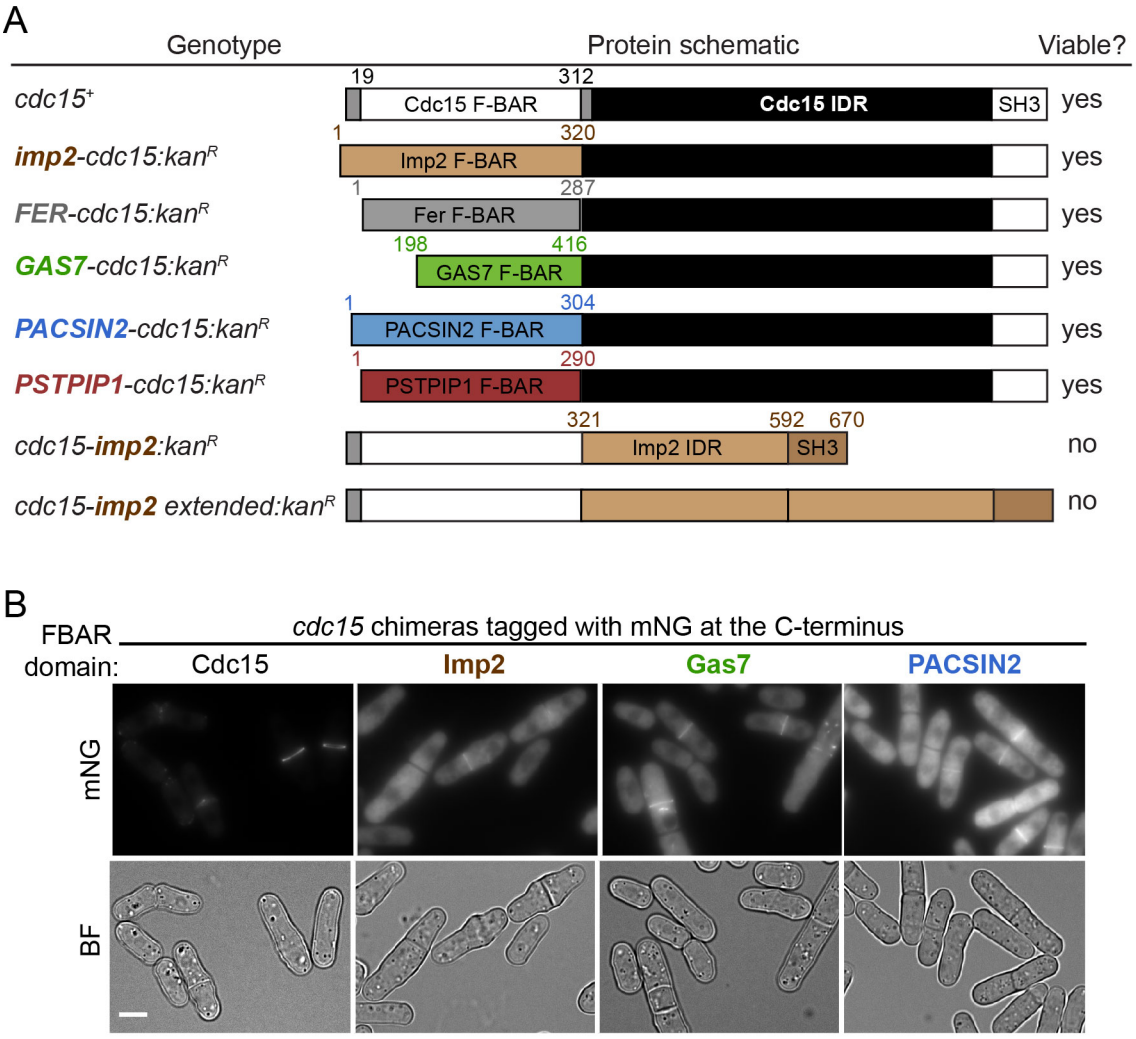

Figure 5. Cdc15 F-BAR but not IDR can be replaced by domains of homologous proteins.

(A) Table of *cdc15* alleles, schematic of gene product (drawn to scale), and ability to rescue *cdc15* null. Numbers indicate aa position. (B) Live-cell images of the indicated haploid strains. A single brightfield (BF) z-slice and sum projections of mNG images are shown. Bar, 5 µm.

Partial loss of the IDR results in cytokinesis defects

To separate the function of the IDR from that of the SH3 domain, which coordinates CR constriction and septum deposition through multiple binding interactions (Tajadura et al., 2004; Morrell-Falvey et al., 2005; Pinar et al., 2008; Roberts-Galbraith et al., 2009; Cortes et al., 2015; Ren et al., 2015; Sethi et al., 2016), we divided the IDR into three segments of 175 aa (Figure 6A) and deleted each segment individually. Each of the three deletion mutants was viable (Figure 6B). However, the three mutants had different phenotypes: *cdc15*-Δ*1* cells were morphologically indistinguishable from WT cells, while *cdc15*-Δ*2* and *cdc15*-Δ*3* cells had defects in morphology and cell division, as evidenced by an increased number of nuclei and septa per cell (Figure 6, B and C). We considered the possibility that the cytokinetic defects observed in *cdc15*-Δ*2* and *cdc15*-Δ*3* resulted from simultaneously removing key aa residues and shortening the separation between the F-BAR and SH3 domains. Therefore, we tested if replacing the IDR with duplicated or triplicated segment 2 (aa 503 to 677) would rescue the morphological defects, but they did not (Figure 6D).

As described above, the shortest viable C-terminal truncation of Cdc15 was at aa 710 (Figure 4A). Therefore, although segment 3 (aa 678 to 854) could be deleted when the SH3 domain was present (Figure 6B), cells required part of segment 3 in the absence of the SH3 domain. This result suggested that there are likely multiple functional motifs along the length of Cdc15 and that loss of some combinations, but not others, might be tolerated. To expand on this idea, we combined deletions of IDR segments and/or the SH3 domain. While *cdc15*-Δ*1*Δ*3* and *cdc15*-Δ*1*Δ*SH3* are viable, *cdc15*-Δ*1*Δ*2, cdc15*-Δ*2*Δ*3,* and *cdc15*-Δ*2*Δ*SH3* are not (Figure 6E). These results indicate that region 2 mediates a particularly important function such that its loss is barely tolerated.

Segments 2 and 3 of Cdc15's IDR contain multiple short stretches that have similar sequence identity among *Schizosaccharomyces* species (Figure 7). Many of these conserved motifs also have high prediction for protein binding (ANCHOR; (Dosztanyi et al., 2009; Meszaros et al., 2009)) (Figure 8A). Therefore, deletions of these short conserved motifs were tested to better define important functional motifs within the IDR. However, none of the smaller deletions resulted in the cytokinetic phenotypes observed for *cdc15*-Δ*2* or *cdc15*-Δ*3* (Figure 8B).

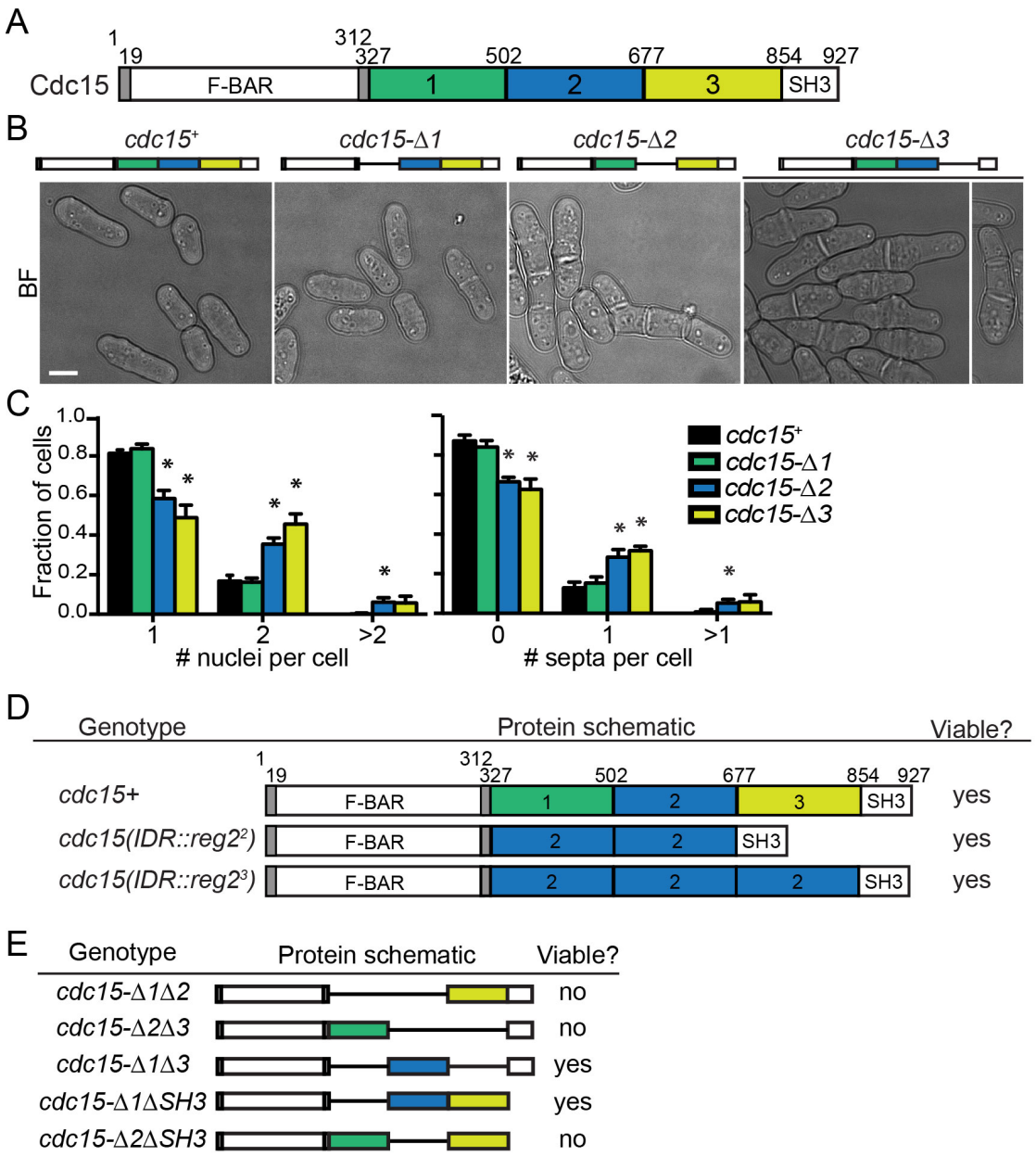

Figure 6. Cdc15 IDR deletion mutants have cytokinesis defects.
(A) Schematic of Cdc15 indicating the aa boundaries of IDR regions. (B) BF images of the indicated strains. Bar, 5 µm. (C) Quantification of the number of nuclei (left) and septa (right) per cell of the indicated strains, determined from cells stained with DAPI and Methyl Blue to visualize DNA and septum, respectively. Results are the mean from three biological replicates, $n > 198$ cells per replicate. Error bars are SD. *, $p<0.05$ Student's T-test. (D-E) Table of *cdc15* alleles, schematic of gene product, and ability to rescue *cdc15* null. Schematics are drawn to scale. Black lines indicate deletion. Numbers indicate aa position.

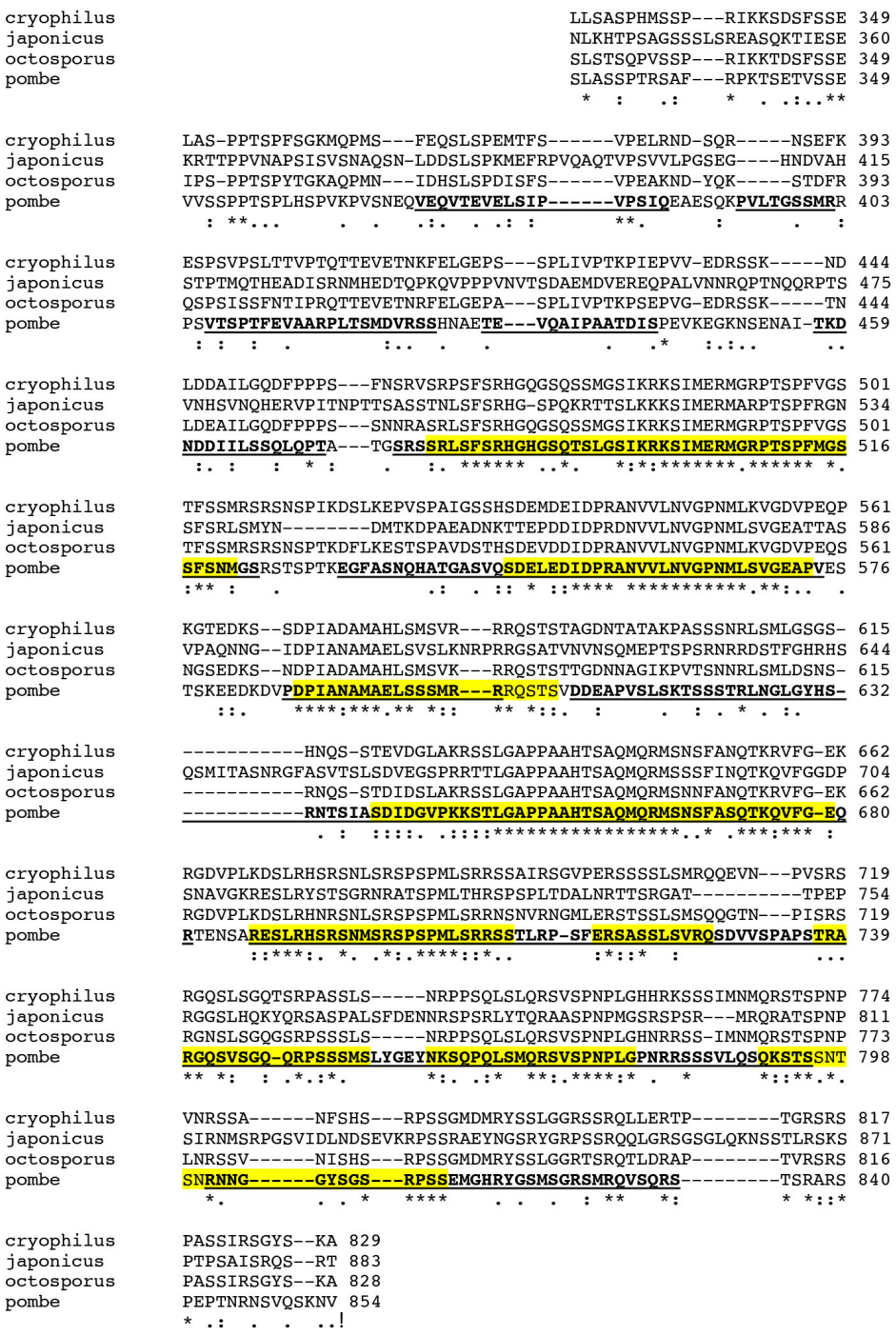

Figure 7. The central region of Cdc15 is conserved across *Schizosaccharomyces* species.

Sequence alignment of *cdc15* central region from *Schizosaccharomyces* species. Predicted binding regions from Figure 8A are underlined and in bold typeface. Small deletions that were tested for morphological defects (listed in Figure 8B) are highlighted in yellow.

A

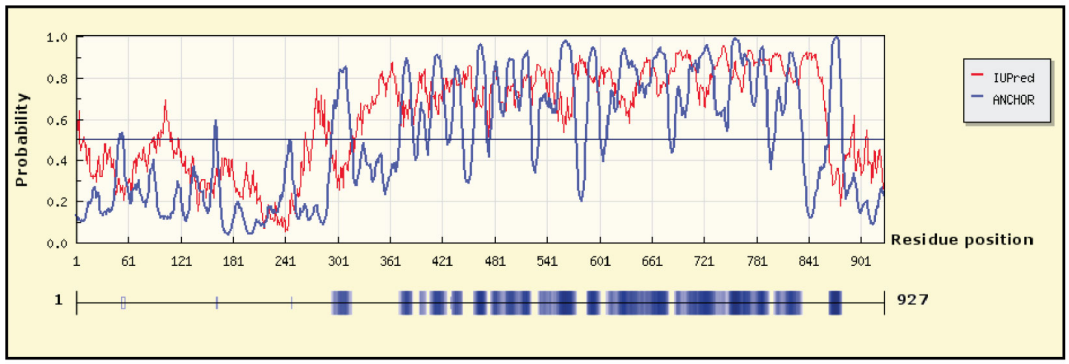

B

Predicted binding regions

371 to 387
394 to 402
406 to 426
431 to 443
456 to 472
476 to 523
531 to 574
586 to 602
609 to 681
687 to 795
801 to 834

C

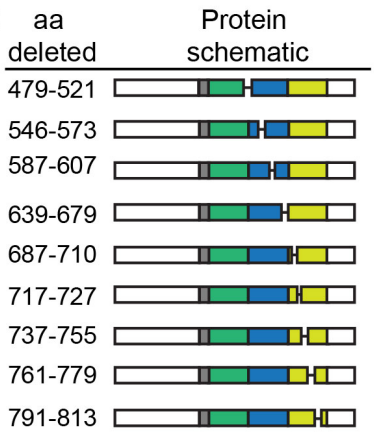

Figure 8. The central region of Cdc15 is predicted to be disordered and has multiple predicted binding regions.

(A) Results of IUPRED and ANCHOR analysis identifying stretches of Cdc15 that have high likelihood for disorder and greater than 50% prediction for binding, respectively. aa that have >50% probability for binding are listed to the right. (B) To-scale schematics of small deletions.

Cdc15 IDR mutants localize to the division site and are phosphoregulated

We confirmed by SDS-PAGE and immunoblotting that Cdc15-Δ1, Cdc15-Δ2, and Cdc15-Δ3 were produced at levels comparable to WT Cdc15 (Figure 9A). Additionally, the three single segment deletion mutants localized to nodes and CRs (Figure 9B).

Next, we examined if the Cdc15 segment deletions were still subject to cell cycle-regulated phosphoregulation as the IDR is the primary site of phosphorylation (Wilson-Grady et al., 2008; Roberts-Galbraith et al., 2010; Koch et al., 2011; Chen et al., 2013; Carpy et al., 2014; Kettenbach et al., 2015; Swaffer et al., 2016; Lee et al., 2018; Swaffer et al., 2018) During interphase, Cdc15 is highly phosphorylated, which is evidenced by slower mobility on SDS-PAGE (Fankhauser et al., 1995; Roberts-Galbraith et al., 2010). During mitosis and cytokinesis, Cdc15 is dephosphorylated (Fankhauser et al., 1995; Roberts-Galbraith et al., 2010). Mutants that abolish phosphorylation exhibit defects in cytokinesis and abnormally localize to the cell cortex during interphase (Roberts-Galbraith et al., 2010). Lambda phosphatase collapse revealed that Cdc15-Δ1, Cdc15-Δ2, and Cdc15-Δ3 were still phosphorylated (Figure 10A). Additionally, we determined that Cdc15-Δ1, Cdc15-Δ2, and Cdc15-Δ3 maintained cell cycle changes in phosphorylation (Figure 10B). Furthermore, mEGFP-Cdc15-Δ2 and mEGFP-Cdc15-Δ3 showed diffuse localization during interphase (Figure 10C), suggesting that the division defects of *cdc15-Δ2* and *cdc15-Δ3* are not mimicking Cdc15 phospho-ablating mutants. In contrast, mEGFP-Cdc15-Δ1 accumulated in cortical puncta during interphase despite the fact that *cdc15-Δ1* have normal morphology (Figure 10C). These findings suggest that phosphorylation events throughout the IDR may have differential effects on Cdc15 function.

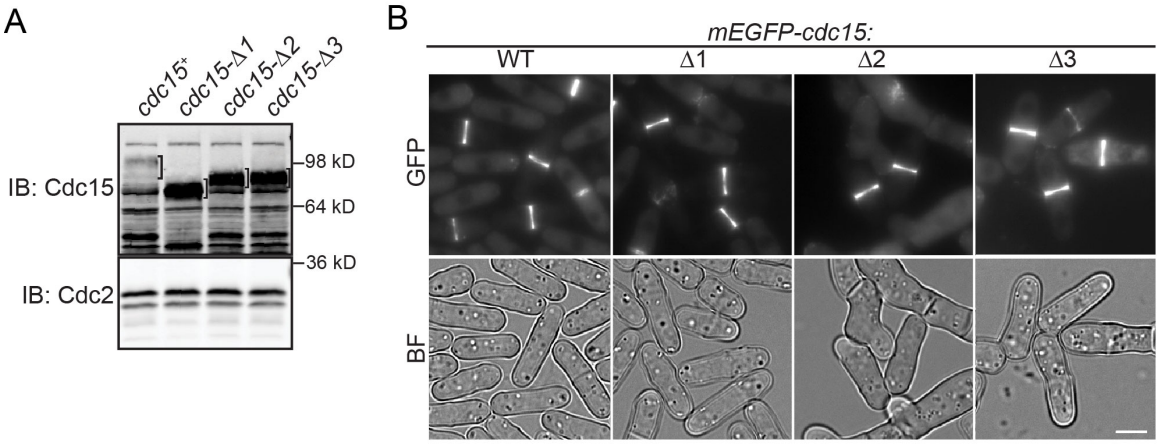

Figure 9. Cdc15 IDR mutants are produced and localize to the division site.
(A) Lysates from indicated strains immunoblotted (IB) for indicated proteins. The bands that are full-length product of *cdc15* allele are indicated by brackets. (B) Live-cell images of the indicated haploid strains. A single BF z-slice and sum projections of mNG images are shown. Bar, 5 μm.

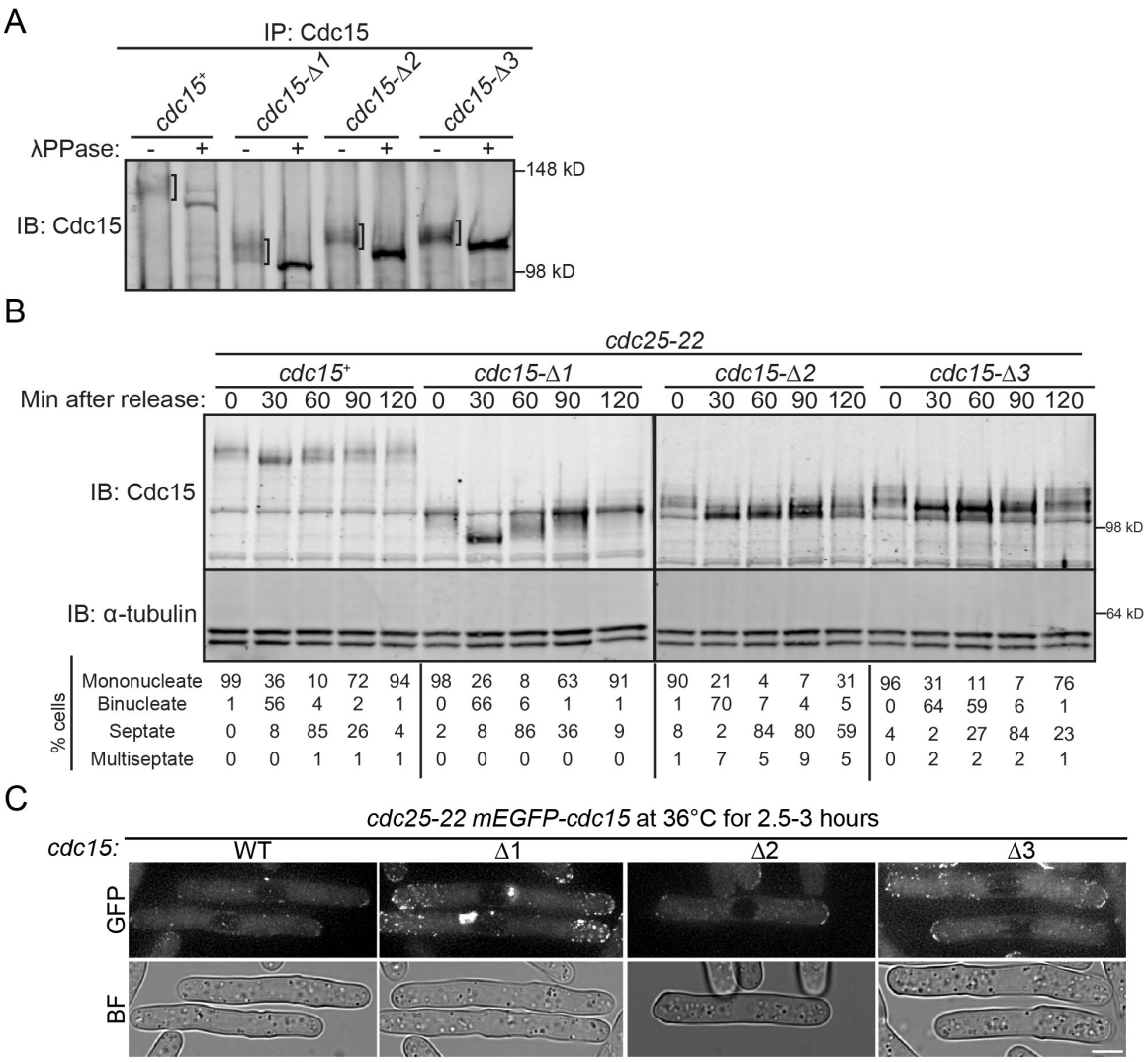

Figure 10. Cdc15 IDR deletion mutants are phosphorylated.
(A) IB of Cdc15 immunoprecipitated (IP) from the indicated strains and then treated with lambda phosphatase (λPPase). Brackets in untreated lanes indicate Cdc15. (B) *cdc25-22* cells with the indicated *cdc15* allele were grown to mid-log phase, shifted to 36°C for 3.75 h, and then released to permissive temperature (25°C). Samples were collected at the indicated times. Denatured lysates were analyzed by IB to detect the indicated proteins. Cell cycle progress was monitored by determining the binucleate and septation indices. (C) Representative images of the indicated strains arrested in G2. A single BF slice and max intensity z-projections of deconvolved GFP images are shown. Bar, 5 μm.

The Cdc15 IDR is important for normal cytokinesis dynamics and CR integrity

To better understand the defects observed in *cdc15* IDR segment deletions, we measured the cytokinesis dynamics of mutants expressing spindle pole body (SPB) protein Sid4-mNG and CR protein Rlc1-mNG, which mark progression through mitosis and cytokinesis, respectively. As expected from the morphological analysis, the cytokinesis dynamics of *cdc15*-Δ*1* were like WT. In contrast, the CR of *cdc15*-Δ*2* cells took longer to constrict while *cdc15*-Δ*3* cells showed increased lengths of both CR maturation (defined as the time between CR assembly and constriction) and CR constriction (Figure 11A).

We were particularly interested in cytokinesis defects of *cdc15*-Δ2 cells since segment 2 was the minimal IDR that supported viability (i.e. *cdc15*-Δ*1*Δ*3* was viable*;* Figure 6E). Interestingly, the increased length of CR constriction in *cdc15*-Δ*2* mutants correlated with a loss of CR integrity upon constriction initiation and subsequent asymmetric deposition of cell wall material (Figure 11B). More precisely, the Rlc1-mNG signal in z-projections became asymmetric and accumulated at one point of the cell, appearing to collapse and lose circularity (Figure 11B; double arrowhead). Shortly after, septum formation was visible at the point(s) where the CR proteins remained (Figure 11B; yellow arrowheads). This was confirmed by imaging Rlc1-mCherry (mCh) to mark the CR and glucan synthase GFP-Bgs4 to mark the position of cell wall deposition in cells oriented vertically (Wang and Tran, 2014) (Figure 12A) and in the standard xy plane (Figure 13A). A Z-series of images of Rlc1-mCh and the membrane marker Acyl-GFP also provided a clear view of asymmetric furrowing in *cdc15*-Δ*2* cells (Figure 12B). The observation that the position of septum formation corresponded to the asymmetric localization of Rlc1 is consistent with a previous report that the CR or actin remnants of the CR locally stimulate cell wall synthesis (Zhou et al., 2015). Asymmetric septation has not been observed in any previously characterized Cdc15 mutant with defective membrane association or oligomerization, or reduced abundance (Huang et al., 2007; Arasada and Pollard, 2014; McDonald et al., 2015). Vice versa, the CR unraveling observed in the absence of both Cdc15's and Imp2's SH3 domains (Roberts-Galbraith et al., 2009) or the CR sliding observed in F-BAR oligomerization and membrane-binding mutants was not observed in *cdc15*-Δ*2* cells during time-lapse live-cell imaging (e.g., Figure 11B) nor did *cdc15*-Δ*2* cells have off-center septa (as measured by long-to-short cell ratio) (Figure 13B). These results suggest that the function of segment 2 is distinct from that of the F-BAR and SH3 domains.

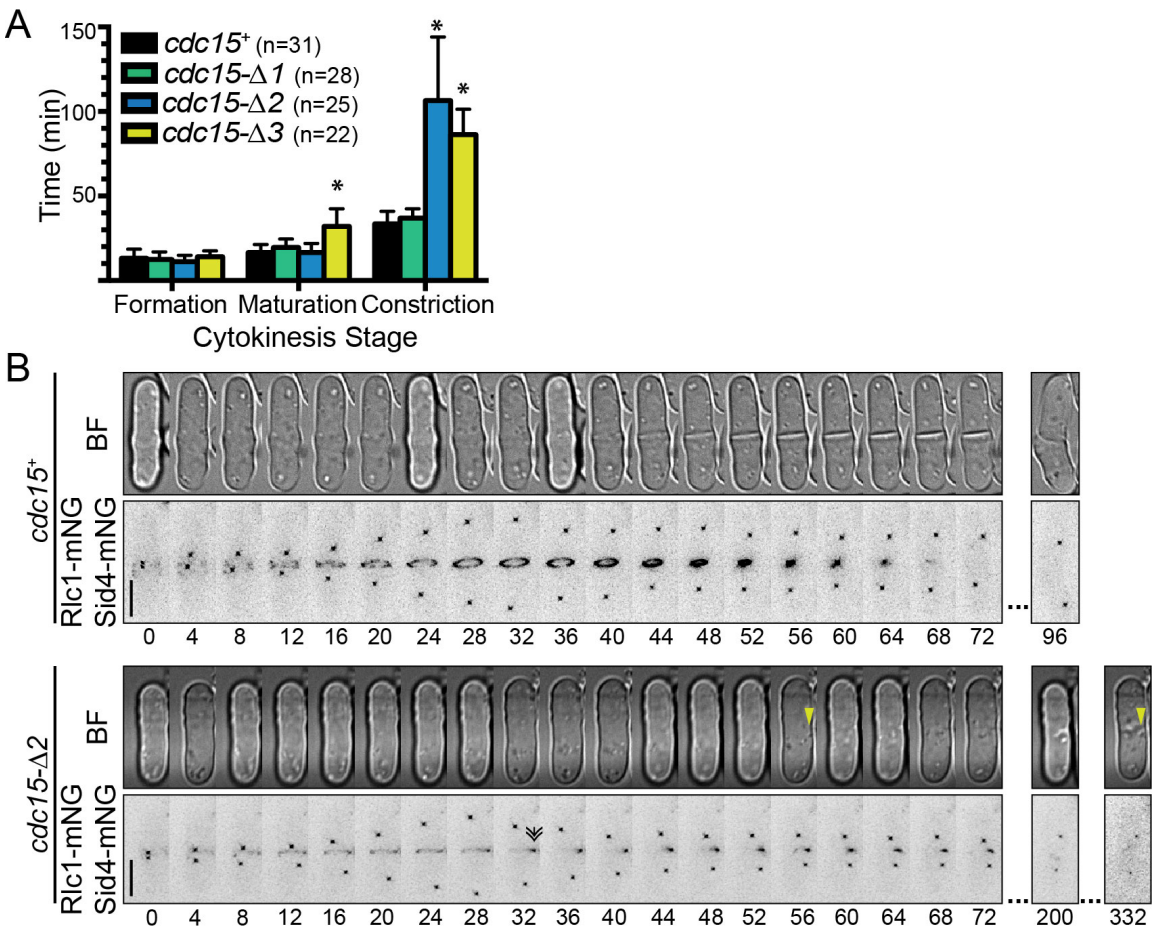

Figure 11. Cdc15 deletions have cytokinesis defects.

(A) Duration of cytokinesis stages determined from imaging as in F of strains expressing the indicated *cdc15* allele plus *rlc1-mNG* and *sid4-mNG* to label the CR and SPB, respectively. Error bars are SD. *, $p < 0.05$ Student's T-Test. (B) Representative time-lapse series of the indicated strains. Images were acquired every 2 min. A single BF slice and max intensity z-projections of deconvolved mNG images are shown. Numbers indicate min from SPB separation. Bar, 5 µm. Double arrow indicates first frame when CR loses ring-like structure. Yellow arrowheads point out first and last frame with visible asymmetric septum deposition.

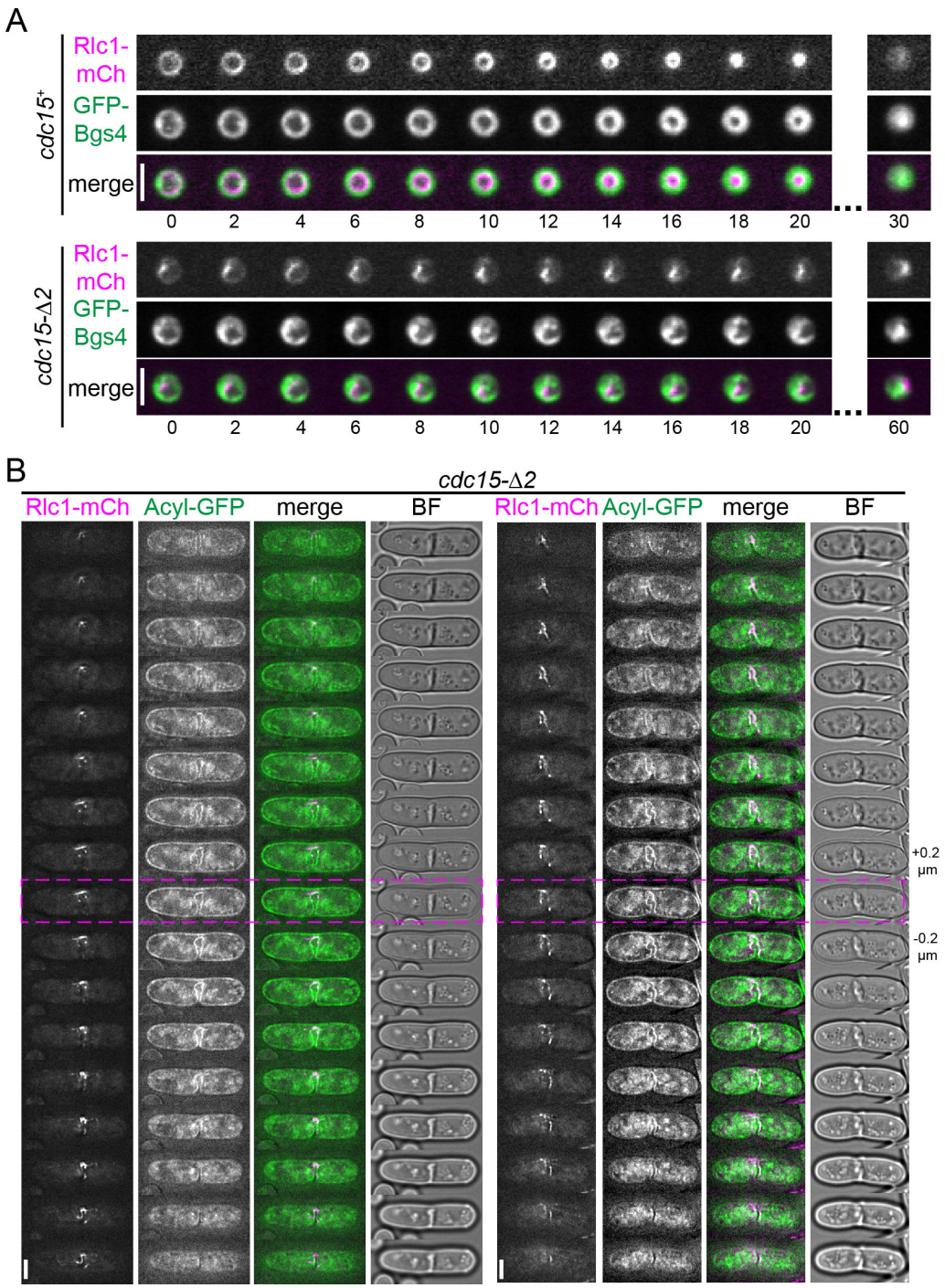

Figure 12. Characterizing the CR defect in *cdc15-Δ2*.
(A) End-on imaging of the indicated strains. Numbers indicate min elapsed since the start of the series. Bar, 5 µm. (B) Z-slices of two representative cells of the indicated genotype. The pink dashed lines mark the middle slice. Z-slices were taken every 0.2 µm through the volume of the cell. Fluorescence images are deconvolved. Bar, 5 µm.

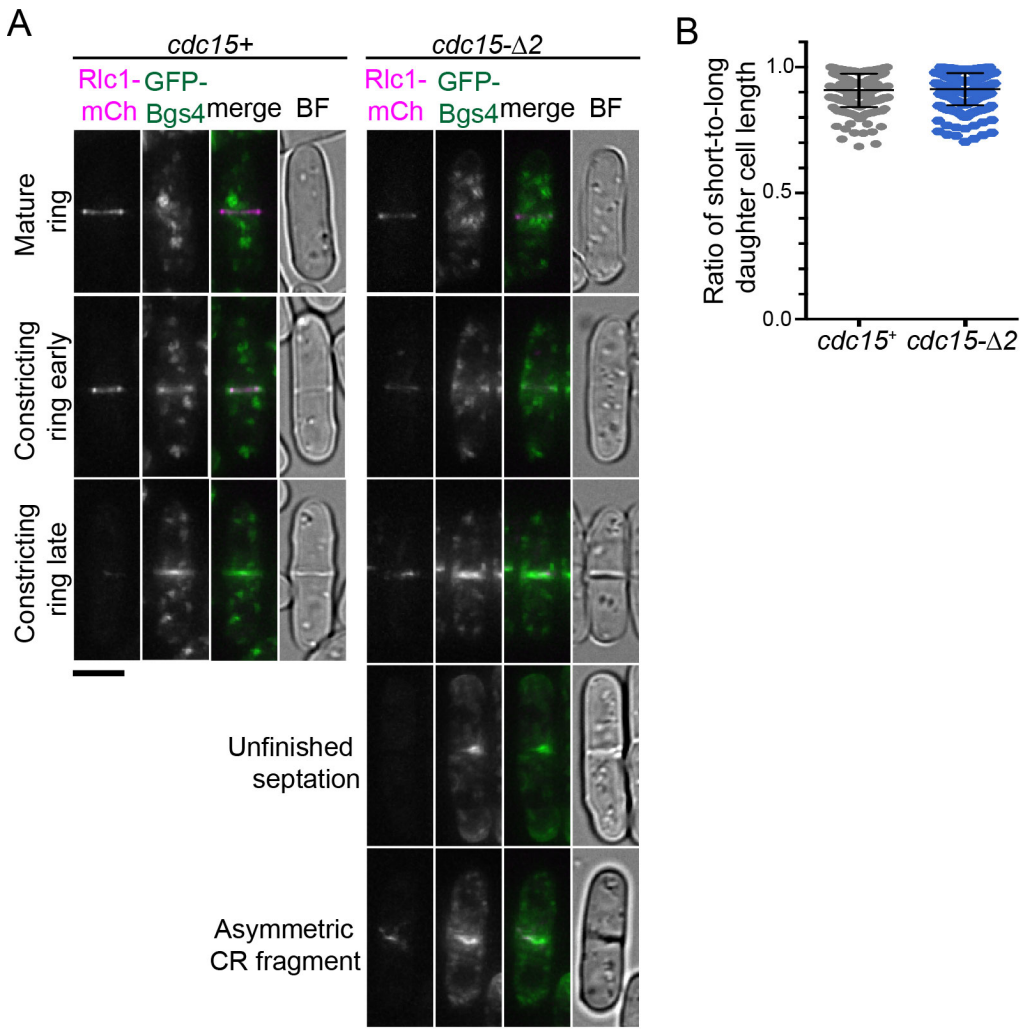

Figure 13. Septum machinery and placement localize to equator.
(A) Representative images of the indicated strains. Bar, 5 µm. (B) The ratio of short-to-long daughter cell length as determined from cells of the indicated genotype that were fixed and stained with DAPI and Methyl Blue. Results are from two biological replicates with n > 87 cells per replicate. Average +/- standard deviation are indicated by black lines.

Cell wall enzymes are trafficked to the division site and active in cdc15-Δ2

The septum is a trilaminar structure. The Bgs1-dependent primary septum is deposited first and sandwiched by secondary septa deposited by Bgs4 and Ags1; enzymatic digestion of the primary septum leads to daughter cell separation (reviewed in (Willet et al., 2015b; García Cortés et al., 2016; Perez et al., 2016). We have already demonstrated that Bgs4 is recruited to the division site (Figures 12A and 13A). However, the Cdc15 IDR has been implicated in the recruitment of Bgs1 (Arasada and Pollard, 2014). Therefore, to test if *cdc15-Δ2* cells failed to adequately recruit Bgs1, we monitored GFP-Bgs1 localization in *cdc15-Δ2* cells. GFP-Bgs1 was recruited to the division site with similar temporal kinetics and abundance in WT and *cdc15-Δ2* (Figure 14A). However, consistent with the asymmetric localization of GFP-Bgs4 (Figure 12A) and deposition of septum material (Figures 11B, 13), GFP-Bgs1 distribution was not always circumferential in *cdc15*-Δ2 cells (Figure 14A). Taken together, these data indicate that cell wall synthesis is activated at the proper time but not necessarily in the proper location in *cdc15-Δ2*. In fact, *cdc15-Δ2* was synthetic lethal with *bgs1-ts/cps1-191* (Figure 15B), indicating that robust cell wall deposition is crucial for division and viability of *cdc15-Δ2.*

CR composition is altered in cdc15-Δ2 cells

The results described above indicate that the asymmetry of CR constriction in *cdc15-Δ2* is not due to a defect in septation per se but rather results from a CR-intrinsic defect that results in loss of a ring structure upon constriction onset and instead CR proteins remain at the division site as arcs or strands. Indeed, *cdc15-Δ2* mutants were sensitive to a low-dose of latrunculin A (Figure 15A), and were synthetically sick or lethal with numerous regulators of the actin cytoskeleton (Figure 15B), indicating lower tolerance to further perturbations of the CR. Therefore, we used fluorescence microscopy to screen actin binding proteins, actin regulators, Cdc15 binding partners, and other CR proteins for changes in their localization to the division site in *cdc15-Δ2* (Figure 15C). The calcineurin phosphatase, which comprises catalytic subunit Ppb1 and regulatory subunit Cnb1, has been found to regulate Cdc15 (Martin-Garcia et al., 2018). Also, the morphologies of *cdc15-Δ2* and *ppb1Δ* (Yoshida et al., 1994) are similar. This prompted us to examine Ppb1's localization in *cdc15-Δ2.* We found that Ppb1 was absent from the CR of *cdc15-Δ2* cells, but it localized normally in other *cdc15* segment deletions (Figure 16A). The localization of Ppb1 to the CR was previously found to depend on Pxl1 (Martin-Garcia et al., 2018) and Pxl1 associates with Cdc15 by Co-IP (Pinar et al., 2008; Roberts-Galbraith et al., 2009). Given that Ppb1 was essentially absent from the CR, it was surprising to find that Pxl1 localized to the division site normally in *cdc15-Δ2* (Figure 16B). This result suggests that Pxl1 is not sufficient for Ppb1 localization to the CR.

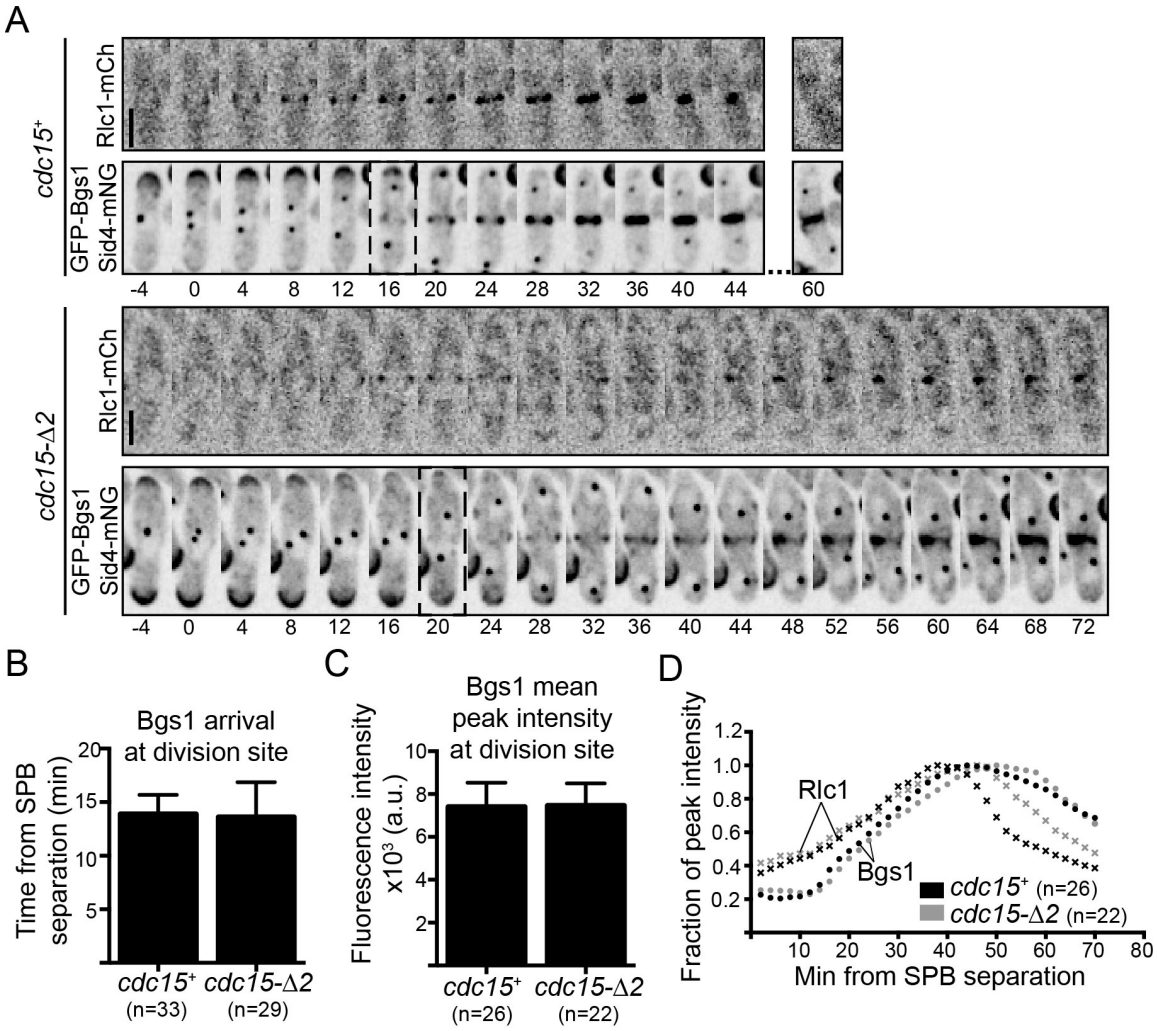

Figure 14. Cell wall synthases are properly trafficked in *cdc15-Δ2.*

(A) Representative time-lapse series of the indicated strains. Sum z-projections are shown. Images were acquired every 2 min. Numbers indicate min from SPB separation. Bar, 5 µm. (B) Timing of GFP-Bgs1 arrival to the division site in the indicated strains also expressing Sid4-mNG and Rlc1-mCh. Error bars are SD. $p = 0.67$ Student's T-test. (C) Average peak fluorescence of GFP-Bgs1 in the indicated strains also expressing Sid4-mNG and Rlc1-mCh. Error bars are SD. $p = 0.85$ Student's T-test. (D) Timing of Rlc1 (×) and Bgs1 (●) peak intensity relative to SPB separation for the indicated strains determined from strains imaged as in (A).

A

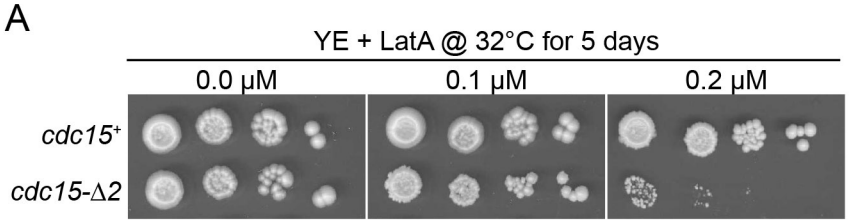

B

Synthetic lethal	Synthetic sick	No interaction
*acp1*Δ	*cdc3-124*	*cdc8-134*
adf1-1	*cdc12-112*	*cwg1-1*
*ain1*Δ	*cdc12-*Δ*C'*	*cwg1-2*
cdc12-4A	*cdc16-116*	
cps1-191	*fim1*Δ	
*efr3*Δ		
*mid1*Δ		
*rlc1*Δ		

C

Protein	Description	At CR in *cdc15-*Δ*2*?
Acp1	Actin capping protein	Yes
Adf1	Actin depolymerizing factor cofilin	Yes
Ain1	Actin crosslinking protein α-actinin	Yes
Cdc12	Formin	Yes
Cyk3	Nebulin-family actin filament anchoring protein	Yes
Fic1	C2 domain protein	Yes
Fim1	Actin bundling protein fimbrin	Yes
Gef2	RhoGEF	Yes
Mid1	Anillin-like protein	Yes
Myo2	Essential myosin-II heavy chain	Yes
Myp2	Non-essential myosin-II heavy chain	Yes
Ppb1	Calcineurin catalytic subunit	No
Rng2	IQGAP protein	Yes
Sbg1	PM-CR linker protein	Yes

Figure 15. Genetic interactions and sensitivities of *cdc15-*Δ*2*.
(A) Growth assay comparing sensitivity of indicated strains to the indicated dose of latrunculin A (LatA). (B) Table of *cdc15-*Δ*2* genetic interactions. (C) List of proteins tested for CR localization in *cdc15-*Δ*2*.

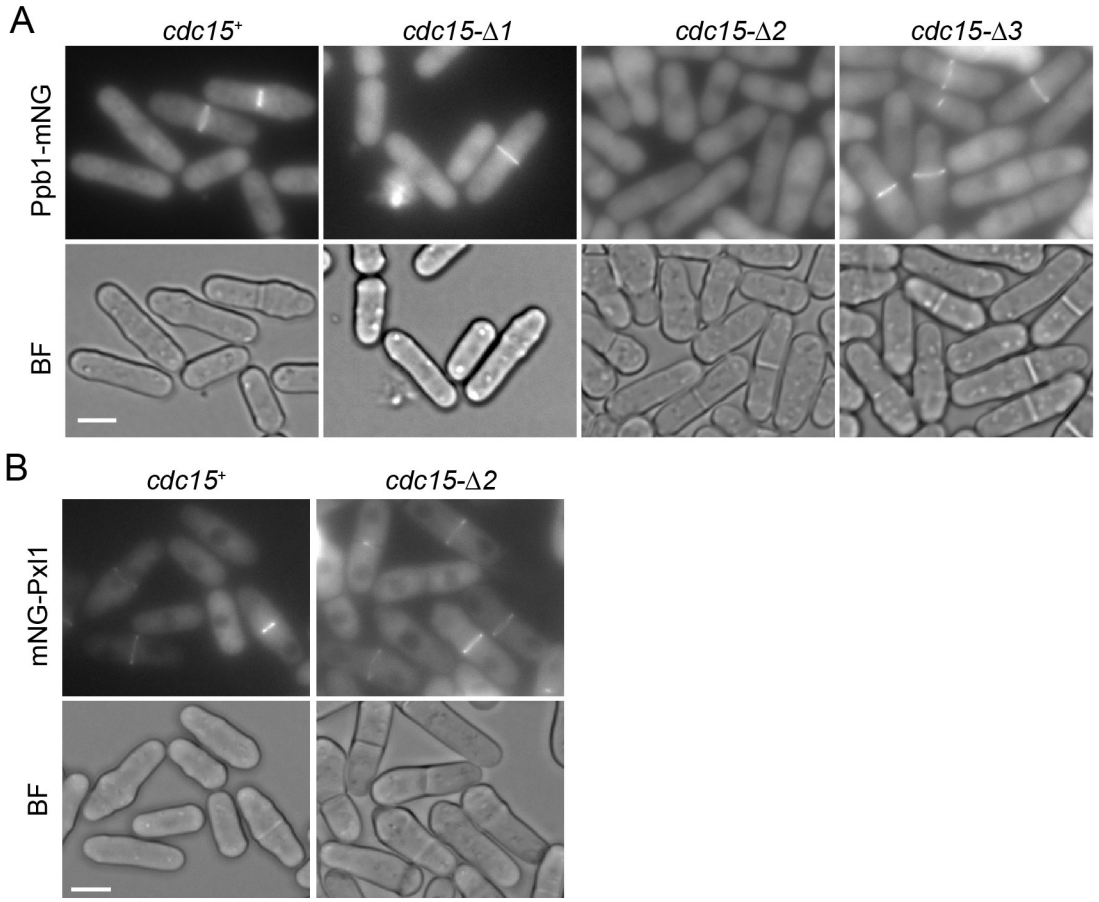

Figure 16. Calcineurin is not recruited to CR in *cdc15*-Δ*2*.
(A and B) Representative sum projections of the indicated strains. Bar, 5 μm.

Discussion

It was unknown what protein feature(s) distinguish the essential Cdc15 from its nonessential paralog Imp2. Using domain-swapping experiments, we determined that the essential function of the F-BAR domain can be replaced by Imp2's F-BAR domain as well as other human F-BAR domains, whereas Cdc15's IDR is uniquely essential and cannot be replaced by that of Imp2. Deletions of segments of the IDR exhibit either lengthened periods of CR maturation and constriction or loss of CR integrity upon constriction onset resulting in asymmetric septum deposition (*cdc15*-Δ*3* and *cdc15*-Δ*2*, respectively). Further, *cdc15*-Δ*2* cells lost CR localization of the calcineurin subunit Ppb1. This identifies a new function for the Cdc15 IDR in recruitment and/or maintenance of calcineurin at the CR and suggests that the CR defects in *cdc15*-Δ*2* may be due to global misregulation of CR components.

The exchangeability of F-BAR domains

Five of the 15 F-BAR domains tested replaced the essential function of Cdc15's F-BAR domain: the F-BAR domains of *S. pombe* Imp2 and human Gas7, PSTPIP1, PACSIN2/syndapin2, and Fer (Table 1). Given that the proteins in which these domains normally reside are involved in a variety of apparently unlinked functions and the F-BAR domains themselves have distinct biochemical characteristics and structures, we conclude that there is significant plasticity among F-BAR domains. This is perhaps not surprising since all F-BAR domains share the ability to interact electrostatically with negatively charged phospholipids and to oligomerize (Table 2) (Tsujita et al., 2006; Shimada et al., 2010; Bai et al., 2012; Goh et al., 2012; Bai and Zheng, 2013; McDonald et al., 2015; McDonald and Gould, 2016; McDonald et al., 2016). Although there are reported differences among F-BAR proteins in phospholipid or curvature specificity, F-BAR domains themselves interact relatively non-specifically with negatively charged phospholipids, and it is only protein features adjacent to the F-BAR domain, such as the FX(C) domain (Itoh et al., 2009; Yamamoto et al., 2018), that convey phospholipid or curvature specificity to the core F-BAR domain (reviewed in (Itoh and De Camilli, 2006)). Thus in the context of the full-length protein, an F-BAR domain acts as a module that concentrates the protein on membranes where other linked modules (e.g. SH3 domains, RhoGAP domains) provide the bulk of specific functions.

In terms of the F-BAR-Cdc15 chimeras that were not functional, multiple explanations can be imagined. In addition to the strong possibility that some fusion proteins were not structurally sound, some F-BAR domains bind directly to other proteins (Shoham et al., 2003; Hansen et al., 2011; Senju et al., 2011; Begonja et al., 2015; Garabedian et al., 2018; Liu et al., 2019), including Cdc15's F-BAR domain that binds the formin Cdc12 (Willet et al., 2015a). Though it is possible that the non-functional F-BAR-Cdc15 chimeras do not bind Cdc12, this seems an unlikely explanation since a mutant that disrupts the Cdc15-Cdc12 interaction is viable (Willet et al., 2015a). However, loss or gain of other protein partners or variations in oligomerization strategies might also be factors contributing to the lack of function of some chimeras (reviewed in (McDonald and Gould, 2016)).

Table 2. Characteristics of F-BAR domains that perform the essential function of Cdc15's F-BAR domain.

F-BAR domain	Lipid specificity	Curvature preference	Oligomerization mode	Tubulation
Cdc15	PS, PIPs[1]	None[1]	Tip-to-tip → Linear*[1]	None[1]
Imp2	PS, PIPs[2]	None[2]	Tip-to-core → Helical[2]	Positive[2]
Fer	$PI(4,5)P_2$, brain lipids[$3]	None[4]	Lateral F-BAR contacts*[1]	None[1,3]
Gas7	n.s.	n.s.	n.s.	None[1]
PACSIN 2	PS, brain lipids[5-6]	n.s.	Tip-to-tip →Spiral[7]; Wedge loop to lateral side of the F-BAR[8]	Positive[5-6,8]
PSTPIP1	$PI(4,5)P_2$, brain lipids[3]	n.s.	n.s.	Positive[3]

PS, phosphatidylserine; PIPs, phosphorylated phosphatidylinositols; n.s., not studied
*Based on homology model; [$]Brain lipids are enriched in PS and PIPs
1- (McDonald et al., 2015), 2- (McDonald et al., 2016), 3- (Tsujita et al., 2006), 4- (Yamamoto et al., 2018), 5- (Goh et al., 2012), 6- (Shimada et al., 2010), 7- (Bai and Zheng, 2013), 8- (Bai et al., 2012)

IDRs in F-BAR proteins

Our study revealed that like the F-BAR domain, Cdc15's IDR is essential, but unlike the F-BAR domain, it cannot be replaced by that of its paralog Imp2. In other contexts as well, the functional specificity of F-BAR proteins must be considered as the combined effect of their F-BAR domains and adjacent protein regions, including globular domains and IDRs. The IDR of *S. cerevisiae* Hof1 mediates its localization to the CR and is important for CR contraction; it also binds septins (Meitinger et al., 2011; Meitinger et al., 2013; Oh et al., 2013). The IDR in FCHO2 binds and allosterically activates AP-2 (Hollopeter et al., 2014; Umasankar et al., 2014). The IDR in FER undergoes a disorder-to-order transition to convey a curvature sensing function (Yamamoto et al., 2018). In the case of Cdc15's IDR, we found that it plays a key role in recruiting the phosphatase calcineurin. Calcineurin localization at the CR depends on the second region of Cdc15's IDR (aa 503 to 677) and Pxl1 (Martin-Garcia et al., 2018), and determining how these two proteins collaborate for proper calcineurin localization will be an important next step. Cdc15-Δ2 is dephosphorylated with timings similar to WT, which indicates that Cdc15's role scaffolding calcineurin at the CR would be separate from its identity as a calcineurin substrate (Martin-Garcia et al., 2018), and furthermore that either other phosphatases are redundant with calcineurin or cytoplasmic calcineurin dephosphorylates Cdc15. Finally, since *cdc15-Δ3* also has cytokinesis defects, but is not required for calcineurin recruitment to the CR, it will be interesting to determine the other functions performed by Cdc15's IDR.

CR strands or fragments direct primary septum deposition

In *cdc15-Δ2,* the CR appears to form normally and the glucan synthases are normally recruited, but upon constriction the CR loses its structure with Bgs1 then co-localizing with the CR-protein strands/arc-like structures that remain. As a result, the septum is deposited—albeit inefficiently—from that point. These behaviors of the CR and Bgs1 in *cdc15-Δ2* cells are consistent with the idea that the primary purpose of the *S. pombe* CR may be to direct efficient cell wall deposition, which in turn provides the force for division (Proctor et al., 2012b; Stachowiak et al., 2014; Thiyagarajan et al., 2015; Willet et al., 2015b; Zhou et al., 2015). The CR has been previously proposed to direct vesicular traffic (Vjestica et al., 2008) and the co-localization of glucan synthases with CR remnants throughout constriction in *cdc15-Δ2* indicates that the CR is indeed a landmark for glucan synthase delivery. CR contraction force has also been proposed to mechanically stimulate glucan synthase activity (Zhou et al., 2015) and it is possible that the CR strands observed in *cdc15-Δ2* are contraction-competent. However, in the absence of all myosin-II activity (*N-degron-myo2 myp2Δ)* primary septum is still deposited (Okada et al., 2019), suggesting that mechanostimulation is not required, although it could provide positive feedback.

cdc15-Δ2 is not the only mutant to display this type of CR behavior. A temperature-sensitive mutant of the essential myosin-II heavy chain *myo2-E1* displays similar CR dynamics at its non-permissive temperature (Palani et al., 2017; Okada et al., 2019). Additionally, a phosphomutant of the formin Cdc12 that prevents its phosphorylation by the SIN kinase Sid2 also has CRs that lose their ring structure during a *cps1-191* arrest when otherwise WT CRs do not (Bohnert et al., 2013). Single time-

point images of the CR and/or septum suggest similar CR behavior in other mutants, including temperature-sensitive cofilin *adf1-1* (Nakano and Mabuchi, 2006b) and deletions of both *acp1* that encodes actin capping protein (Kovar et al., 2005; Nakano and Mabuchi, 2006a) and *fim1* that encodes the actin bundler fimbrin (Wu et al., 2001). Altogether it seems that perturbations in CR architecture destabilize the ring, resulting in nonconcentric and inefficient primary septum deposition. In *cdc15*-Δ*2*, CR destabilization could be due to misregulation of multiple CR components due to loss of calcineurin at the division site.

CHAPTER 3

CDK PHOSPHORYLATES *S. POMBE* PAXILLIN TO INHIBITS ITS CYTOKINETIC RING LOCALIZATION

Abstract

During the cell cycle, division of the genetic material and the cytoplasm are coordinated spatially and temporally to ensure genome integrity. This is mediated in part by the major cell cycle regulator cyclin-dependent kinase (CDK). CDK activity peaks during mitosis but then during mitotic exit/cytokinesis CDK activity is reduced and reversed by various phosphatases including Cdc14, PP1 and PP2A phosphatases. CDK has previously been shown to phosphorylate various components of the actin- and myosin-based cytokinetic ring (CR) that mediates division of yeast and animal cells. Here we establish that *Schizosaccharomyces pombe* CR-component paxillin Pxl1 is also regulated by CDK. Abolishing phosphorylation on CDK sites causes precocious recruitment of Pxl1 to the division site and increased duration of CR constriction. We determined that both the Cdc14 phosphatase Clp1 and the PP1 phosphatase Dis2 reverse Pxl1 phosphorylation. This study describes a novel *S. pombe* CDK substrate and also provides an example of multiple phosphatases collaborating to reverse CDK phosphorylation of a single protein during cytokinesis.

Introduction

Cytokinesis is the final stage of the cell cycle, during which daughter cells physically separate. Yeast and animal cells divide using a conserved actin- and myosin-based contractile apparatus called the cytokinetic ring (CR) (Glotzer, 2017; Mangione and Gould, 2019) and substantial insight into the process has been gained from studying model organisms such as *Schizosaccharomyces pombe* (Bathe and Chang, 2010; Pollard and Wu, 2010b; Willet et al., 2015b). Multiple forward genetic screens identified essential and non-essential proteins for cytokinesis, which include both CR structural components and regulatory proteins (Nurse et al., 1976; Minet et al., 1979; Chang et al., 1996; Balasubramanian et al., 1998; Kim et al., 2010; Hayles et al., 2013; Chen et al., 2015; Chen et al., 2016), many of which are conserved in the budding yeast *S. cerevisiae* and metazoan cells (reviewed in (Pollard and Wu, 2010b)). Subsequent fluorescence imaging studies determined the timing of cytokinesis events relative to the events of mitosis in *S. pombe* (Wu et al., 2003; Wu and Pollard, 2005; Wu et al., 2006). The CR assembles during metaphase from clusters of early cytokinetic proteins called "cytokinesis nodes." Nodes are organized by the anillin-like protein Mid1 (Sohrmann et al., 1996; Paoletti and Chang, 2000; Wu et al., 2003; Rincon and Paoletti, 2012). They contain type-II myosin heavy chain Myo2 (Kitayama et al., 1997; May et al., 1997) and its light chains Rlc1 (Le Goff et al., 2000; Naqvi et al., 2000) and Cdc4 (McCollum et al., 1995), IQGAP actin bundling protein Rng2 (Eng et al., 1998; Takaine et al., 2009; Padmanabhan et al., 2011; Tebbs and Pollard, 2013), the F-BAR protein Cdc15 (Fankhauser et al., 1995; Wachtler et al., 2006), and the formin Cdc12 (Chang et al., 1997). Cdc12 nucleates and elongates F-actin from nodes that eventually coalesces into the CR (Kovar et al., 2003; Laporte et al., 2011; Zimmermann et al., 2017). The CR then undergoes a maturation period during which it accumulates more components such as

type-II myosin heavy chain Myp2 (Bezanilla et al., 1997; Motegi et al., 1997), the F-BAR protein Imp2 (Demeter and Sazer, 1998), and cell wall regulators Fic1 (Roberts-Galbraith et al., 2009), Pxl1 (Pinar et al., 2008; Cortes et al., 2015; Ren et al., 2015), and Rgf3 (Tajadura et al., 2004; Morrell-Falvey et al., 2005; Ren et al., 2015). Then, the CR constricts to bring together opposing membranes behind which a cell wall structure called the "septum" is deposited. The septum is trilaminar with a primary septum sandwiched by two secondary septa. Digestion of the primary septum leads to liberation of the two daughter cells (reviewed in (Willet et al., 2015b; García Cortés et al., 2016; Perez et al., 2016)).

These events are carefully regulated spatially and temporally to protect genomic integrity and ensure cytokinetic success. This is accomplished in part by the major cell cycle regulator cyclin-dependent kinase (CDK). High levels of CDK activity promote mitosis while inhibiting cytokinesis (Wheatley et al., 1997) (reviewed in (Wolf et al., 2007)). CDK inhibition and simultaneous reversal of CDK phosphorylation by opposing phosphatases (Stegmeier and Amon, 2004; Clifford et al., 2008a; Wu et al., 2009; Bloom et al., 2011; Wurzenberger and Gerlich, 2011; Grallert et al., 2015; Kuilman et al., 2015) are required for the events of mitotic exit, which includes anaphase and cytokinesis. In yeasts, multiple cytokinetic proteins have been identified as substrates of CDK including *S. pombe* formin Cdc12 (Willet et al., 2018), *S. cerevisiae* IQGAP protein Iqg1 (Holt et al., 2009; Naylor and Morgan, 2014), and *S. cerevisiae* C2 domain protein Inn1/Fic1 (Palani et al., 2012; Kuilman et al., 2015). Multiple large-scale proteomics studies have determined that Pxl1 is phosphorylated (Koch et al., 2011; Carpy et al., 2014; Kettenbach et al., 2015; Swaffer et al., 2016, 2018) and indicated that Pxl1 is a CDK substrate (Swaffer et al., 2016).

Although not essential, *pxl1*Δ have severe cytokinesis defects with CR sliding and splitting during anaphase (Ge and Balasubramanian, 2008; Pinar et al., 2008). Pxl1 arrives to the CR during maturation (Ren et al., 2015). It binds the F-BAR protein Cdc15 (Roberts-Galbraith et al., 2009), and the presence of Cdc15's SH3 domain is important for its assembly into the CR throughout cytokinesis (Martin-Garcia et al., 2018). The N-terminus of Pxl1 is important for its CR localization (Pinar et al., 2008) while its C-terminus comprises three tandem LIM domains that are important for its function (Figure 19A) (Ge and Balasubramanian, 2008; Pinar et al., 2008). Pxl1 is a negative regulator of Rho1 GTPase (Pinar et al., 2008), which is important for promoting cell wall deposition at the division site (Arellano et al., 1996; Nakano et al., 1997). The mechanism that dictates timing of Pxl1 arrival at the division site is unknown, as is whether Pxl1 activity itself is regulated. Here we confirm that Pxl1 is indeed a CDK substrate and characterize how CDK phosphorylation impacts Pxl1 activity.

Results

Pxl1 is phosphorylated in a cell cycle dependent manner

As reported previously, we observed that HA-Pxl1 levels fluctuate throughout the cell cycle (Figure 17A) (Ge and Balasubramanian, 2008; Pinar et al., 2008). Also, we noted that HA-Pxl1 migration by SDS-PAGE varies throughout mitosis/cytokinesis, with a notable retardation 30 minutes after release from a G2 arrest that is reversed by 60 minutes after release (Figure 17A). Consistent with the findings of several

phosphoproteomic screens, treatment with lambda protein phosphatase collapsed immunoprecipitated HA-Pxl1 to a single distinct band, indicating that these changes in migration are due to changes in phosphorylation (Figure 17B).

Pxl1 is phosphorylated by cyclin-dependent kinase

Previous studies and our own analysis of purified Pxl1 identified multiple phosphorylation sites on Pxl1, many of which match the CDK minimal consensus sequence of [S/T]P (Table 3 and Figure 18) (Koch et al., 2011; Carpy et al., 2014; Kettenbach et al., 2015; Swaffer et al., 2016, 2018). Therefore, we tested if Cdc2-Cdc13 (active CDK) could phosphorylate recombinant MBP-Pxl1. CDK phosphorylated both an N-terminal fragment (N) and full-length Pxl1 (FL), but not a C-terminal fragment (C) (Figure 19A-B). These results were expected because all of the identified [S/T]P phosphorylation sites reside in the N-terminus of Pxl1 (Figure 19A). Phospho-amino acid analysis indicated that CDK phosphorylates both serines and threonines in MBP-FL and MBP-N (Figure 20A), and comparison of the tryptic phosphopeptide maps of MBP-FL and MBP-N confirmed that all phosphorylation sites reside in the N-terminus of Pxl1 (Figure 20B).

Mutating all nine of the CDK sites in the N-terminus of Pxl1 to alanine abolished Pxl1 phosphorylation by CDK *in vitro* (Figure 19C). To determine the consequence of Pxl1 phosphorylation on these sites, we replaced $pxl1^{+}$ with alleles encoding HA-tagged *pxl1* phosphomutants: all nine residues matching the [S/T]P consensus sequence were mutated to alanine (9A) or aspartic acid (9D) to ablate or mimic phosphorylation, respectively. Unlike the migration of HA-Pxl1, HA-Pxl1(9A) and HA-Pxl1(9D) migrated as single bands on SDS-PAGE. Furthermore, HA-Pxl1(9D) migrated more slowly than HA-Pxl1(9A), which co-migrated with dephosphorylated HA-Pxl1 (Figure 21A). While treatment of HA-Pxl1 with lambda protein phosphatase collapsed the protein smear into one band, the migrations of HA-Pxl1(9A) and HA-Pxl1(9D) were unaltered by the treatment. We also monitored the phosphomutant protein throughout the cell cycle (Figure 21B) and did not observe any changes in protein migration as the cells progress from G2 through mitosis and cytokinesis, indicating that the majority of Pxl1 phosphorylation was eliminated in the 9A and 9D mutants.

Immunoblotting suggested that HA-Pxl1(9A) protein levels were increased compared to HA-Pxl1 and HA-Pxl1(9D). Therefore, we compared the whole-cell fluorescence intensities of Pxl1 wildtype and phosphomutants tagged at the N-terminus with mNeonGreen (mNG) (Shaner et al., 2013; Willet et al., 2015a). mNG-Pxl1(9A) whole-cell fluorescence intensity was increased ~2-fold compared to mNG-Pxl1 and mNG-Pxl1(9D), with a proportional increase in the amount of mNG-Pxl1(9A) in the CR (Figure 22A-C).

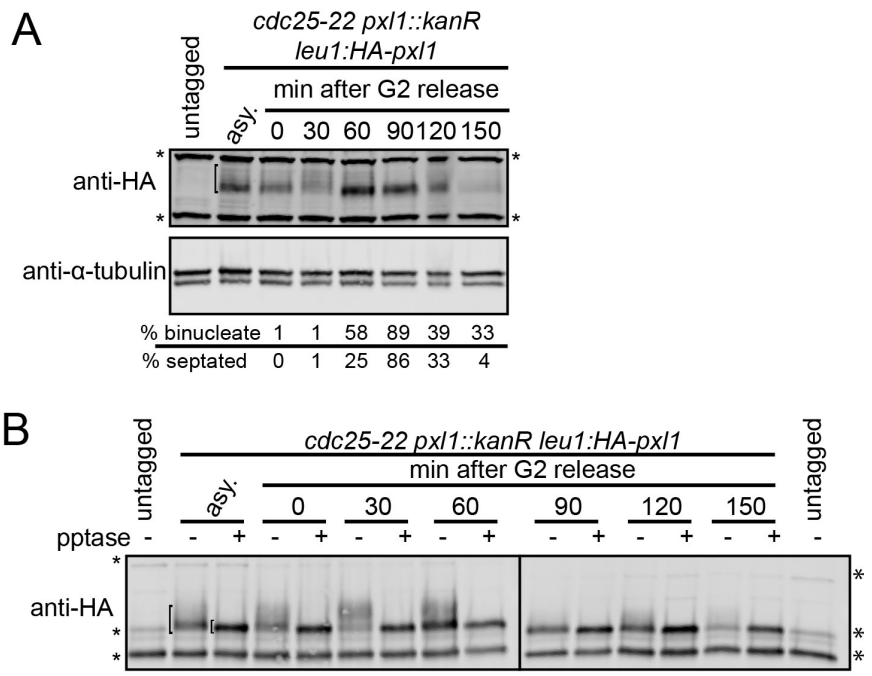

Figure 17. Pxl1 phosphorylation changes throughout the cell cycle.
cdc25-22 pxl1::kan^{R} *leu1:HA-pxl1* cells were grown to mid log phase, shifted to 36°C for 4 h, and then released to permissive temperature (25°C). Samples were collected at the indicated times. Denatured protein extracts (A) and immunoprecipitation(IP)-phosphatase (pptase) samples (B) were separated by SDS-PAGE and analyzed by immunoblot analysis with HA and tubulin antibodies. Completion of mitosis was determined by monitoring binucleate formation and septation index. Asterisks indicate background bands and the bracket in asynchronous (asy.) samples indicate HA-Pxl1.

Table 3. Identification of [S/T]P phosphorylation sites in the Pxl1 N-terminus.

1- (Carpy et al., 2014), 2- (Kettenbach et al., 2015), 3- (Koch et al., 2011), 4- (Swaffer et al., 2016), 5- (Swaffer et al., 2018)

[S/T]P Site	Spectral count from MS analysis of GFP-Pxl1 purification	Identified in these other studies
S3	Not detected	2, 4, 5
S24	6	2, 5
S31	15	2, 5
T55	12	2, 5
T64	33	2, 5
S67	142	1, 2, 5
S97	7	1, 2, 3, 5
S136	8	n.a.
T214	Not detected	n.a.

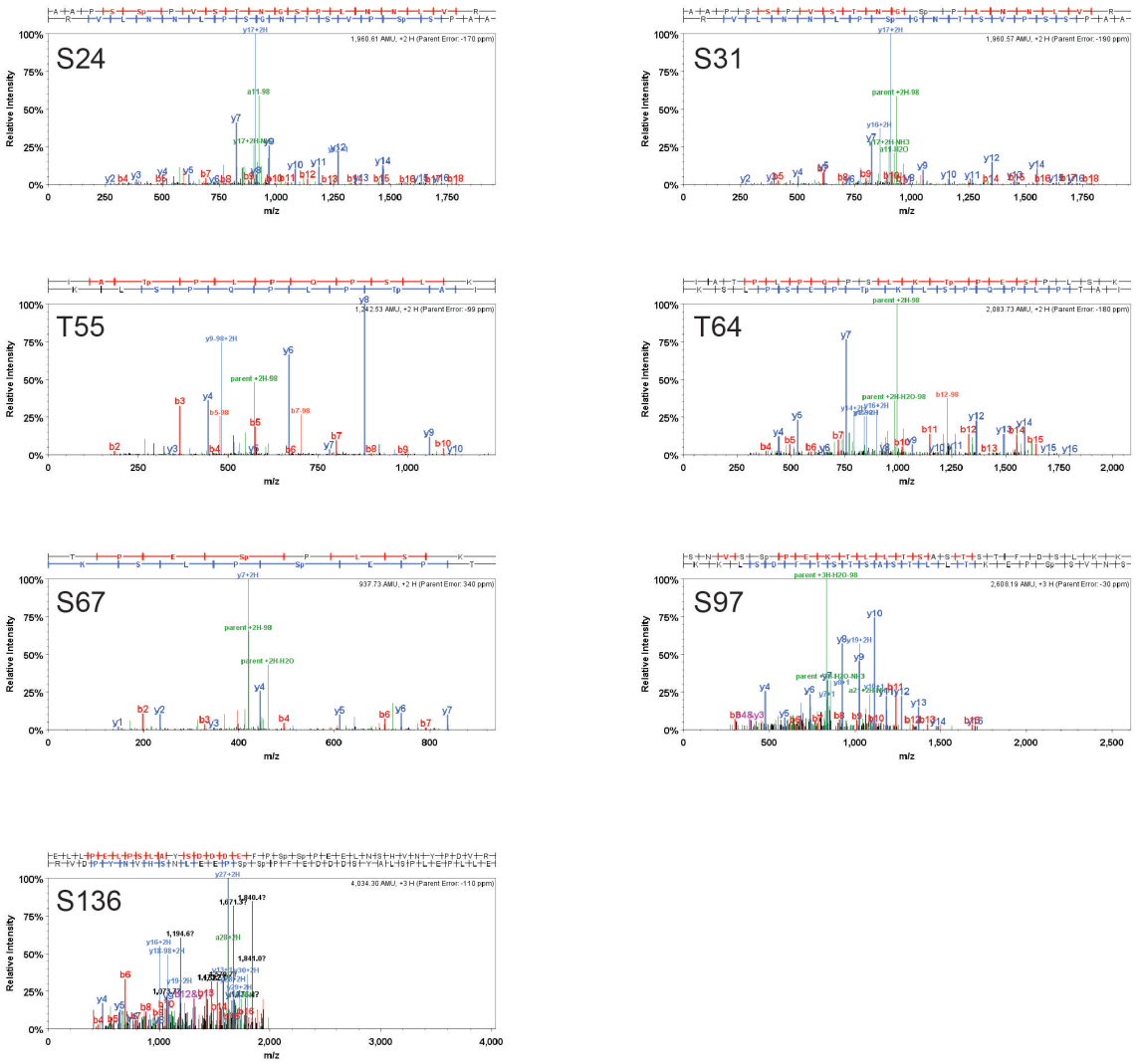

Figure 18. Mass spectra of a representative phosphopeptide from each of the identified CDK phosphorylation sites on Pxl.

These mass spectra were extracted from Scaffold PTM with matched b and y ions highlighted in red and blue, respectively. Ions resulting from neutral loss are highlighted in green. For most of the phosphorylation sites, both MS/MS (MS2) and MS/MS/MS (MS3, i.e. further MS/MS fragmentation of the ion which results from the neutral loss of phosphate of the parent ion during MS2 scan) spectra were acquired. In these cases, only MS2 spectra are shown here. Sp/Tp: phosphorylated serine/threonine.

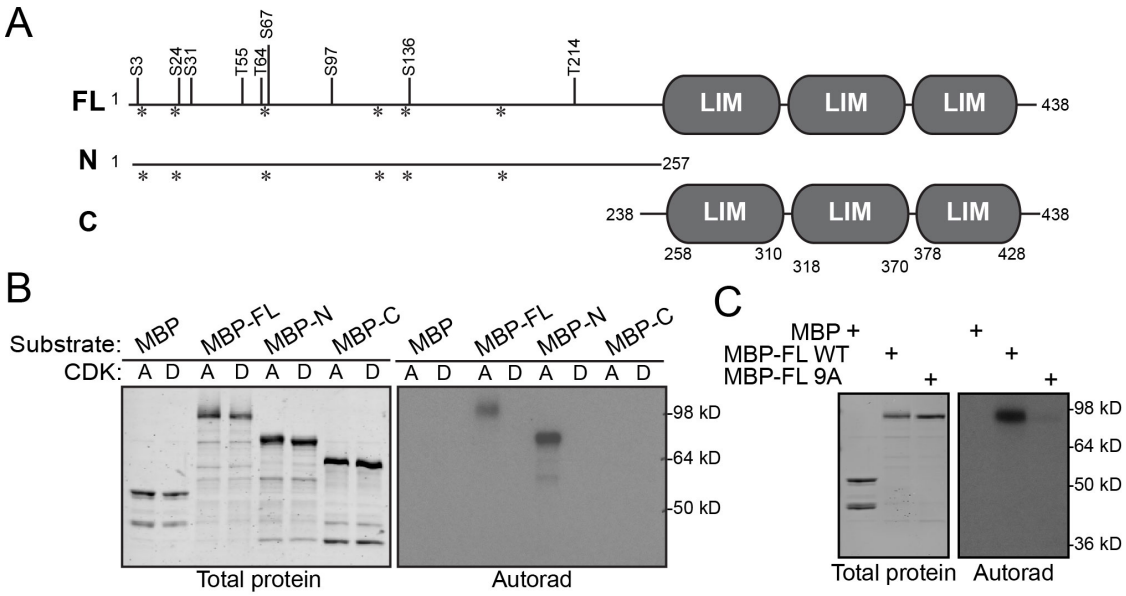

Figure 19. Pxl1 is phosphorylated by CDK.
A) To-scale schematics of Pxl1 full-length (FL) and N- and C-terminal fragments used in B and C. Numbers indicate amino acid positions. Asterisks indicate PXXP motifs. LIM domains are shown as gray ovals. Black lines indicate the 9 sites in the N-terminus that match the [S/T]P consensus sequence and are mutated in Pxl1(9A) or Pxl1(9D). B) *In vitro* kinase assays using active (A) or dead (D) CDK, the indicated substrate, and radiolabeled ATP were separated by SDS-PAGE, transferred to PVDF, stained with Revert Total Protein Stain, and then exposed to film (Autorad). C) *In vitro* kinase assays using active CDK, the indicated substrate, and radiolabeled ATP were separated by SDS-PAGE, transferred to PVDF, stained with Coomassie to visualize total protein, and then exposed to film (Autorad).

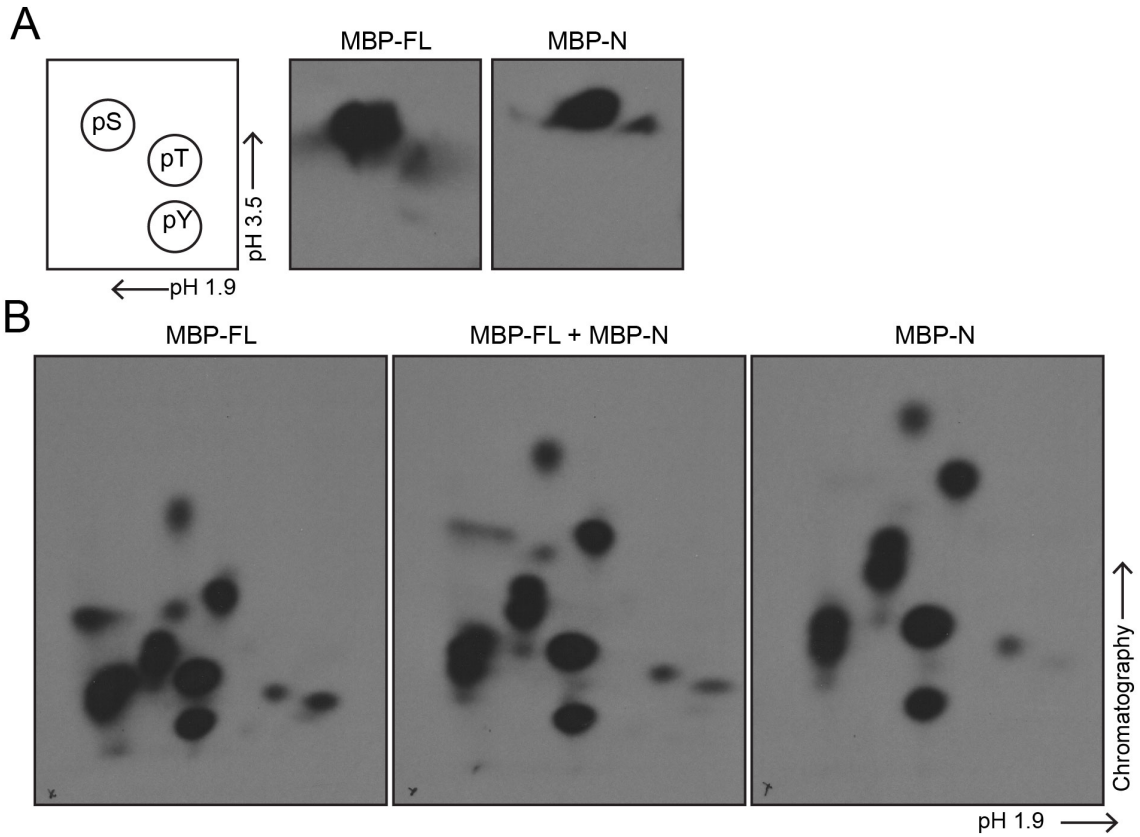

Figure 20. The Pxl1 N-terminus is phosphorylated by CDK on Thr and Ser.
A) Phospho-amino acid analysis of Pxl1 phosphorylated by CDK. B) Tryptic peptide mapping of Pxl1 full-length (FL) and N-terminal (N) fragments phosphorylated by CDK. Reactions were run individually and mixed.

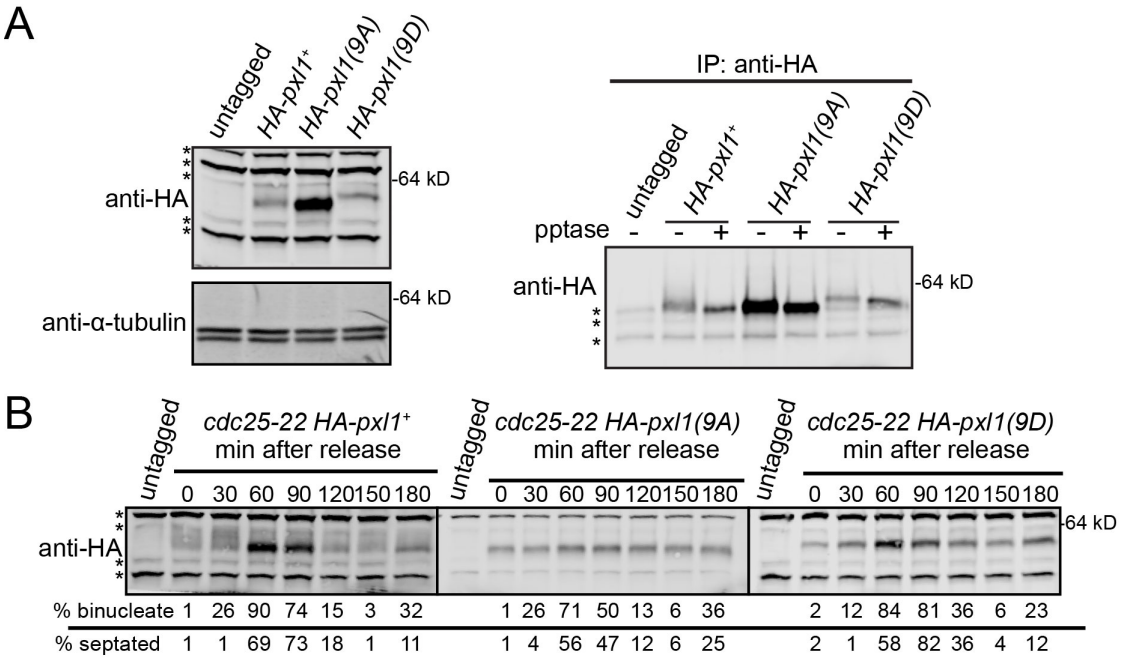

Figure 21. CDK phosphomutants abolish Pxl1 phosphorylation *in vivo*.
A) Lysates from the indicated strains (left) and subsequent IP-pptase (right) were separated by SDS-PAGE and immunoblotted for indicated proteins. Asterisks indicate background bands. B) Cells of the indicated genotype were grown to mid log phase, shifted to 36°C for 4 h, and then released to permissive temperature (25°C). Samples were collected at the indicated times. Denatured protein extracts were separated by SDS-PAGE and analyzed by immunoblot analysis with HA antibody. Completion of mitosis was determined by monitoring binucleate formation and septation index. Asterisks indicate background bands.

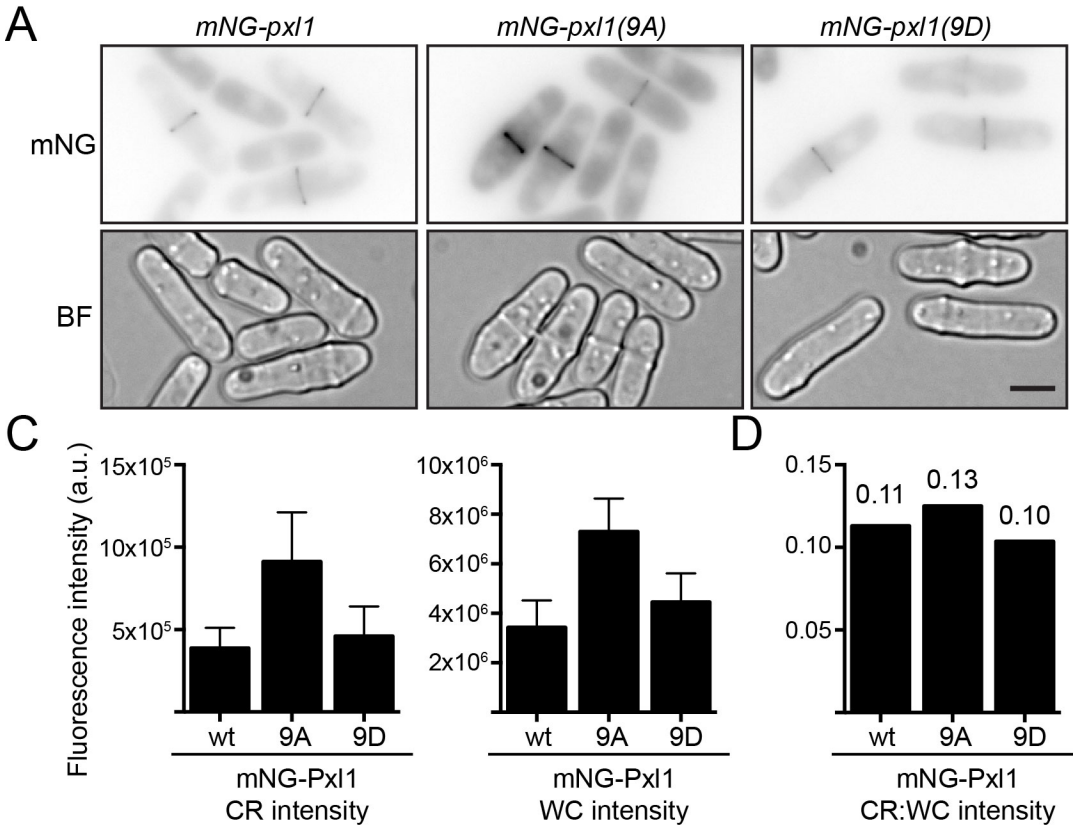

Figure 22. Phosphoablated Pxl1 mutant has increased protein abundance.
A) Sum projections (mNG) or brightfield (BF) representative images of the indicated strains. Scale bars are 5 μm. B) Average CR and whole cell (WC) intensity of the indicated proteins. Error bars are SD. C) Ratio of average CR and average WC intensity from the data collected in C.

Phosphorylation regulates the timing of Pxl1 localization to the CR

CDK phosphorylation of *S. pombe* formin Cdc12 (Willet et al., 2018), *S. cerevisiae* IQGAP Iqg1 (Naylor and Morgan, 2014), and *S. cerevisiae* C2 domain protein Inn1 (Palani et al., 2012; Kuilman et al., 2015) temporally regulates their recruitment to the CR. Therefore, we imaged mNG-Pxl1, mNG-Pxl1(9A), and mNG-Pxl1(9D) in cells that also produced Sid4-mNG, a spindle pole body (SPB) marker for monitoring progression through mitosis. We performed time-lapse imaging of these cells to determine when mNG-Pxl1 arrived at the division site relative to SPB separation (Figure 23A-B). mNG-Pxl1(9A) arrived earlier (14.7 +/- 5.2 min; 47 cells) than either mNG-Pxl1 (19.0 +/- 3.4 min; 31 cells) or mNG-Pxl1(9D) (19.9 +/- 3.1 min; 27 cells). Thus abolishing phosphorylation on Pxl1 results in its early localization to the CR.

Loss of Pxl1 phosphorylation alters cytokinesis timings

We next asked whether early recruitment to the CR and increased amount of Pxl1 at the CR affected cytokinesis dynamics. To do this we performed time-lapse imaging of cells producing Sid4-mNG and the CR marker Rlc1-mNG in *pxl1*$^{+}$ (wt)*, pxl1(9A),* and *pxl1(9D)* (Figure 24A). Then, we quantified the duration of CR formation (i.e., the period from SPB separation to CR formation), maturation (i.e., the period between formation and constriction), and constriction (Figure 24B, left). While there were no significant differences in the durations of formation and maturation, constriction took longer in *pxl1(9A)* compared to *pxl1*$^{+}$ and *pxl1(9D)* (Figure 24B, right). This suggests that phosphorylation delays Pxl1 until the proper time, and that early recruitment has negative downstream consequences on the efficiency of cytokinesis.

pxl1 phosphomutants have synthetic growth defects with rgf3 mutants

Consistent with Pxl1 being a negative regulator of Rho signaling at the division site (i.e. opposing Rho activation by Rgf3) (Pinar et al., 2008), *pxl1*Δ suppresses the temperature-sensitivity of the *rgf3* mutant *ehs2*-1 (Morrell-Falvey et al., 2005). Given that phosphorylation appears to inhibit Pxl1 (i.e. loss of phosphorylation results in earlier and more Pxl1 at the CR), we hypothesized that *pxl1(9D)*—for which we had not yet identified a phenotype—might suppress an *rgf3* mutant similar to *pxl1*Δ while *pxl1(9A)* would show a negative interaction. As predicted, *pxl1(9A)* was synthetically sick with *lad1-1* but *pxl1(9D)* did not suppress this *rgf3* mutant (Figure 25). While this result is consistent with phosphorylation inhibiting Pxl1, it also indicates that *pxl1(9D)* is likely not a true phosphomimetic.

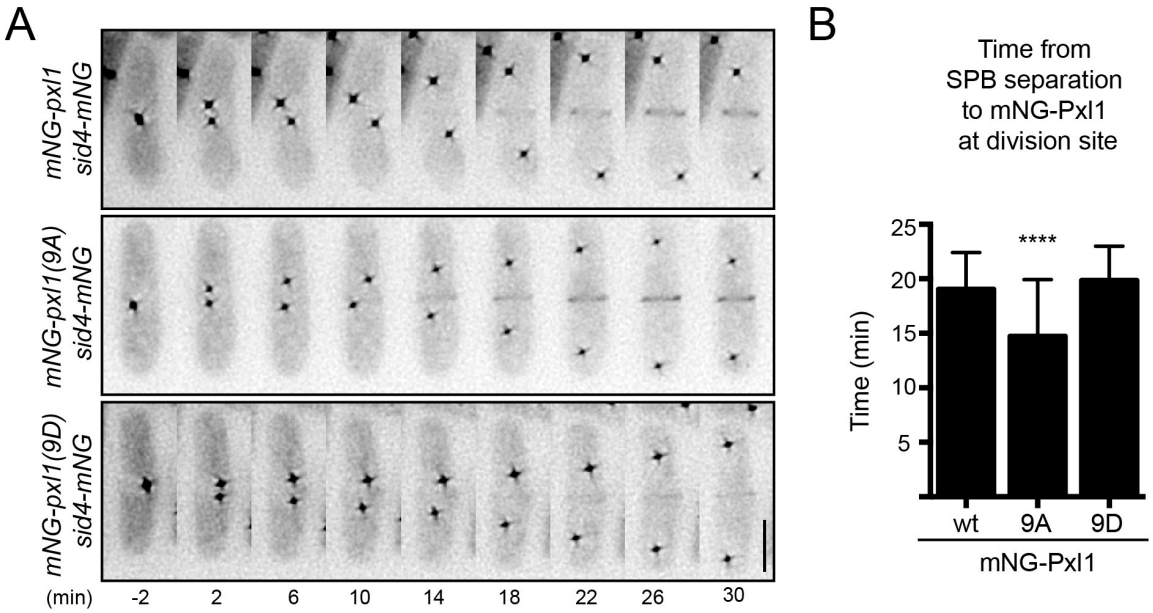

Figure 23. Loss of CDK phosphorylation leads to early recruitment of Pxl1 to the CR.

A) Representative montages of single cells taken from time-lapse fluorescence imaging of the indicated strains. Images were acquired every 2 min and every other time point is shown. Time 0 is set as the first frame with 2 SPBs (not shown). B) Graph of average time between SPB separation to division site localization of the indicated Pxl1 proteins. **** $p < 0.0001$, One-way ANOVA with multiple comparisons to wt. Error bars are SD. Scale bars are 5 μm.

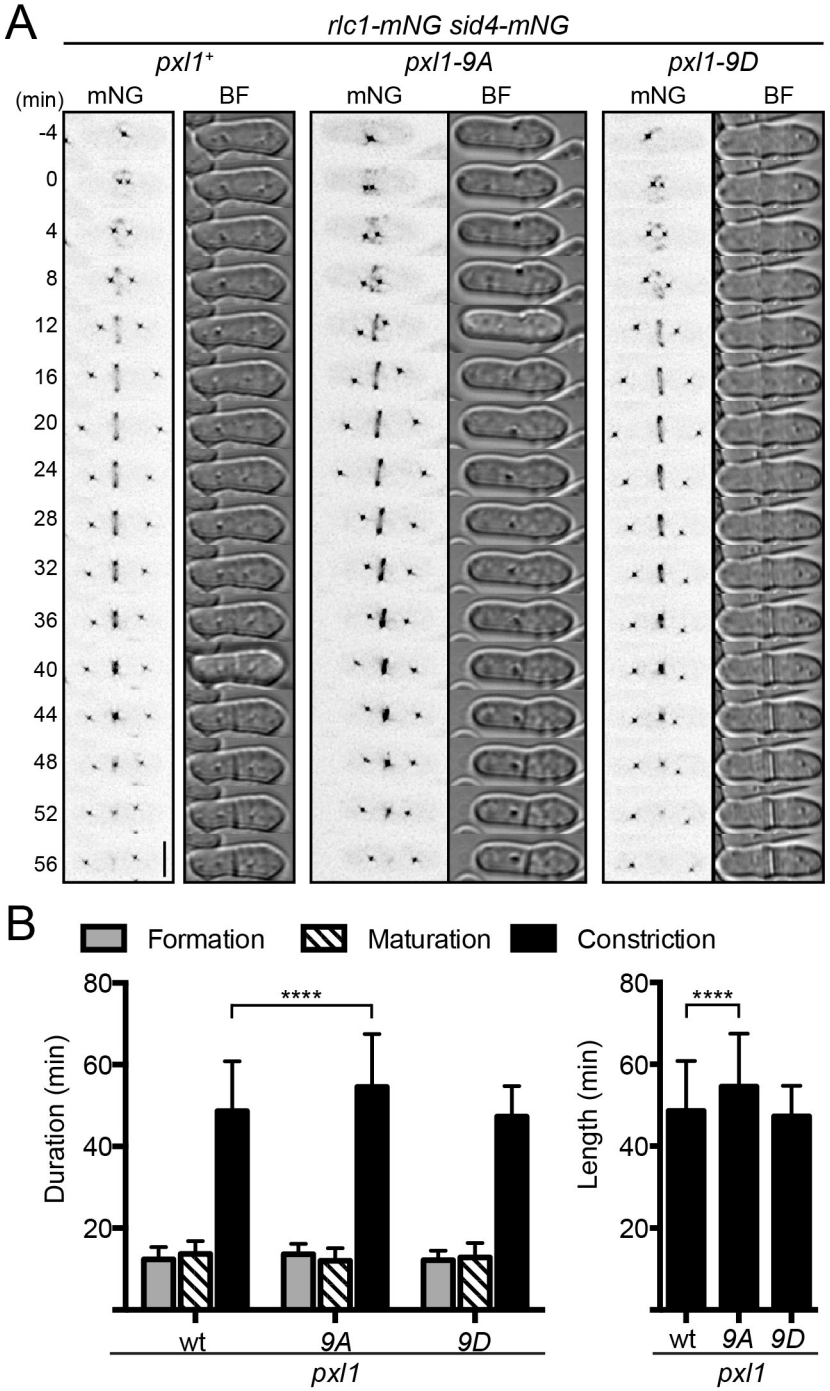

Figure 24. Cells with abolished Pxl1 phosphorylation have increased duration of constriction.

A) Representative fluorescence (mNG) or BF montages of single cells taken from time-lapse imaging of the indicated strains. Images were acquired every 2 min and every other time point is shown. Time 0 is set as the first frame with 2 SPBs. Scale bar is 5 μm. B) Graph of average duration of the indicated cell cycle stages (left), with the duration of constriction shown alone on the right graph. **** $p < 0.0001$, Two-way ANOVA with Tukey correction and multiple comparisons to wt. Error bars are SD.

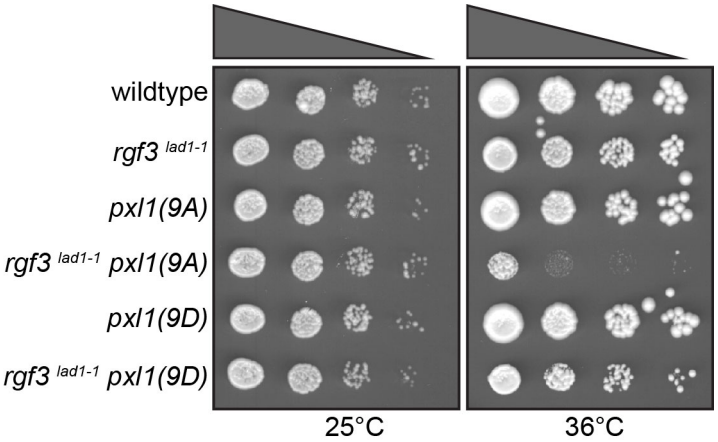

Figure 25. *pxl1* and *rgf3* have synthetic growth defects.
Serial growth assay of the indicated strains grown at the indicated temperatures for four days.

Cdc14 phosphatase Clp1 and PP1 phosphatase Dis2, but not calcineurin, regulate Pxl1 dephosphorylation

While Pxl1 is rapidly phosphorylated as cells enter mitosis, it is also rapidly dephosphorylated during anaphase (Figure 17). We wanted to know which phosphatase(s) regulates Pxl1 dephosphorylation. The Cdc14 phosphatase Clp1 opposes CDK activity by removing phosphorylation from [S/T]P sites (Clifford et al., 2008b; Chen et al., 2013). Consistent with Clp1 regulating Pxl1 dephosphorylation, the slower migrating bands corresponding to phosphorylated Pxl1 were increased in *clp1*Δ compared to *clp1*$^{+}$ (Figure 26A).

Pxl1 is important for recruitment of the phosphatase calcineurin to the mature CR (Martin-Garcia et al., 2018). To test if Pxl1 is itself a substrate of calcineurin, we released cells from a G2 arrest for 30 minutes and then treated with calcineurin inhibitor FK506 to test if this prevented Pxl1 dephosphorylation, but it did not (Figure 26B). This indicates that Pxl1 is not a substrate of calcineurin, despite its requirement for recruiting calcineurin to the division site.

Lastly, searching the ELM database (Gouw et al., 2018) for linear motifs in Pxl1 that could provide insight into its regulation and/or function identified a protein phosphatase 1 catalytic subunit (PP1c) interacting motif (Egloff et al., 1997; Aggen et al., 2000) at amino acids 78-84. Furthermore, the catalytic subunit of *S. pombe* PP1 Dis2 was pulled-down in a GFP-TRAP experiment of lysates from cells producing GFP-Pxl1 and blocked in prometaphase by *nda3*-KM311 arrest (Table 4). Pxl1 phosphorylation in lysates from *dis2*Δ was increased, similar to what was observed in *clp1*Δ cells (Figure 26C), consistent with PP1 regulating Pxl1 dephosphorylation.

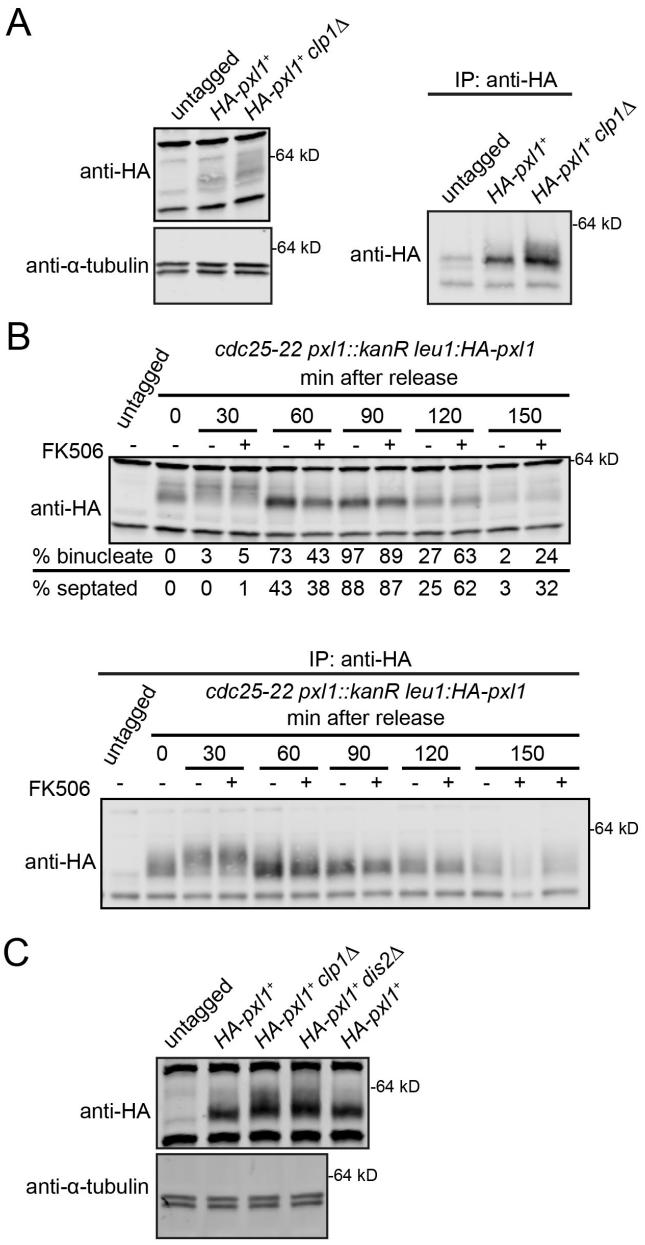

Figure 26. Pxl1 is regulated by the Cdc14 and PP1 phosphatases, but not by calcineurin.

A) Denatured lysates (left) and IP (right) samples separated by SDS-PAGE and immunoblotted for indicated proteins. B) Cells of the indicated genotype were grown to mid log phase, shifted to 36°C for 4 h, and then released to permissive temperature (25°C). The calcineurin inhibitor FK506 or DMSO control was added to cell cultures at 30 minutes after release from G2 arrest. Samples were collected at the indicated times. Denatured protein extracts (top) and IP (bottom) were separated by SDS-PAGE and analyzed by immunoblot analysis with HA antibody. Completion of mitosis was determined by monitoring binucleate formation and septation index. C) Denatured lysates separated by SDS-PAGE and immunoblotted for indicated proteins.

Table 4. Selected proteins that were pulled down by GFP-Pxl1 from prometaphase-arrested cells.

Protein	Exclusive spectrum count	% Sequence coverage	Molecular weight (kD)
Pxl1	887	98.6	49.0
Cdc15	310	68.2	102.1
Dis2	219	89.6	37.6

Discussion

Here we confirmed the results of several large scale phosphoproteomics studies that CDK phosphorylates Pxl1. Analysis of mutants that ablate CDK phosphorylation indicate that Pxl1 localization to the CR is inhibited by phosphorylation. Further supporting a gain-of-function phenotype, *pxl1* phosphoablating mutants had increased constriction duration and they had negative genetic interactions with a mutant of *rgf3*, which encodes the essential RhoGEF that positively regulates Rho1 GTPase activity (Arellano et al., 1996; Tajadura et al., 2004; Morrell-Falvey et al., 2005; Ren et al., 2015). Although *pxl1* phosphoablating mutants had essentially wildtype morphology, this is consistent with the idea that CDK has many substrates and that multiple redundant mechanisms exist to regulate the timing of cytokinesis.

It will be interesting to determine the mechanism by which phosphorylation inhibits Pxl1 recruitment to the CR. The N-terminus of Pxl1 is the site of CDK phosphorylation and it also contains CR targeting information (Pinar et al., 2008), so one conspicuous hypothesis is that phosphorylation prevents binding to a Pxl1 protein partner. Candidates include the SH3 domain of the F-BAR protein Cdc15 (Roberts-Galbraith et al., 2009), the F-BAR protein Rga7 (Martin-Garcia et al., 2014), myosin-II light chain Rlc1 (Pinar et al., 2008), or plasma membrane-CR linker Sbg1 (Sethi et al., 2016). Phosphorylation could directly inhibit the interaction, promote a conformational change that obscures or changes the interaction site on Pxl1, or generate a novel interaction site for phospho-peptide modules such as 14-3-3 proteins that regulates Pxl1 function.

We also identified two phosphatases that regulate Pxl1 dephosphorylation: the Cdc14 phosphatase Clp1 and the PP1 phosphatase Dis2. Both Cdc14 and PP1 phosphatases have been implicated in reversing CDK phosphorylation and promoting mitotic exit (Stegmeier and Amon, 2004; Clifford et al., 2008a; Clifford et al., 2008b; De Wulf et al., 2009; Wu et al., 2009; Mocciaro and Schiebel, 2010; Bloom et al., 2011; Bouchoux and Uhlmann, 2011; Wurzenberger and Gerlich, 2011; Palani et al., 2012; Grallert et al., 2015; Kuilman et al., 2015; Orii et al., 2016). Additional phosphatases are implicated in mitotic exit in *S. pombe* and metazoans including PP2A (Cundell et al., 2013; Grallert et al., 2015; Wlodarchak and Xing, 2016) and calcineurin/PP2B (Yoshida et al., 1994; Mochida and Hunt, 2007; Nishiyama et al., 2007; Martin-Garcia et al., 2018). We tested if calcineurin could also regulate Pxl1 phosphorylation because Pxl1 has been shown to mediate recruitment of the calcineurin catalytic subunit Ppb1 to the CR (Martin-Garcia et al., 2018). Interestingly, calcineurin does not seem to be a major

regulator of Pxl1 phosphorylation. Combining this with our previous finding that Pxl1 is not sufficient to recruit Ppb1 (Chapter 2, Figure 16) provides compelling evidence that the Pxl1-Ppb1 interaction is more complex. It's not clear whether the Pxl1-Ppb1 interaction is indirect or part of a multi-protein complex, or if Ppb1 recruitment is downstream of Pxl1-influenced signaling. Determining what other CR components are absent or mis-regulated in *ppb1*Δ will be an important next step to teasing apart this interaction.

Still, Pxl1 is a CDK substrate that is regulated by multiple phosphatases. Pxl1 phosphostatus changes when either phosphatase is deleted indicating they act on Pxl1 non-redundantly. By detailed analysis of Pxl1 phosphorylation, we can gain insight into whether Clp1 and Dis2 act simultaneously or sequentially, what residues are modified by each phosphatase and if they overlap, and if there are any differences between complete and partial de-phosphorylation of Pxl1. Inconveniently for these studies, we suspect that the *pxl1(9D)* is not a true phosphomimetic since *pxl1(9D)* had a mild growth defect with *rgf3* mutants, while previously *pxl1*Δ was shown to rescue the growth defect of *rgf3* (Pinar et al., 2008). However, perhaps by preventing phosphatase interaction with Pxl1 (i.e. by mutating docking motifs), we can force Pxl1 hyper-phosphorylation in an otherwise wildtype setting and test how this alters Pxl1 behavior and cytokinesis. Through studies of Pxl1, we will gain insight into how CDK-counteracting phosphatases collaborate to regulate mitotic exit and cytokinesis in eukaryotic cells.

CHAPTER 4

PHOSPHORYLATION OF THE F-BAR PROTEIN CDC15 BY THE DYRK-FAMILY KINASE POM1 PREVENTS DIVISION AT CELL TIPS BY INHIBITING CDC15 SCAFFOLD FUNCTION

Abstract

In many organisms, positive and negative signals cooperate to position the contractile ring (CR) for cytokinesis. In the rod-shaped fission yeast *Schizosaccharomyces pombe*, symmetric division is achieved at mid-cell through anillin/Mid1-dependent positive cues released from the central nucleus and negative signals from the DYRK-family polarity kinase Pom1 at cell tips. The F-BAR protein Cdc15, a major scaffold of the CR, has been implicated as a Pom1 substrate important for preventing CR placement at cell tips. Here we test this hypothesis by mapping and mutating the full cohort of twenty-two Pom1 phosphorylation sites on Cdc15 and characterizing the behavior of the resultant Cdc15 phosphomutants. Although a Cdc15 mutant that ablates phosphorylation on Pom1 sites results in faster cytokinesis and early division site recruitment of Cdc15 and another CR component myosin light chain Rlc1, it does not cause tip division—even when Mid1/anillin-dependent signaling is disrupted. On the other hand, a Cdc15 phosphomimetic partially suppresses division at cell tips in cells with disruption of both Mid1 and Pom1 signaling. Additionally, deletion of Cdc15 binding partners Fic1, Pxl1, and Cyk3 partially suppresses division at cell tips. Furthermore, Pom1 phosphorylation of Cdc15 directly inhibits binding to Pxl1 *in vitro,* which is mediated by a novel collaboration between Cdc15's disordered region and SH3 domain. Our data are consistent with a model in which the dephosphorylation of Cdc15 is necessary but not sufficient for CR formation in fission yeast, and indicate that one mechanism by which Pom1 inhibits cytokinesis at cell tips is via direct Cdc15 phosphorylation.

Introduction

The position of the cell division site is crucial for both cellular function and integrity. Studies in prokaryotic and eukaryotic systems revealed two major positioning systems: local positive signals and distal inhibitory ones (Oliferenko et al., 2009). In rod-shaped bacteria, the division plane is positioned mainly via inhibitory signals arising from the cell poles and the nucleoids, leaving only the cell middle as permissive for ring assembly (Almonacid and Paoletti, 2010). In animal cells, the mitotic spindle positions the division site by conferring both positive signals to the medial cortex and distal relaxation signals (Eggert et al., 2006b; Glotzer, 2017).

Stimulatory and inhibitory mechanisms for division site positioning have also been described in the fission yeast Schizosaccharomyces pombe (Rincon and Paoletti, 2012). Like animal cells, *S. pombe* cells use an actomyosin contractile ring (CR) for division, which is assembled at mid-cell for symmetric division. CR placement in *S. pombe* is positively regulated by the position of the nucleus (Daga and Chang, 2005; Tolic-Norrelykke et al., 2005), which is centered in the cell by microtubule pushing forces (Tran et al., 2001). The positive CR placement cue is provided by the anillin-like Mid1 that shuttles in and out of the nucleus during interphase and localizes to overlying

cortical nodes, which are early precursors of the CR (Chang et al., 1996; Sohrmann et al., 1996; Paoletti and Chang, 2000). Cortical nodes are restricted to mid-cell by negative signals at the cell tips that depend on the DYRK-family Pom1 kinase, which is transported to cell tips on microtubules by the Tea1/Tea4 complex (Padte et al., 2006; Hachet and Simanis, 2008) (Martin et al., 2005; Celton-Morizur et al., 2006).

At mitotic entry, equatorial Mid1-containing nodes mature into cytokinetic nodes, recruiting CR proteins such as myosin II Myo2, the F-BAR protein Cdc15 and the formin Cdc12 (Laporte et al., 2011; Akamatsu et al., 2014). Node-anchored Cdc12 nucleates F-actin that is bound by myosin-II, which pulls on F-actin and thus can pull neighboring nodes closer together until they coalesce into a ring (Vavylonis et al., 2008; Zimmermann et al., 2017). In the absence of *mid1*, although cells remain competent for division, the CR forms late and appears to condense either from strands of cytokinetic proteins scattered over the cortex or from a single location rather than from nodes (Huang et al., 2008; Roberts-Galbraith and Gould, 2008; Saha and Pollard, 2012). In these cells, CR orientation and placement is aberrant, leading to oblique, frequently off-center CRs relative to the long axis of the cell (Chang et al., 1996; Sohrmann et al., 1996). However, inhibitory signals arising from the cell tips remain in place to prevent the assembly of the cytokinesis apparatus at the cell tips, such that division is restricted to the medial portion of the cell(Huang et al., 2007)]. The *mid1*-independent inhibitory cell end signals require the Tea1/Tea4 complex and the Pom1 kinase. Indeed, deletion of any of these cell end factors is synthetic lethal with *mid1*Δ, and double mutants form septa at cell ends(Huang et al., 2007).

Because a c*dc15-GFP* allele blocked tip septation in *tea1*Δ *mid1-18* double mutants (Huang et al., 2007), it was hypothesized that the F-BAR protein Cdc15 could be a target of this so-called "tip occlusion pathway." Cdc15 is an abundant (Wu and Pollard, 2005) and essential component of the CR (Fankhauser et al., 1995). It has an N-terminal F-BAR domain that oligomerizes and binds membranes and the formin Cdc12 (Carnahan and Gould, 2003; McDonald et al., 2015; Willet et al., 2015a), and a C-terminal SH3 domain that binds multiple CR components (e.g. paxillin Pxl1, the C2 domain protein Fic1) and stabilizes the CR during anaphase (Roberts-Galbraith et al., 2009; Arasada and Pollard, 2014; Ren et al., 2015). Cdc15 activity is under strong cell cycle-dependent phospho-regulation: it is phosphorylated during G2 phase on many sites (>35) and hypo-phosphorylated during cytokinesis to allow its oligomerization, membrane binding and CR scaffolding activities (Fankhauser et al., 1995; Roberts-Galbraith et al., 2010). Phosphoproteomic screens implicated Cdc15 as a target of Pom1 and the MARK/PAR-1 family kinase Kin1 to influence CR stability but whether Pom1-mediated Cdc15 phosphorylation is important to prevent CRs forming at cell tips has not been determined(Kettenbach et al., 2015; Lee et al., 2018). In this study, we show that Pom1 directly phosphorylates Cdc15 on up to twenty-two sites and antagonizes Cdc15 function. Furthermore, mimicking Pom1 phosphorylation on Cdc15 partially rescues the formation of tip septa in cells that lack both positive Mid1 cues and Pom1 signaling. Thus, Pom1 kinase activity provides negative signal at cell poles and promotes medial septation in part through local inhibition of Cdc15.

Results

Pom1 kinase activity is required to prevent division septum assembly at cell tips

To investigate whether the signals for tip occlusion require Pom1 kinase activity, we used the conditional allele *pom1*(T778G) (*pom1*^{as}) to specifically inhibit kinase activity with 3MB-PP1(Padte et al., 2006) (Bhatia et al., 2014), and we introduced this allele into *mid1Δ* cells (Chang et al., 1996; Sohrmann et al., 1996), which have misplaced and/or tilted septa and a very small percentage of tip septa (Huang et al., 2007). After 2 hours of treatment with 3MB-PP1, we observed tip septation in almost all *pom1*^{as1} *mid1Δ* cells (Figure 27A-B). Tip septa were of three types (Figure 27C): 1) one or two septa at the very cell ends; 2) septa anchored at both cell ends and spanning the long cell axis; 3) septa anchored at one cell end. The percentage of cells with tip septa in the *pom1*^{as1} *mid1Δ* double mutant increased with time (Figure 27D), with >95% of cells showing tip septa after a 2 hour incubation with 1μM 3MB-PP1. These phenotypes were not observed in either single mutant or in the double mutant treated with vehicle (Figure 27A-B). Collectively, these experiments suggest that among Tea1, Tea4, and Pom1 implicated in tip occlusion (Huang et al., 2007), the specific signals that prevent formation of division septa at cell tips arise from Pom1 kinase activity.

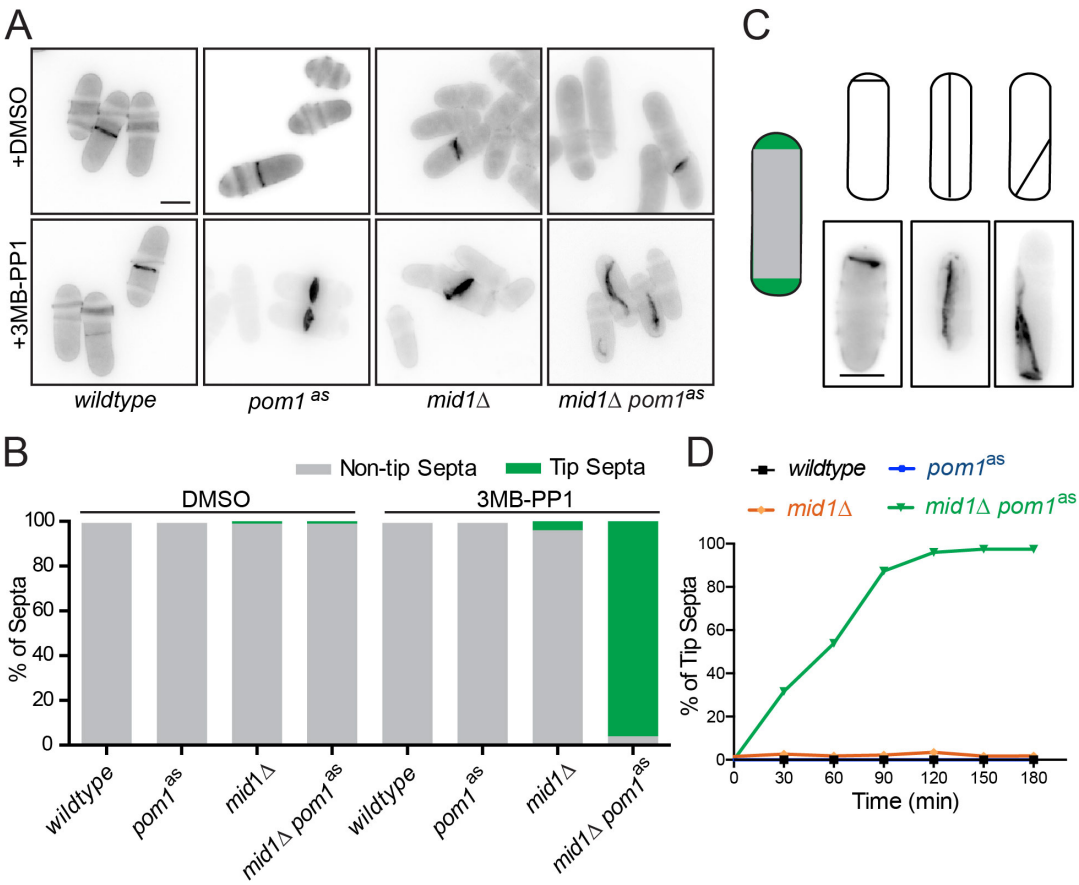

Figure 27. Pom1 kinase activity is required to inhibit tip septa.
A) Representative images of cells of the indicated genotype that were grown to log-phase at 32°C and then treated for 2 hours with either DMSO or 3MB-PP1 to inhibit analog-sensitive Pom1. Cells were fixed in 70% ethanol at 4°C and then stained with Calcofluor White. Scale bar is 5 µm. B) Quantification of tip septa phenotype from images acquired as in A. Graph is average of three replicates. C) Schematic and representative images of types of tip septa. Scale bar is 5 µm. D) Time-course of tip septa appearance when cells of the indicated genotype were treated with 3MB-PP1 and grown at 32°C. Samples were prepared as described in A.

Pom1 can phosphorylate Cdc15 on 22 sites

C-terminal tagging of Cdc15 with GFP (*cdc15-gc1*) prevented tip septa formation in *mid1-18 tea1Δ* cells suggesting that this allele is hypomorphic and that inhibition of Cdc15 function is required for tip occlusion (Huang et al., 2007). We found that the *cdc15-gc1* allele also prevented tip septation in the $pom1^{as1}$ *mid1Δ* double mutant (Figure 28A).

Given this result and knowing that Cdc15 is phosphorylated on many sites during interphase (Fankhauser et al., 1995; Roberts-Galbraith et al., 2010) and that multiple of these phosphorylation events are reduced upon Pom1 inhibition (Kettenbach et al., 2015), we and others (Huang et al., 2007; Lee et al., 2018) hypothesized that Pom1 phosphorylates Cdc15. Consistent with Cdc15 being a Pom1 substrate, the slow migrating, phosphorylated forms of Cdc15 were partially reduced in *pom1Δ* cells (Figure 28B), and recombinant Pom1 efficiently phosphorylated N-terminal (Cdc15N; aa1-460) and C-terminal (Cdc15C; aa441-end) fragments of Cdc15 *in vitro* (Figure 28C; (Lee et al., 2018)). Phosphoamino acid analysis revealed that Pom1 phosphorylates Cdc15C predominantly on serines and phosphorylates Cdc15N on both serine and threonine residues (Figure 29A). Thus, Cdc15 is phosphorylated in a *pom1*-dependent manner *in vivo* (Figure 28B; Kettenbach 2015) and directly by Pom1 *in vitro* (Figure 28C; (Lee et al., 2018)).

To identify Cdc15 sites phosphorylated by Pom1, we performed mass spectrometry (MS) analysis of Cdc15C phosphorylated *in vitro* by recombinant Pom1. Of the 17 sites in Cdc15C that match the consensus sequence for DYRK kinases (Himpel et al., 2000), MS analysis identified 13 as phosphorylated *in vitro* (Figure 30). All of these sites were previously identified as phosphorylated *in vivo* (Wilson-Grady et al., 2008; Roberts-Galbraith et al., 2010) (Kettenbach et al., 2015; Swaffer et al., 2018). The remaining four sites matching the DYRK consensus sequence (S813, S821, S831, S836) were not identified in our MS analysis, possibly because these residues are on small tryptic peptides, although S813 and S836 were identified in other phosphoproteomic datasets (Kettenbach et al., 2015; Swaffer et al., 2018). A Cdc15C mutant with 16 of the 17 consensus sites mutated to alanine was still phosphorylated by Pom1 (data not shown). Thus, we mutated the remaining RXXS site (S710) and two additional residues that we identified by MS as highly phosphorylated *in vitro* (T492, S732); this essentially abolished Cdc15C phosphorylation by Pom1 *in vitro* (Figure 29B). We identified 3 sites (S43, S405, T419) in Cdc15N that both (1) match an RXXS/T consensus sequence and (2) had been shown to be phosphorylated *in vivo* (Roberts-Galbraith et al., 2010; Kettenbach et al., 2015).. Mutating these sites to alanine abolishes phosphorylation of Cdc15N by GST-Pom1 (Figure 29C). Taken together, 22 sites throughout Cdc15 can serve as Pom1 phosphorylation sites (Figure 28D).

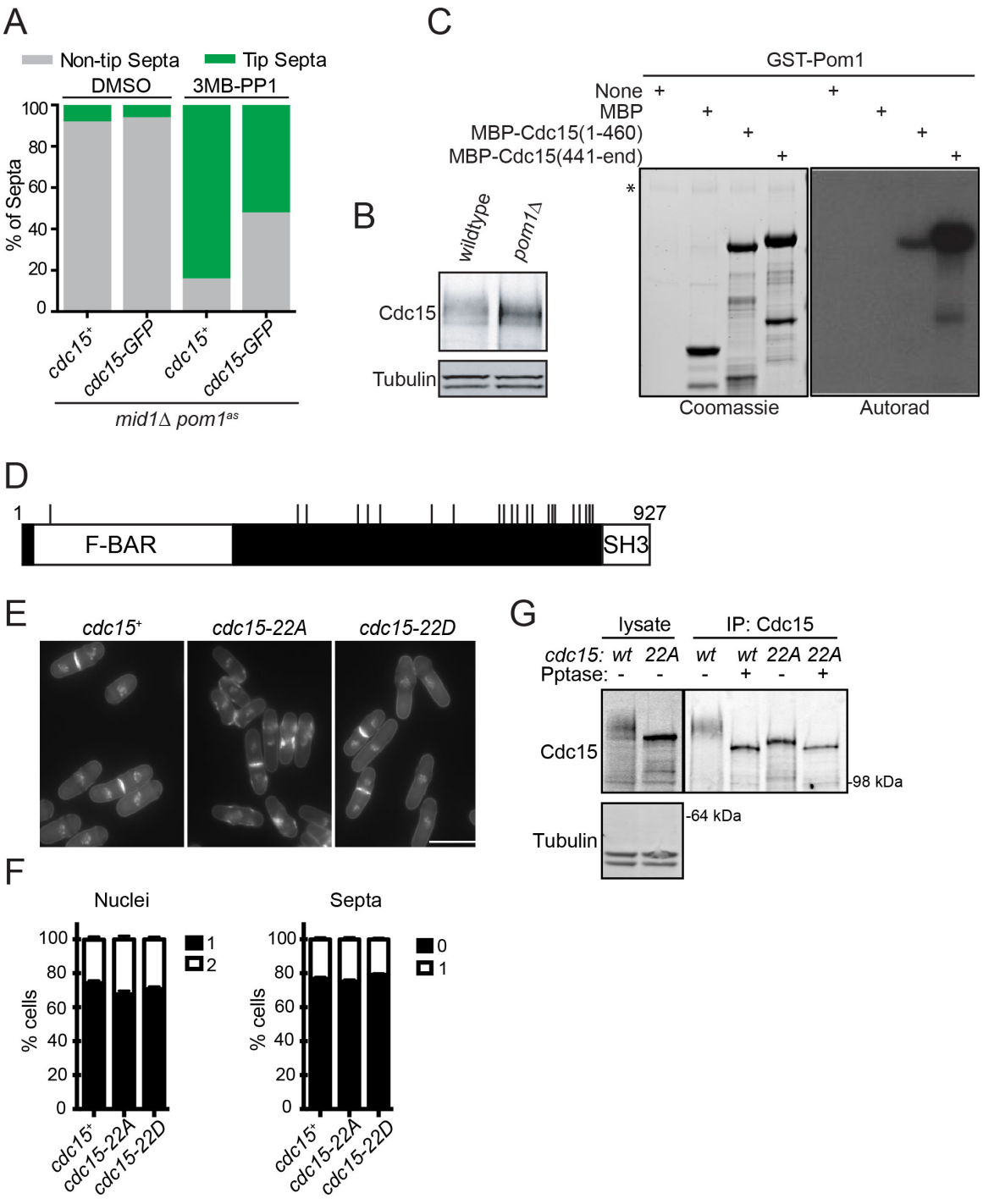

Figure 28. Pom1 can phosphorylate Cdc15 on 22 sites.

A) Quantification of tip septa phenotype. Cells of the indicated genotype were grown to log-phase in YES at 32°C and then treated with DMSO or 3MB-PP1 for 2 hours before fixation with 70% ethanol at 4°C. Fixed cells were stained with Calcofluor White to visualize septa. Graph is average from three replicates. B) Denatured lysates from the indicated strains were separated by SDS-PAGE and then immunoblotted for the indicated proteins. C) *In vitro* kinase reactions using radiolabeled ATP,

recombinant GST-Pom1 and indicated substrate proteins were separated by SDS-PAGE. Coomassie-stained gels of inputs and autoradiography detection of ^{32}P incorporation are shown. Asterisk indicates GST-Pom1. D) Scale schematic of Cdc15 structure with 22 sites phosphorylated by Pom1 indicated with black line. E) Representative images of DAPI and Methyl Blue stained cells of the indicated *cdc15* genotype. Scale bar is 5 μm. F) Quantification of nuclei and septation indices from images acquired as in E; n ≥ 300 for each strain. G) Denatured lysates were prepared from either *cdc15+* (*wt*) or *cdc15-22A* (*22A*) strains. Anti-Cdc15 was used to immunoprecipitate (IP) Cdc15, which was then treated with lambda protein phosphatase (Pptase) or water. Lysates and IPs were separated by SDS-PAGE and immunoblotted for the indicated proteins.

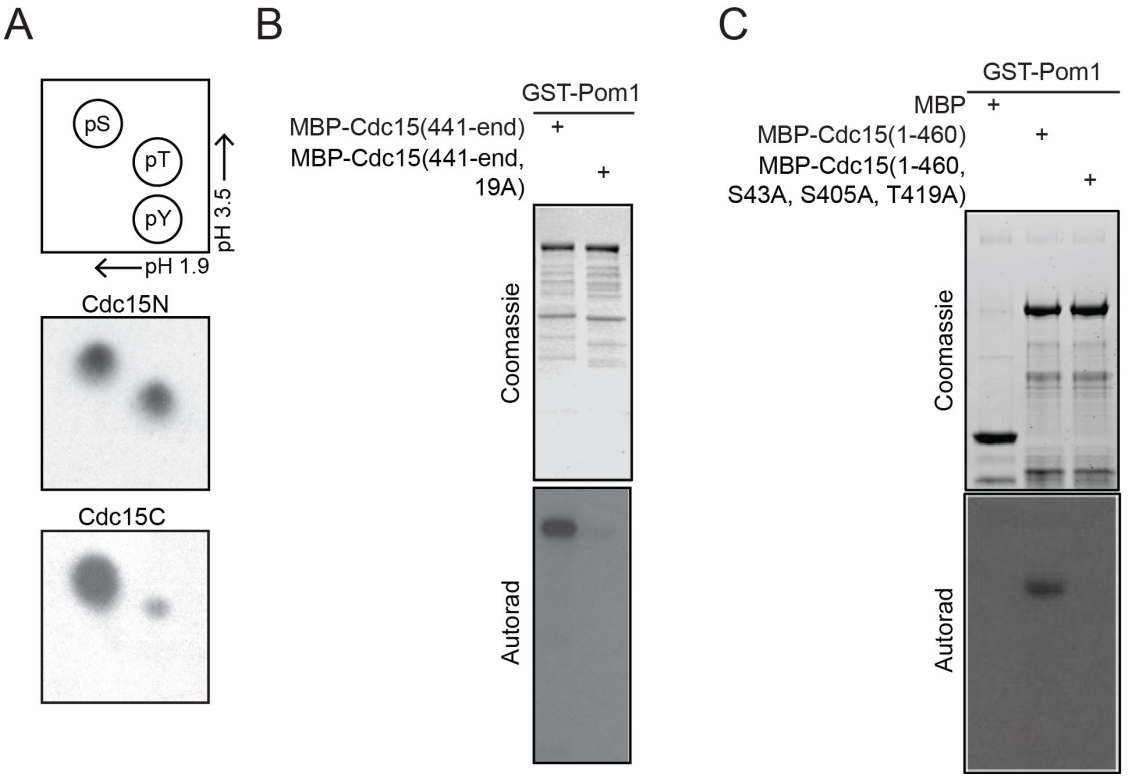

Figure 29. Cdc15 phosphomutants abolish Pom1 phosphorylation.
A) Phosphoaminoacid analysis of indicated substrate proteins phosphorylated *in vitro* by GST-Pom1. The positions of standard phosphorylated amino acids are indicated (top). Phosphoaminoacids were detected by autoradiography (bottom). Cdc15N, MBP-Cdc15(1-460); Cdc15C, MBP-Cdc15(441-end). B-C) *In vitro* kinase assays using radiolabeled ATP, recombinant GST-Pom1 and indicated substrate proteins were separated by SDS-PAGE. Coomassie-stained gels of inputs (top) and autoradiography detection of ^{32}P incorporation (bottom) are shown.

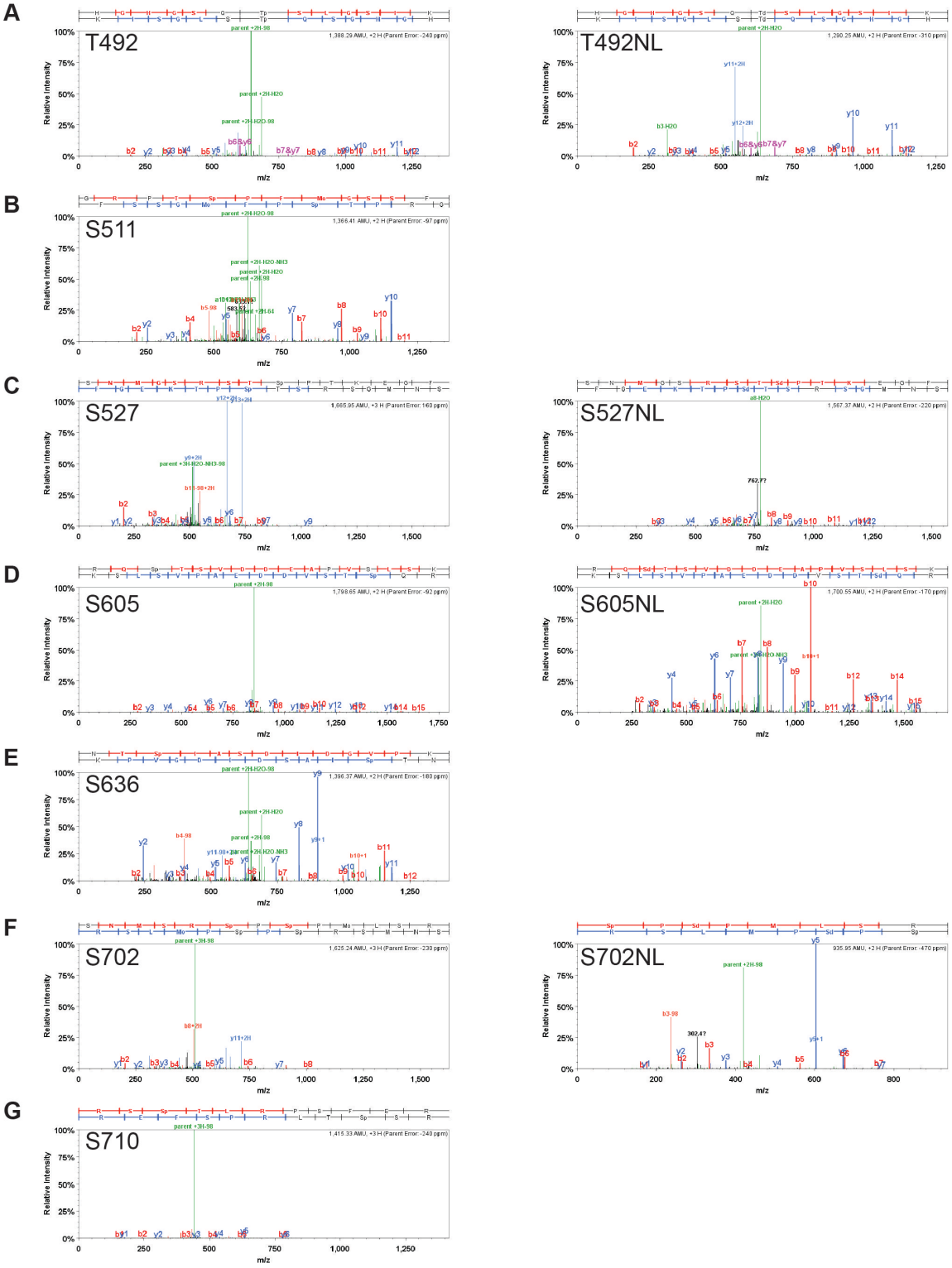
A
T492
T492NL
B
S511
C
S527
S527NL
D
S605
S605NL
E
S636
F
S702
S702NL
G
S710
Relative Intensity
m/z

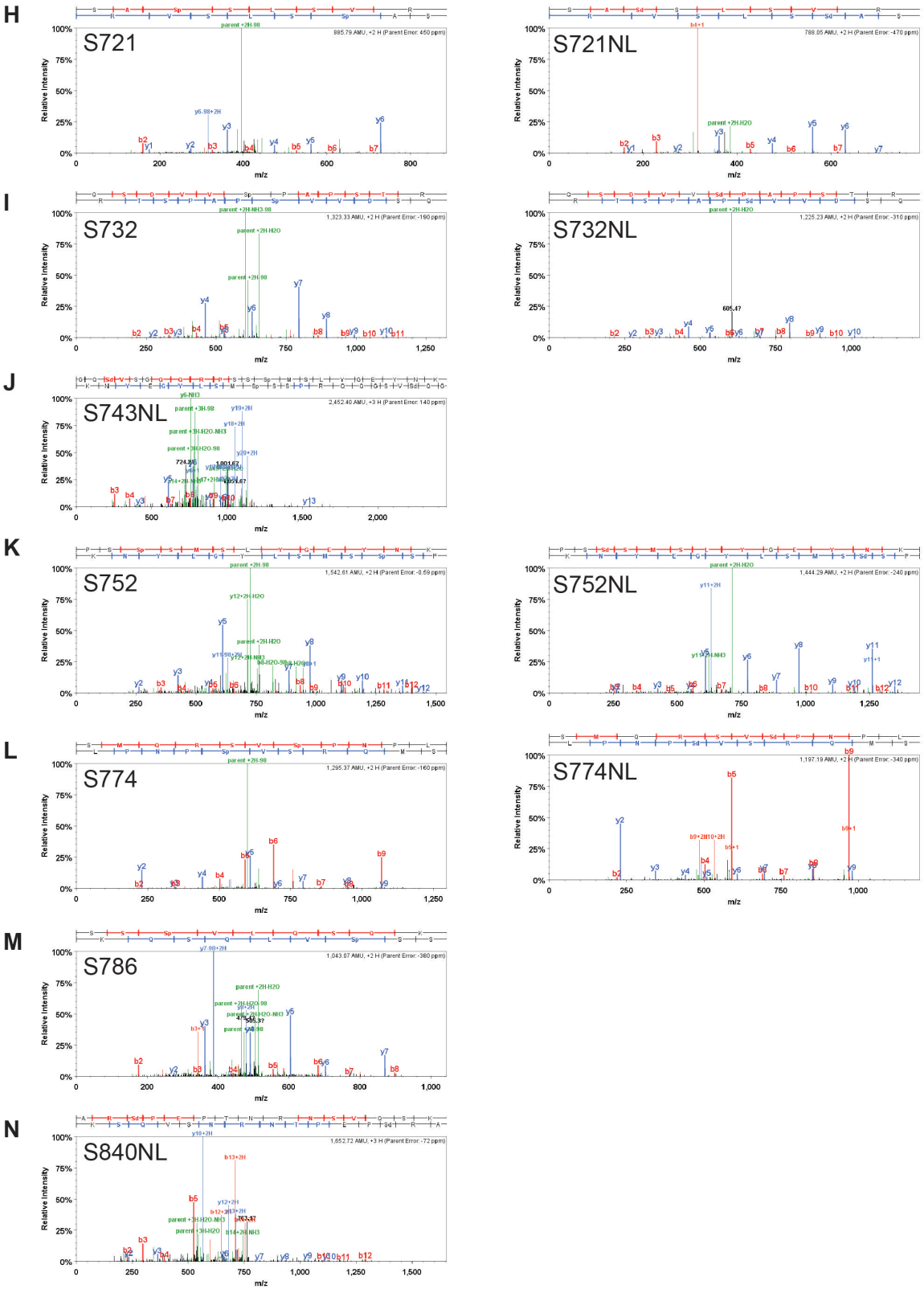

Figure 30. Cdc15 residues phosphorylated by Pom1.
A-N) Spectra identifying phosphorylation of the indicated residue.

Pom1 coordinates with other kinases to regulate Cdc15 phosphostatus

To test the function of these phosphorylation sites *in vivo*, we mutated them to alanine (to abolish phosphorylation) or aspartic acid (to partially mimic phosphorylation) and integrated the mutant *cdc15* alleles at the endogenous locus. Both phosphomutants were viable with normal mitotic and septation indices and no off-center or tip septa were observed (Figure 28E-F). Analysis of the SDS-PAGE mobility of Cdc15-22A showed that much of the phosphorylation-induced retardation of Cdc15 was eliminated by these mutations (Figure 28G). The increase in migration of Cdc15-22A was much greater than that observed for Cdc15 from *pom1*Δ background cells (Figure 28B) or from *pom1*^{as1} cells that were acutely inhibited (Figure 31A), suggesting that multiple kinases phosphorylate these residues on Cdc15 *in vivo*. Indeed, the polarity kinase Kin1 has been previously identified as a regulator of Cdc15, although it was proposed to phosphorylate non-overlapping sites on Cdc15 (Lee et al., 2018). We confirmed that Kin1 phosphorylates Cdc15 *in vitro* (Figure 31B). Additionally, we found that indeed dual inhibition of Kin1 and Pom1 results in an additive decrease in Cdc15 phosphorylation (Figure 31A). However, *kin1*Δ combined with 22A does not result in additive decrease in Cdc15 phosphorylation (Figure 31C) suggesting that Kin1 and Pom1 target largely overlapping sites *in vivo* and also, yet more kinases target at least a subset of these same sites.

We identified two other kinases that regulate Cdc15 phosphorylation by screening kinase gene deletions and temperature-sensitive mutants (data not shown). These are the p21-activated kinase Shk1(Orb2/Pak1) and the protein kinase C Pck1 (Figure 32). Both kinases co-localize with Cdc15 at the cell division site (Figure 34) and have been implicated in regulating cytokinesis. Shk1 phosphorylates Rlc1 to regulate timing of CR constriction (Loo and Balasubramanian, 2008). Pck1 is downstream of Rho1 GTPase that regulates septum deposition (Toda et al., 1993; Kobori et al., 1994; Arellano et al., 1999; Sánchez-Mir et al., 2014). *In vitro* kinase assays confirmed that Cdc15 is directly phosphorylated by these kinases (Figure 33) As we determined for Kin1, the Cdc15-22A is still phosphorylated when Shk1 or Pck1 is inactivated (Figure 35). Taken together, these findings indicate that Cdc15 is phosphorylated by at least four kinases—Pom1, Kin1, Shk1, and Pck1—on largely overlapping sites. That Cdc15-22A is still phosphorylated hen Kin1, Pck1, or Shk1 activity is lost suggests that the remaining phosphorylated residues are redundantly regulated by those three kinases or that as yet unidentified kinases also regulate Cdc15.

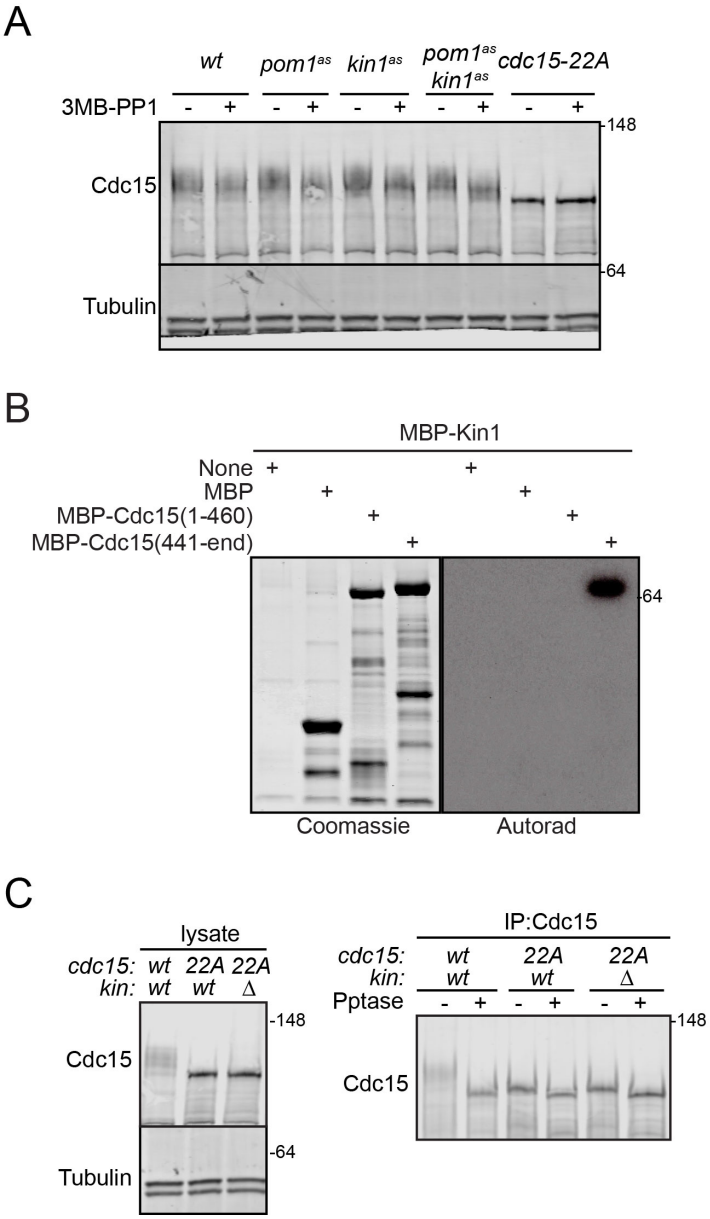

Figure 31. Cdc15 is also phosphorylated by Kin1.
A) Denatured lysates from the indicated strains were separated by SDS-PAGE and then immunoblotted for the indicated proteins. B) *In vitro* kinase assays using radiolabeled ATP, recombinant MBP-Kin1 and indicated substrate proteins were separated by SDS-PAGE. Coomassie-stained gels of inputs and autoradiography detection of ^{32}P incorporation are shown. C) Denatured lysates were prepared from the indicated strains. Anti-Cdc15 was used to IP Cdc15, which was then treated with lambda pptase or water. Lysates and IPs were separated by SDS-PAGE and immunoblotted for the indicated proteins.

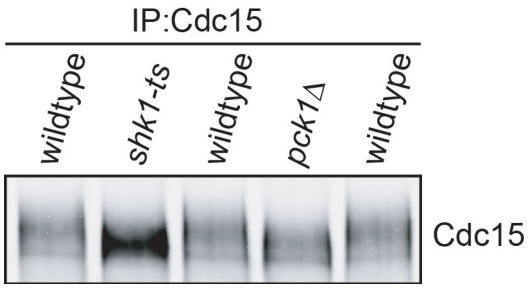

Figure 32. Shk1 and Pck1 also regulate Cdc15 phosphorylation.
Denatured lysates were prepared from the indicated strains. Anti-Cdc15 was used to IP Cdc15. IPs were separated by SDS-PAGE and immunoblotted for Cdc15.

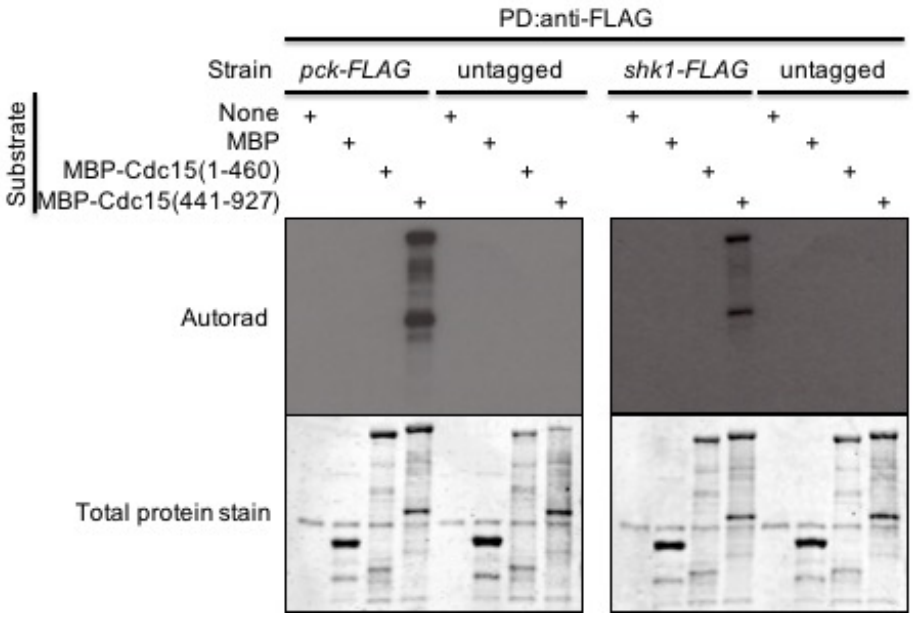

Figure 33. Shk1 and Pck1 directly phosphorylate Cdc15.
Native lysates were prepared for the indicated strains and anti-FLAG was pulled down using Protein G beads. Beads were added to *in vitro* kinase assays with the indicated substrate protein and radio-labeled ATP. Assays were separated by SDS-PAGE and transferred to PVDF membrane. Revert Total Protein Stain and autoradiography detection of ^{32}P incorporation are shown.

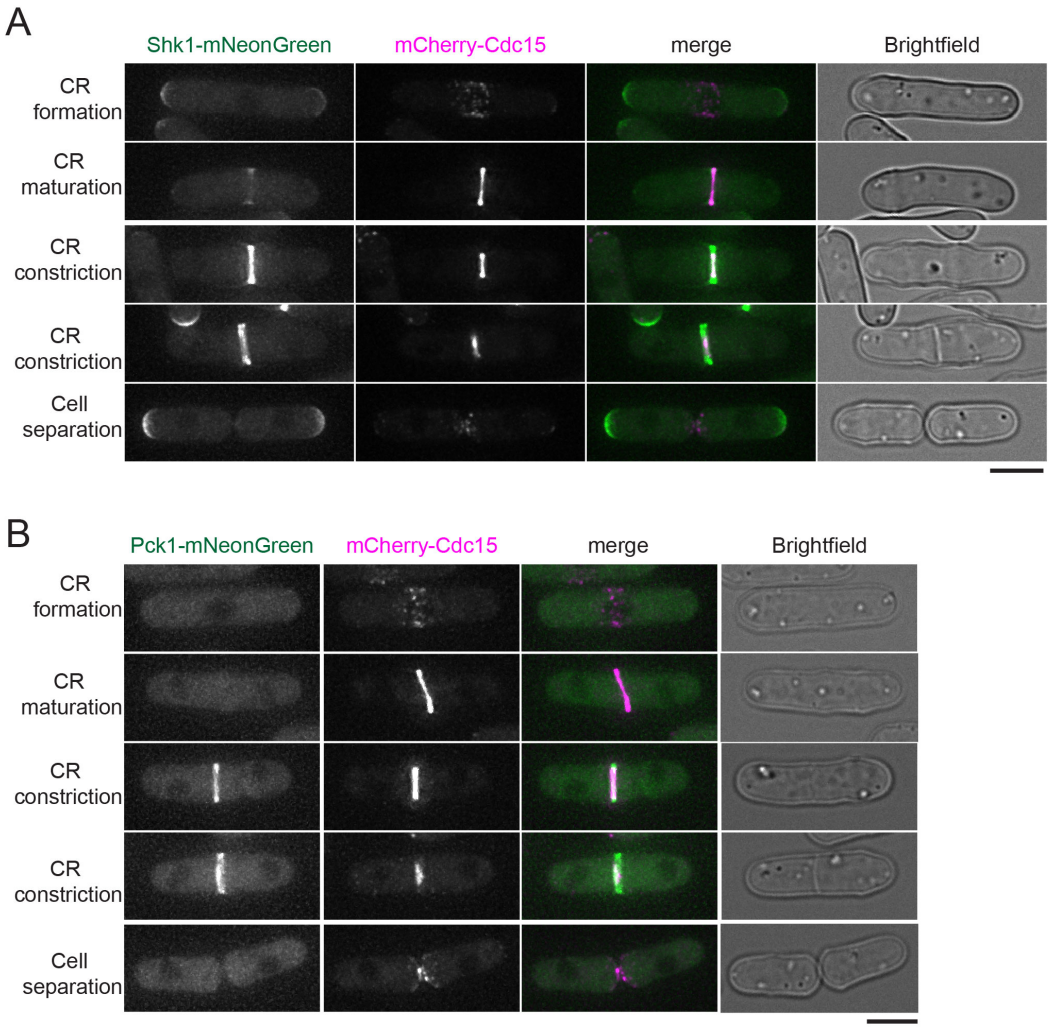

Figure 34. Shk1 and Pck1 co-localize with Cdc15.
Representative cells were selected from max projections of deconvolved images of strains producing the indicated tagged proteins and imaged live. Scale bar 5 µm.

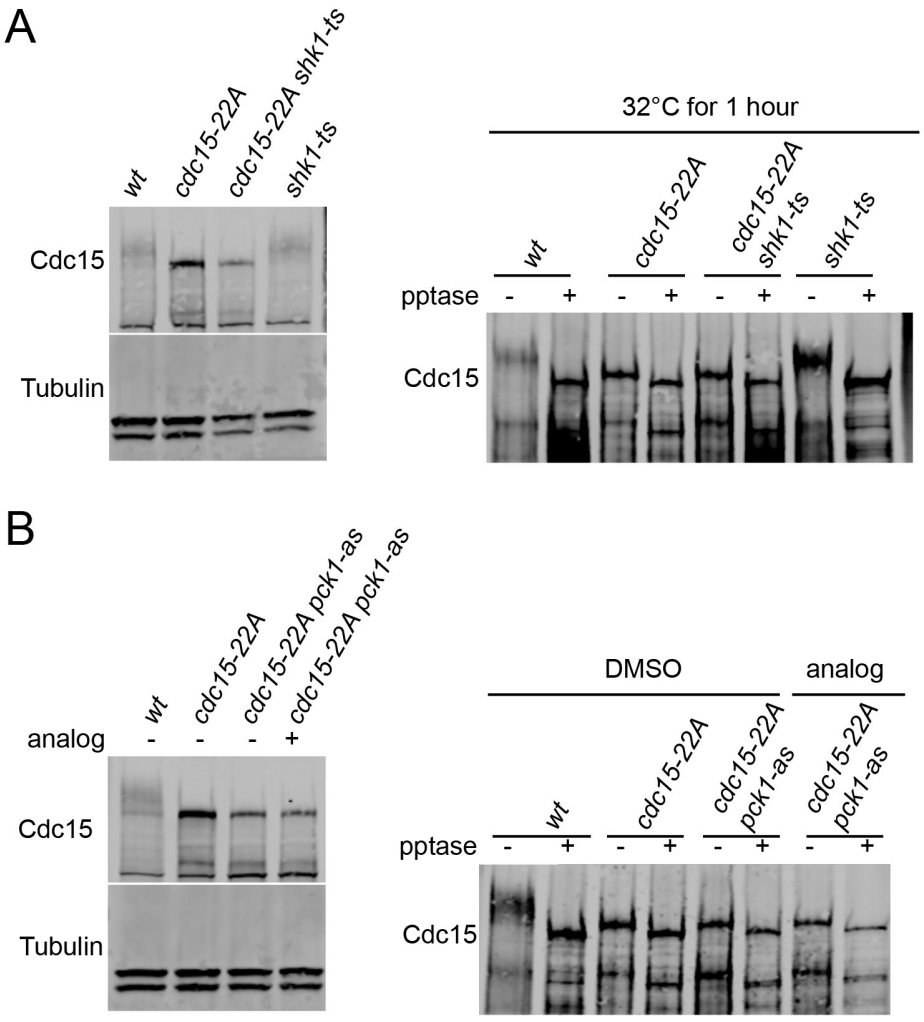

Figure 35. Pom1 phosphorylates overlapping sites with Shk1 and Pck1.
A-B) Denatured lysates were prepared from the indicated strains (right). Anti-Cdc15 was used to IP Cdc15, which was then treated with lambda pptase or water. Lysates and IPs were separated by SDS-PAGE and immunoblotted for the indicated proteins. A) All samples were grown to log-phase at the permissive permissive temperature and then shifted to the restrictive temperature (32°C) for 1 hour prior to sample collection. B) All samples were grown to log-phase. The ATP analog 3-BrB-PP1 or vehicle control (DMSO) was added to samples for 1 hour before samples were collected.

Pom1 phosphorylation regulates Cdc15 localization

Next we visualized phosphomutants by tagging them at the N-terminus with mNeonGreen (mNG) (Willet et al., 2015a). As was previously described for other phosphoablating Cdc15 mutants (Roberts-Galbraith et al., 2010), the fluorescent fusion protein mNG-Cdc15-22A localizes abnormally to cortical puncta even during interphase, arriving at the division site 19.8 +/- 6.6 minutes before mitotic onset (i.e. spindle pole body (SPB) separation) compared to 0.5 +/- 1 and 1.3 +/- 1.3 minutes for mNG-Cdc15 and mNG-Cdc15-22D (Figure 36A-B). mNG-Cdc15-22A abundance in the CR is also increased, although the whole cell fluorescence intensities of mNG-Cdc15, mNG-Cdc15-22A, and mNG-Cdc15-22A are comparable **(**Figure 36C**).**

Given these changes in both timing and abundance of Cdc15 recruitment to the CR, we carefully examined cytokinesis dynamics using time-lapse imaging of *cdc15* Pom1-phosphomutants expressing Rlc1-mNG and Sid4-mNG to mark the CR and SPB, respectively (Figure 36D). The length of CR formation was similar in wildtype, *cdc15*-22A, and *cdc15*-22D. However, the periods of maturation and constriction were shorter in *cdc15*-22A and longer in *cdc15*-22D (Figure 36E).

Pom1-mediated Cdc15 phosphorylation prevents septum formation at cell tips

The wildtype-like septation of Cdc15 phosphoablating mutants (Figure 28E-F) is consistent with the fact that *pom1*Δ do not have tip septa. However, we wondered how Cdc15 phosphomutants affect septa formation in the absence of Mid1. Combining the phosphoablating mutant *cdc15-22A* with *mid1*Δ did not drive tip septa formation (Figure 37A), indicating that Cdc15 is not sufficient for CR formation, consistent with studies of other Cdc15 phosphoablating mutants (Roberts-Galbraith et al., 2010).

We hypothesized that a Cdc15 phosphomimetic would suppress tip septa formation even in cells lacking both Mid1 and Pom1 position cues. Although not completely suppressed, the percentage of tip septa is substantially reduced by introducing the *cdc15-22D* allele to *mid1*Δ*pom1*^{as1} cells (Figure 37B). Together these results indicate that Cdc15 is a key substrate for Pom1-mediated inhibition of tip septa, although likely not the only substrate.

To characterize the molecular consequences of Pom1-mediated Cdc15 phosphorylation, we sought to identify other factors involved in the Pom1-Cdc15 regulatory pathway by searching for mutants that prevented septa formation at tips in *pom1*^{as1} *mid1*Δ cells. Loss-of-function in several actomyosin ring components (Rlc1, Fim1, Ain1, Myp2, Rng2, Cdc12 and F-actin) failed to restore tip occlusion to *mid1-18 tea1Δ* cells (Huang et al., 2007). By contrast, deletion of CR components Cyk3, Fic1, or Pxl1 restored tip occlusion in *pom1*^{as1} *mid1Δ* cells (Figure 37C-F). This suggests that Cyk3, Fic1, and Pxl1 are required to form tip septa. Cyk3, Fic1, and Pxl1 have been shown to interact directly or indirectly with Cdc15 (Roberts-Galbraith et al., 2009; Bohnert and Gould, 2012; Ren et al., 2015; Davidson et al., 2016; Sethi et al., 2016; Martin-Garcia et al., 2018). In the context of tip septa formation, Cyk3, Fic1, or Pxl1 could be downstream of Cdc15 activation or they could be additional substrates of Pom1. Pxl1 is

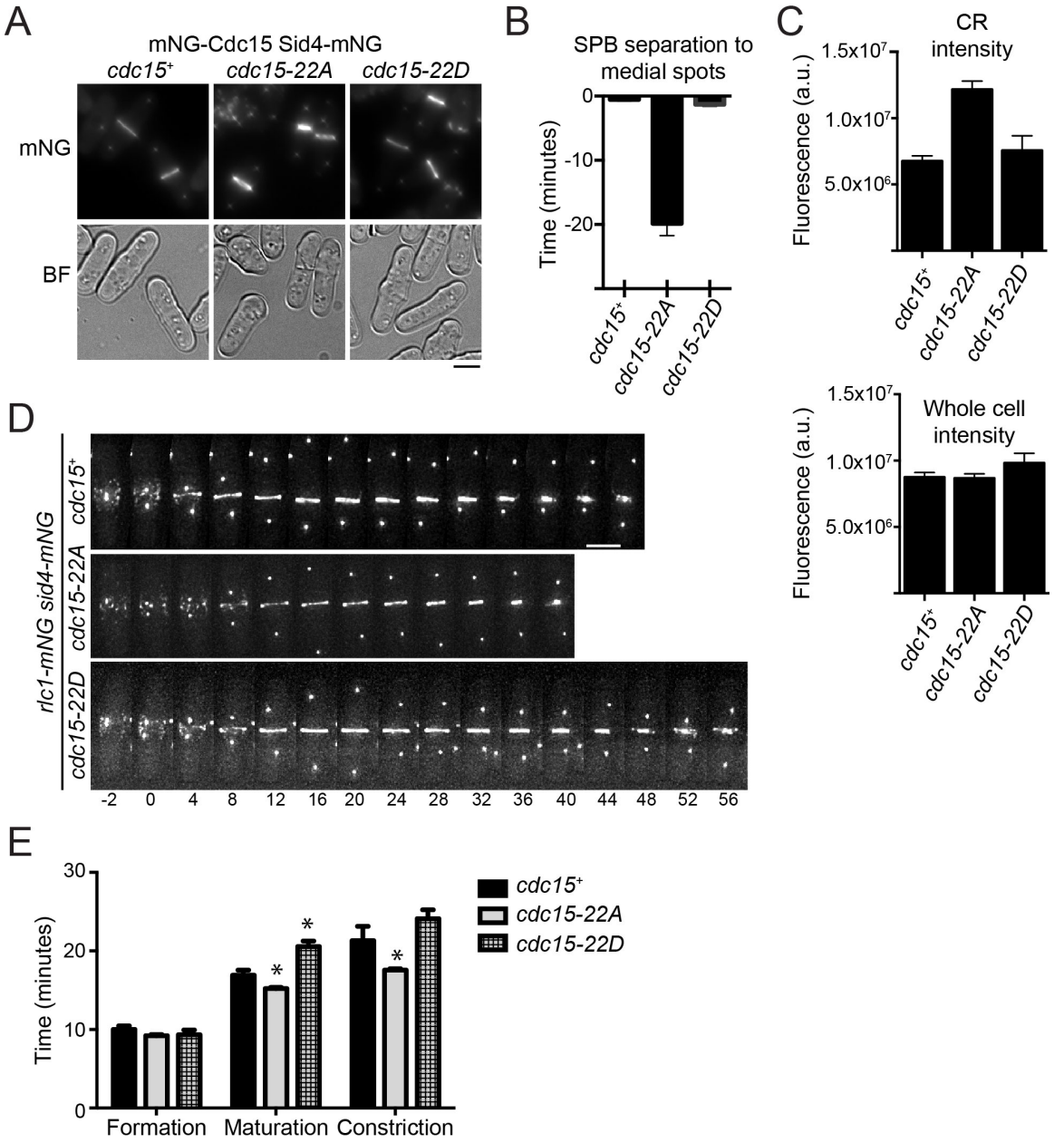

Figure 36. Pom1 phosphorylation regulates Cdc15 localization.
A) Sum projections (mNG) or brightfield (BF) representative images of the indicated strains. Scale bars are 5 μm. B) Average time of arrival of Cdc15 at the division site relative to SPB separation (time 0). Error bars indicate standard error of the mean. C) Average CR and whole cell (WC) intensity of the indicated proteins. Error bars are SD. D) Representative montages from live-cell, time-lapse imaging of indicated strains. Numbers indicate minutes from SPB separation, which is set to time 0. Scale bar is 5 μm. E) Length of cytokinesis stages for indicated genotypes based on time-lapse imaging of cells expressing CR and SPB markers Rlc1-mNG and Sid4-mNG, respectively. Error bars indicate standard error of the mean. *, $p < 0.05$ one-way ANOVA.

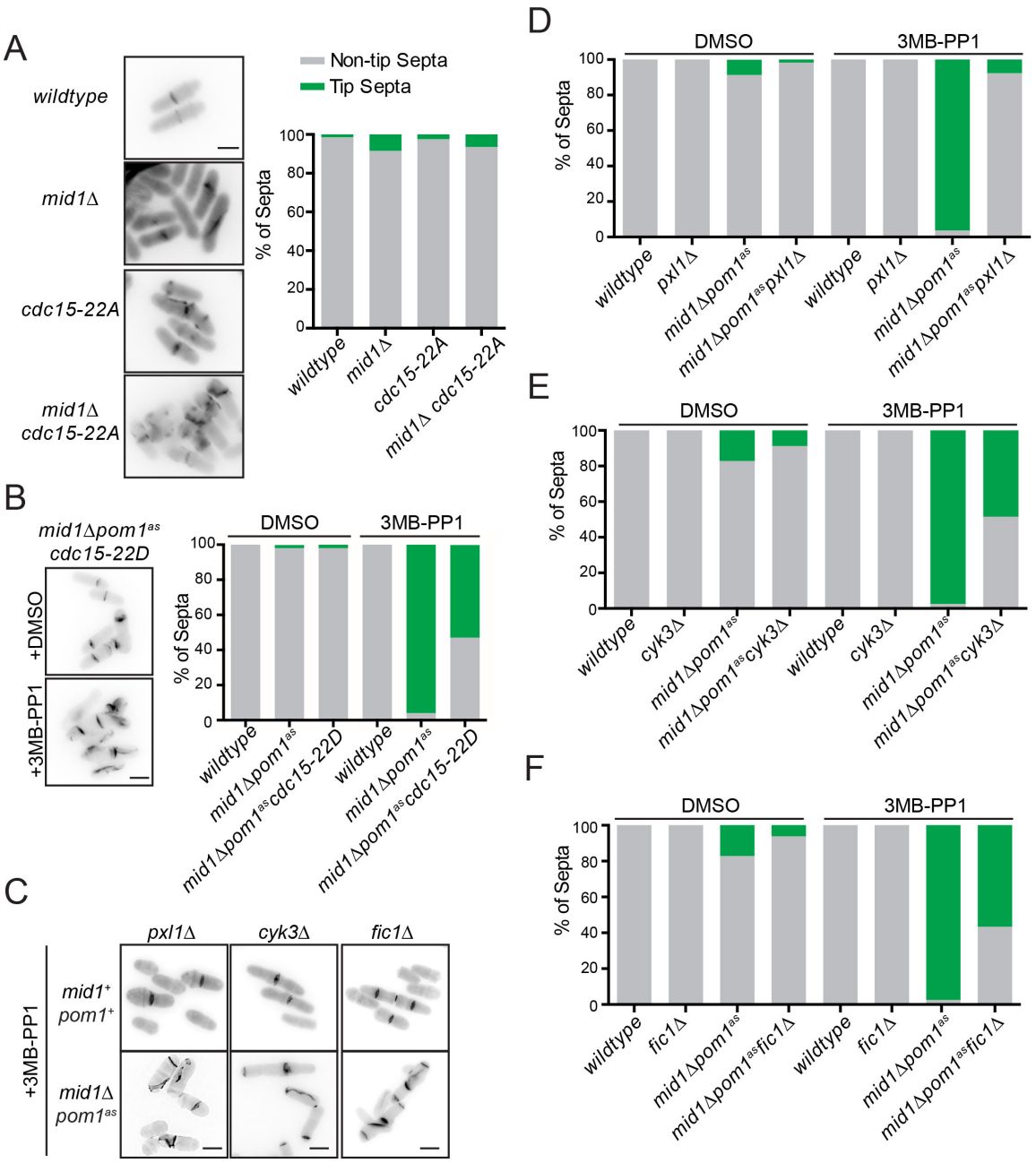

Figure 37. Cdc15 phosphomimetic rescues tip septa formation.
A-F) Quantification of tip septa phenotype. Graph is average of three replicates. Images are representative of cells of the indicated genotype and treatment. Cells were fixed in 70% ethanol at 4°C and then stained with Calcofluor White. Scale bar is 5 µm. For Pom1 inhibition experiments, cells were grown to log-phase at 32°C and then treated for 2 hours with either DMSO or analog 3MB-PP1 to inhibit analog-sensitive Pom1. D, F-H)

not appreciably phosphorylated by Pom1 *in vitro* (data not shown) nor is the phosphostatus of Fic1 and Pxl1 regulated by Pom1 *in vivo* (Kettenbach et al., 2015); data not shown). Therefore, we next tested whether Pom1-mediated phosphorylation regulates their interaction with Cdc15.

Pom1 inhibits Cdc15 binding to Pxl1 in vitro

The C-terminus of Cdc15 interacts with Fic1 and Pxl1 in an SH3 domain-dependent manner (Roberts-Galbraith et al., 2009; Bohnert and Gould, 2012; Ren et al., 2015). Previous studies proposed that phosphorylation of Cdc15 triggers a conformational change that prevents interaction with partners such as Fic1 and Pxl1 (Roberts-Galbraith et al., 2010). According to this model, the loss of Pom1-mediated phosphorylation would result in mis-localized and mis-timed interaction of Cdc15 with Fic1 and Pxl1. However, whether phosphorylation itself directly inhibits Cdc15 interaction with binding partners has not been tested. Therefore, we tested using an *in vitro* kinase assay coupled to an *in vitro* binding assay whether Pom1-mediated phosphorylation inhibits Cdc15 binding to Fic1 and Pxl1. Whereas phosphorylation of MBP-Cdc15C did not affect its interaction with Fic1, Pom1-mediated phosphorylation of GST-Cdc15C blocked its association with Pxl1 (Figure 38A-B). Of note, these experiments were performed with a C-terminal fragment of Cdc15 and thus even though Pom1-mediated phosphorylation of Cdc15C did not prevent interaction with Fic1, it remains possible that phosphorylation of full-length Cdc15 would prevent interaction with Fic1, in accordance with our previously proposed model of the full-length dimer exhibiting a phospho-mediated conformational switch that regulates its interaction with membranes and protein partners (Roberts-Galbraith et al., 2010).

The phosphorylation of Cdc15 C-terminus occurs in the central, intrinsically disordered region (IDR) and not in the SH3 domain (Figure 38A). This suggested that perhaps Pxl1 was interacting at least in part with the central IDR. Therefore, we performed a set of binding experiments to determine which region of Cdc15 interacts with Pxl1. First, we found that the Cdc15 SH3 domain is not sufficient for Pxl1 interaction *in vitro* (Figure 38C). Next, we tested whether canonical SH3 binding is required for Cdc15 interaction with Pxl1. Mutating the SH3 domain to abolish canonical SH3 binding (W903S) eliminates interaction with Fic1 *in vitro* (Figure 39A). However, Cdc15(W903S) can still interact with Pxl1, although with apparently reduced affinity (Figure 39B). This was confirmed by performing quantitative binding assays that determined K_d (Figure 39C). Taken together, these results indicate that Cdc15 binds to Pxl1 using both a canonical SH3 domain interaction plus its IDR.

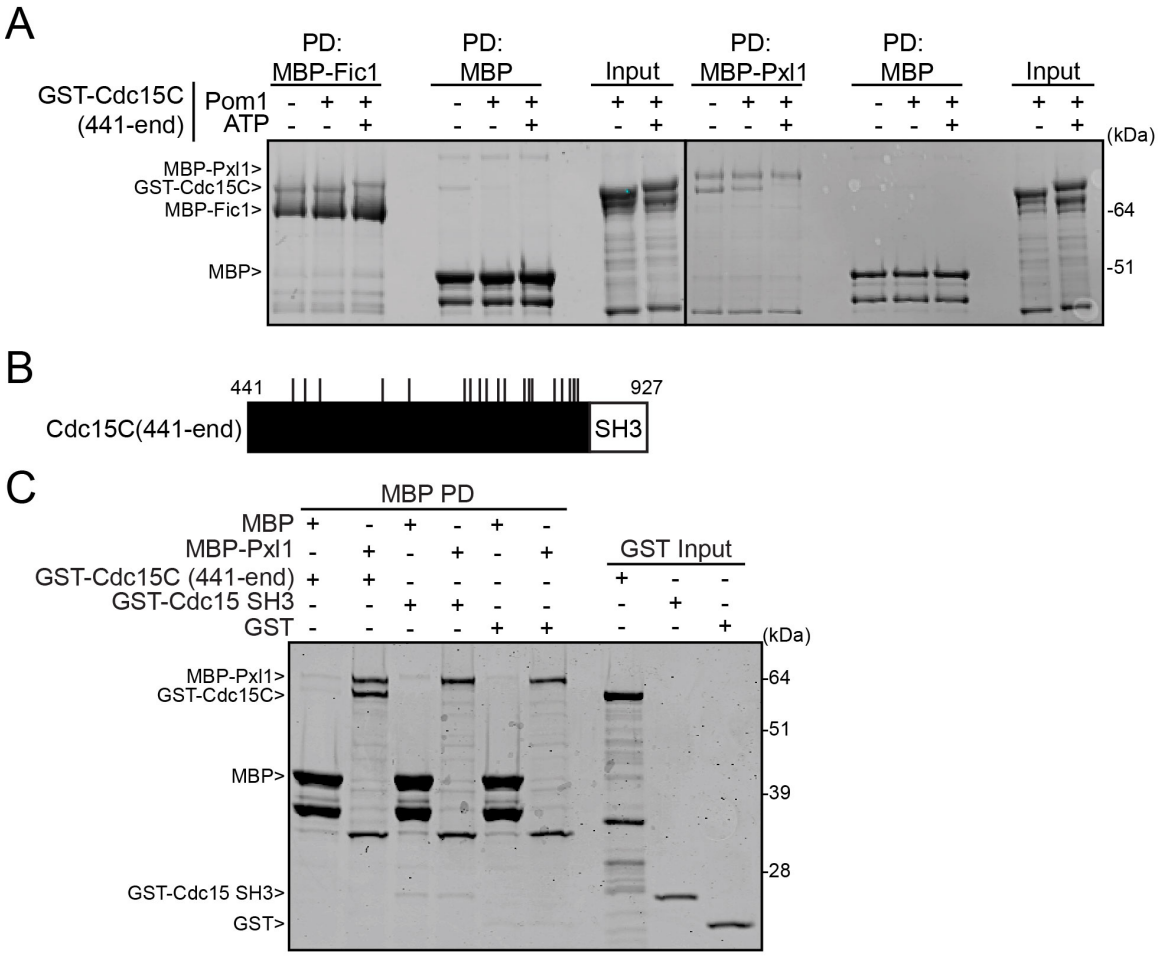

Figure 38. Cdc15 IDR is required for interaction with Pxl1 and Pom1 phosphorylation regulates interaction of Cdc15 with Pxl1.
A) *In vitro* kinase assays with recombinant GST-Pom1 and GST-Cdc15C were added to the indicated MBP-tagged proteins. Amylose resin was used to pull down proteins. B) Schematic of C-terminal fragment of Cdc15 used in binding assays. Pom1 phosphorylation sites are indicated with black lines. C) Binding assays between the indicated MBP-tagged and GST-tagged proteins. Amylose resin was used to pull down proteins.

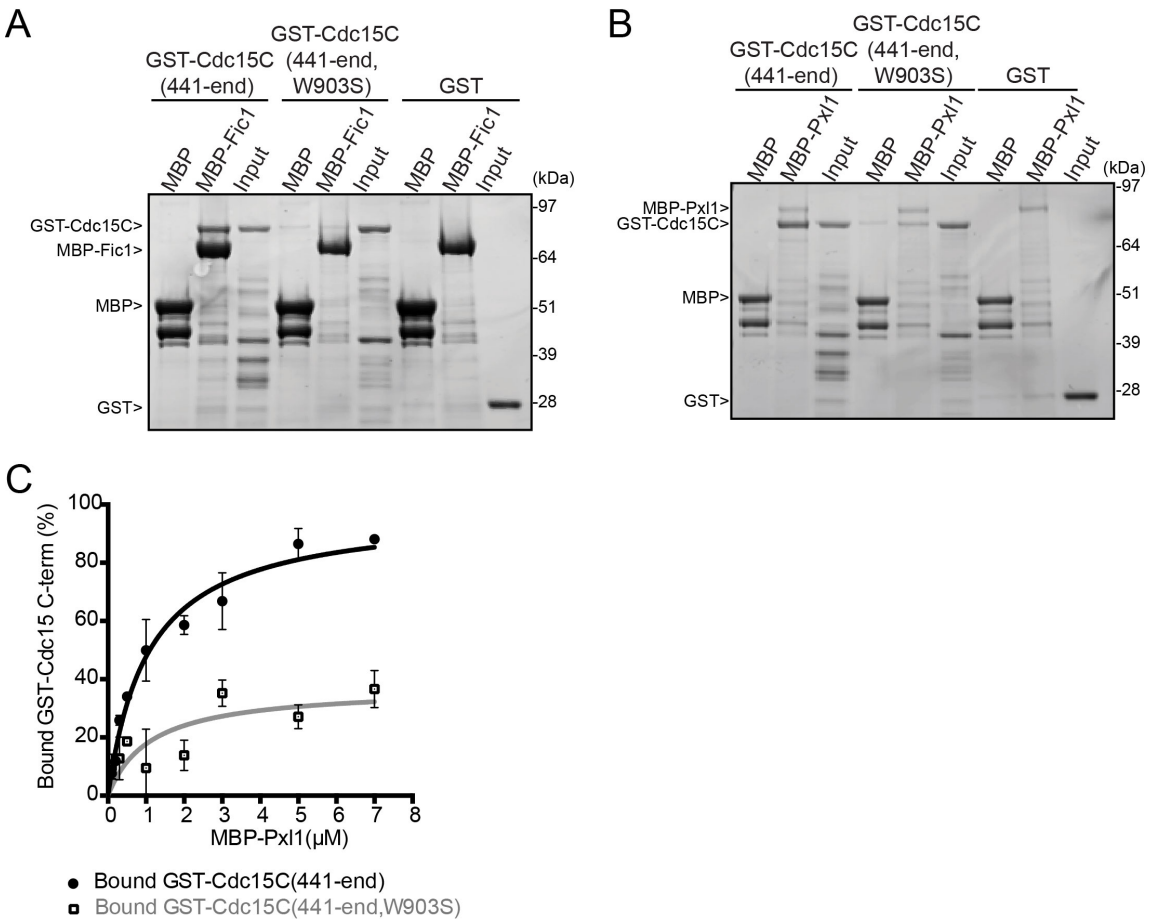

Figure 39. Cdc15 SH3 domain is required for interaction with Fic1 and participates in binding Pxl1.

A-C) Binding assays between the indicated MBP-tagged and GST-tagged proteins. Amylose resin was used to pull down proteins.

Discussion

The DYRK-family kinase Pom1 has been shown to be critical for preventing septation at cell tips (Huang et al., 2007) and in this study we confirm the hypothesis that this is due in part to phosphorylation of the F-BAR protein Cdc15. Although Cdc15 phospho-regulation is established (Fankhauser et al., 1995; Wachtler et al., 2006; Roberts-Galbraith et al., 2010) (Kettenbach et al., 2015; Lee et al., 2018), this is the first comprehensive mapping of the complete cohort of Cdc15 residues phosphorylated by a single kinase. Phosphomutants made based on this analysis revealed that Pom1 phosphorylation regulates Cdc15 cortical localization and abundance in the CR. Furthermore, mutants that mimic Pom1 phosphorylation partially rescue tip septation when both positive Mid1-mediated and negative Pom1-mediated cues are absent. Deleting CR proteins and cell wall regulators that are scaffolded downstream of Cdc15—Cyk3, Fic1, and Pxl1—also partially rescues tip septation. Taken together, these results suggest that Pom1 inhibits division at cell tips in part by suppressing Cdc15 scaffolding.

What other proteins are regulated by Pom1 to prevent tip division?

The Cdc15 phospho-ablating mutant *cdc15-22A* did not induce tip septa formation in *mid1*Δ, indicating that it is not the sole protein regulated by Pom1 to inhibit division site placement. Other potential substrates include CR proteins Cyk3, Rga7, and Imp2, whose phosphorylation status has been shown to be regulated by Pom1 (Kettenbach et al., 2015). Imp2 and Cdc15 redundantly scaffold a network of proteins important for septum formation, which includes Cyk3, Fic1, and Pxl1. Rga7 has been shown to associate with Imp2 *in vivo* and is essential for proper septum formation. The consequences of phosphorylation of Cyk3, Rga7, and Imp2 have not been studied and it will be interesting to explore if Pom1 regulates this network globally for a common purpose.

How does phosphorylation inhibit Cdc15 molecularly?

The Cdc15-22A mutant localizes in puncta at the tips throughout the cell cycle, possibly due to loss of inhibitory Pom1 phosphorylation at cell ends. This phenotype is similar to other *cdc15* phospho-ablating mutants (Roberts-Galbraith et al., 2010). However, the previously studied *cdc15-27A* mutant took longer to form the CR and to constrict than *cdc15*$^{+}$ (Roberts-Galbraith et al., 2010),while *cdc15-22A* constricts earlier and faster than *cdc15*$^{+}$. The sites in the *cdc15-22A* and *cdc15-27A* mutants are overlapping but not identical, and *cdc15-27A* is not specific to a single kinase. This prompts the questions

How do different phosphorylation events affect Cdc15?

Previous investigations of Cdc15 regulation determined that phosphorylation inhibits its cortical localization and interaction with downstream CR proteins (Roberts-Galbraith et al., 2010). Additionally, phosphorylation seemed to regulate the ability of Cdc15 to oligomerize into linear assemblies (Roberts-Galbraith et al., 2010). This led to a model in which phosphorylation triggers a switch from a closed, inhibited conformation to an open conformation (Roberts-Galbraith et al., 2010), which has been proposed for other F-BAR proteins (Rao et al., 2010; Stanishneva-Konovalova et al., 2016). This paper shows for the first time that phosphorylation directly inhibits Cdc15 interaction with Pxl1. We also discovered that interaction with Pxl1 requires both Cdc15's SH3 domain and the IDR where the bulk of Pom1-mediated phosphorylation occurs. However, the interaction

between the C-terminus of Cdc15 and Fic1 was not inhibited by Pom1-mediated phosphorylation *in vitro* even though hyper-phosphorylated Cdc15 from G2 doesn't pull-down Fic1 but a Cdc15 phosphoablation mutant does (Roberts-Galbraith et al., 2010). Unlike Pxl1, the Cdc15 SH3 domain is sufficient to bind Fic1, presumably through one or more of the multiple poly-Proline sequences in its N-terminus (Bohnert and Gould, 2012). Therefore, it's possible phosphorylation of full-length Cdc15 both triggers a conformational switch that masks the binding pocket on the SH3 domain and directly inhibits interaction with Pxl1. It's particularly intriguing to consider this with the knowledge that Cdc15 is never completely dephosphorylated (Roberts-Galbraith et al., 2010) and thus a complex hierarchy of phosphorylation events could be regulating its multiple scaffolding activities. An important next step will be determine the structure of full-length Cdc15 to determine if this conformational switch is actually a method of inhibition.

How does Cdc15 integrate signaling from multiple kinases to time cytokinesis?

Although this paper primarily characterized the role of Pom1 phosphorylation in regulating Cdc15 for proper CR placement, we also identified three other kinases that collaborate to phosphorylate Cdc15: Kin1 (Lee et al., 2018), Shk1, and Pck1. Our data suggest that these kinases phosphorylate largely overlapping sites on Cdc15 given that the Cdc15-22A mutant abolishes most phosphorylation on Cdc15 and there does not seem to be an additive effect when combined with other kinase mutants. This was somewhat unexpected as a previous study reported that Kin1 and Pom1 phosphorylate non-overlapping sites (Lee et al., 2018). However, the previous study did not use mutational analysis or phospho-site mapping to verify the phosphorylated residues identified by MS. This is necessary given that most sites are located in the IDR of Cdc15 where 1 in every 5 residues is a Ser or Thr, which makes it difficult to accurately identify which residue in a phospho-peptide is phosphorylated. It will be interesting to follow up these findings by careful mapping of the sites modified by Shk1, Pck1, and Kin1 to determine how much overlap exists.

CHAPTER 5

CONCLUSIONS AND FUTURE DIRECTIONS

This thesis comprises three separate but related studies to provide molecular insight into the regulation and execution of cytokinesis using the model organism *S. pombe*. All three studies are rooted in the essential cytokinetic scaffold Cdc15. In Chapter 2, we described that the IDR contributes to its essential function and identified a role for it in recruiting calcineurin. Additional scaffolding functions of the IDR and the F-BAR domain remain to be uncovered. Chapter 3 branched off Cdc15, studying the regulation of its binding partner of Pxl1. By studying a single protein, we have opened doors to understanding general principles of how phosphatases collaborate to regulate cytokinesis. Finally, in chapter 4 we studied the regulation of Cdc15 itself. Given the many sites of phosphorylation on Cdc15 and its strong cell cycle regulation, we have long considered it an integration point for kinase-mediated signaling. In this thesis, we confirmed that multiple kinases do indeed converge on Cdc15 and we determined the cellular effect of phosphorylation by one of them. However, we have much more to learn about these different inputs and the resulting molecular output.

F-BAR protein IDRs: unchartered territories

Chapter 2 described structure-function studies of the essential CR scaffold Cdc15. This work discovered that the essential function of Cdc15's F-BAR domain can be replaced by the F-BAR domains of other proteins. This work also revealed that the central IDR is essential for Cdc15 function, but unlike the F-BAR domain, it cannot be swapped with the IDR of paralog Imp2. Characterization of mutants with partial deletion of the IDR revealed that in addition to being phosphorylated, the IDR contributes to scaffolding functions in the CR.

One defect that we observed with removal of aa 503-677 (*cdc15-Δ2*) is loss of calcineurin localization at the CR. The role of Cdc15's IDR in recruiting calcineurin to the CR is the project of another graduate student in the lab, Chloe Snider. An interaction between Cdc15 and calcineurin has not been detected (Chloe Snider, unpublished data). Calcineurin localization at the division site requires Pxl1 (Martin-Garcia et al., 2018), and we showed in Chapter 4 Pxl1 interacts with Cdc15's IDR and SH3 domain. However, we found that Ppb1 is absent even when Pxl1 is present at the division site, and interaction is not detected even when all 3 molecules are present (Chloe Snider, unpublished data), indicating that the recruitment of calcineurin is more complicated and could involve an unidentified partner of Cdc15's binding region.

cdc15-Δ2 mutants display an abnormal CR behavior that is unique to the deletion of aa 503-677. I tested if forcing calcineurin to the CR in *cdc15-Δ2* would rescue the CR defect. I fused the calcineurin catalytic subunit Ppb1 to the N-terminus of Pxl1, which contains CR-targeting information (Pinar et al., 2008). This fusion protein has been previously used to force Ppb1 to the division site in a *pxl1Δ* (Martin-Garcia et al., 2018). We confirmed that this fusion product does localize to the CR in *cdc15-Δ2* when it replaces *ppb1*$^{+}$ at the endogenous locus, although the double mutant still had defects. I also integrated the fusion gene at the *leu1* locus so cells expressed *ppb1*$^{+}$ from the endogenous locus and combined it with *cdc15-Δ2*; this mutant also still had defects. This

indicates that aa 503-677 are mediating another function—perhaps recruiting, maintaining, or precisely localizing another protein—that is important for CR integrity.

cdc15-Δ*3* also had cytokinetic defects, although it did not exhibit the same CR behavior. In this case, CR contraction proceeded extremely slowly, although CRs did not slide away from the division site. One possibility is that the primary defect in *cdc15*-Δ*3* is a reduced rate of septum synthesis. Further characterization of this defect could lead to insight into how CR contraction and septum synthesis are coupled. In chapter 4, we discovered that the part of the IDR deleted in *cdc15*-Δ*3* is important for interaction with Pxl1 *in vitro,* suggesting one possible molecular defect that could explain the phenotype of *cdc15*-Δ*3*.

Taken together, Cdc15's IDR could be mediating multiple interactions, adding further complexity to the network of proteins that are known to be scaffolded by its F-BAR and SH3 domains. A few other F-BAR proteins' IDRs have been implicated in their function (Meitinger et al., 2011; Meitinger et al., 2013; Oh et al., 2013) (Hollopeter et al., 2014; Umasankar et al., 2014) (Yamamoto et al., 2018), and it will be interesting to see if in fact all IDRs are important for F-BAR protein function.

Collaboration between phosphatases to control mitotic exit and cytokinesis

The studies of chapter 3 were prompted by a hypothesis that I generated to explain the CR defect in *cdc15*-Δ*2.* Although subsequent experiments disproved that hypothesis, my efforts to test it led to the confirmation of a novel CDK cytokinetic substrate that is regulated by at least two phosphatases and opened the door to future studies. Multiple large-scale phospho-proteomics identified Pxl1 as a phospho-protein regulated by CDK, although Pxl1 phosphorylation had not been studied. I confirmed that Pxl1 is phosphorylated *in vivo* and that CDK directly phosphorylates Pxl1. Not only did I confirm that Pxl1 is regulated by CDK, but I also identified two phosphatases that regulate it: the Cdc14 phosphatase Clp1 and PP1 Dis2. Clp1 is known to antagonize CDK phosphorylation, which further supports that Pxl1 is a CDK substrate *in vivo*. Dis2 is one of two PP1 catalytic subunits in *S. pombe*. The other is Sds21 (Ohkura et al., 1989; Dawson and Holmes, 1999). Although Sds21 was not a major protein pulled down by GFP-Pxl1 (Table 4), future studies can test whether Sds21 also regulates Pxl1. This will provide insight into how PP1 orthologs collaborate to regulate cell biological processes and whether there is any division of labor. It also offers the potential to dissect how catalytic subunits have substrate specificity, whether this is through intrinsic molecular features that dictate binding of catalytic or regulatory subunits to substrate or by temporal and spatial regulation of phosphatase localization and thus access to substrates.

It will also be interesting to determine how multiple phosphatases collaborate to regulate a single substrate. Although the Pxl1(9D) did not seem to be a true phosphomimetic, future studies can begin to probe the effect of hyper-phosphorylation by interfering with substrate-phosphatase interaction. There is a predicted PP1 docking motif in the N-terminus of Pxl1 at aa 78-84, right between two sets of CDK phosphorylation sites (T64/S67 and S97) (Figure 40). In future experiments, we will test whether mutating the PP1 docking motif as was done in previous studies (Grallert et al., 2015) results in Pxl1 hyperphosphorylation. Additionally, we will monitor PP1 localization in the Pxl1 PP1 docking mutant to determine if Pxl1 is more than a substrate but also a CR scaffold for PP1. This will be important for interpreting the cytokinesis phenotypes of the Pxl1

PP1 docking mutant to know if the primary molecular perturbation is Pxl1 hyperphosphorylation in an otherwise wildtype setting (i.e. Dis2 is still acting on other substrates) or if larger-scale perturbations are occurring due to loss of PP1 activity at the CR. Although a docking site has not been described for Clp1, its homolog in *S. cerevisiae,* Cdc14*,* has been shown to dock on PxL sites (Kataria et al., 2018). The residues on Cdc14 that bind with the PxL motif are conserved in Clp1, suggesting that this docking mechanism could be conserved. This is another potential way to perturb Pxl1 dephosphorylation and characterize how multiple phosphatases regulate it.

Even though calcineurin doesn't regulate Pxl1, its localization at the division site and the gross cytokinesis defects of *ppb1*Δ cells indicate that it is still important for regulating cytokinesis. Indeed, PP1, PP2A, PP2B/calcineurin, and Cdc14 phosphatases are all implicated in cytokinesis in *S. pombe* and in metazoan cells to varying degrees. Combining reductionist studies like those I propose for Pxl1 with more systematic studies such as proteomics studies to identify phosphatase substrates can be used to unravel how multiple phosphatases distribute responsibility.

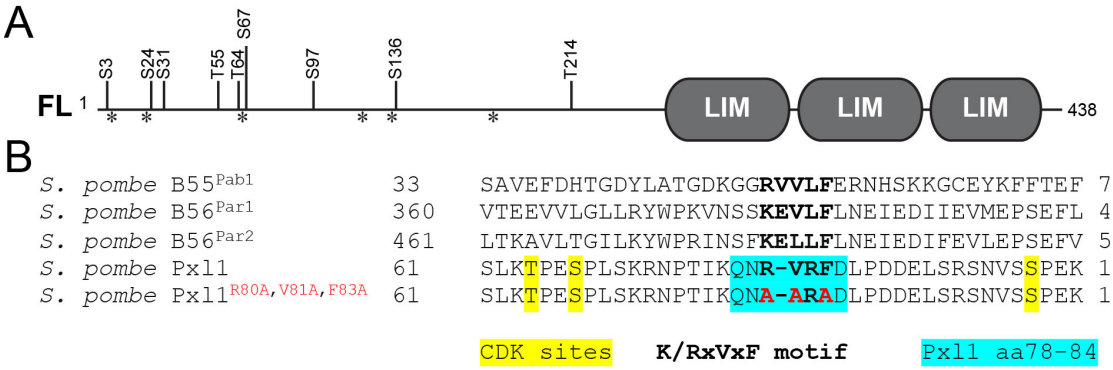

Figure 40. PP1 docking site in the N-terminus of Pxl1.
A) Schematic of Pxl1. Numbers indicate amino acid position of [S/T]P motifs in the N-terminus of Pxl1. Asterisks indicate PxxP motifs. B) Alignment of PP1 docking motifs. Red residues indicate mutations that can be made to disrupt the docking motif.

CDK regulation of F-BAR protein scaffolding

After establishing that CDK phosphorylates Pxl1, I proceeded to make phosphomutants that ablated or mimicked CDK phosphorylation and to characterize the cell biology of those phosphomutants. Analysis of phospho-ablating mutants indicated that Pxl1 localization to the CR is inhibited by phosphorylation, and the cytokinesis defects of *pxl1(9A)* indicate that this timing is important for efficient execution of cytokinetic events. The N-terminus of Pxl1 contains CR targeting information (Pinar et al., 2008), and given that all of the CDK phosphorylation sites are in the N-terminus, we hypothesized that phosphorylation directly inhibits an interaction at the CR. The first interaction that we tested was Pxl1's interaction with the C-terminus of Cdc15 (Pinar et al., 2008; Roberts-Galbraith et al., 2009; Martin-Garcia et al., 2018), which we confirmed is direct in Chapter 4. Cdc15 is one of the earliest proteins at the division site arriving before SPB separation (Wu et al., 2003; Roberts-Galbraith et al., 2009; Ren et al., 2015). Although we showed in Chapter 4 that phosphorylation of Cdc15 C-terminus inhibits binding to Pxl1, Cdc15 is dephosphorylated prior to Pxl1's localization at the CR (Roberts-Galbraith et al., 2010). Therefore, it is possible that Pxl1 must itself be inhibited to prevent interaction with Cdc15 and delay its recruitment to the CR until maturation. To test this, we phosphorylated bead-bound MBP-Pxl1 with CDK and then added a C-terminal fragment of Cdc15 to see if the two proteins could still interact. We found that GST-Cdc15C bound equally to non-phosphorylated and phosphorylated MBP-Pxl1 (Figure 41). Thus the interaction between Pxl1 and the C-terminus of Cdc15 is regulated by phosphorylation of Cdc15 (see Chapter 4), not by regulation of Pxl1.

Pxl1 phosphorylation could be regulating another of its interactions at the CR, such as interaction with Rga7, Rlc1, or Sbg1 (Pinar et al., 2008; Roberts-Galbraith et al., 2009; Martin-Garcia et al., 2014; Foltman et al., 2016; Sethi et al., 2016). More unpublished data shows that Pxl1 can also directly bind to the F-BAR domain of Cdc15 (Chloe Snider). That CDK phosphorylation could regulate binding to the F-BAR domain is an attractive hypothesis because it has been previously shown to regulate the binding of formin Cdc12 to the F-BAR domain (Willet et al., 2018). To test this, we phosphorylated bead-bound MBP-Pxl1 with CDK and then added recombinant Cdc15 F-BAR to see if the two proteins could still interact. Phosphorylation of MBP-Pxl1 reduced its interaction with Cdc15 F-BAR domain by approximately 50% *in vitro* (Figure 41). Interestingly, though both Pxl1 and Cdc12 are phosphorylated by CDK at similar times of the cell cycle, Cdc12 arrives at the division site much earlier than Pxl1. The different timing of these proteins could be due to the order in which they are dephosphorylated. Alternatively, other regulatory mechanisms could redundantly regulate protein recruitment as a Cdc12 CDK phosphomutant is still highly phosphorylated *in vivo* (Willet et al., 2018). Considering our new understanding of the nanoscale architecture of the CR and that the Cdc15 F-BAR domain is at the membrane (McDonald et al., 2017), another possibility is that CDK phosphorylation specifically regulates Pxl1 and Cdc12 localization to the membrane via F-BAR docking.

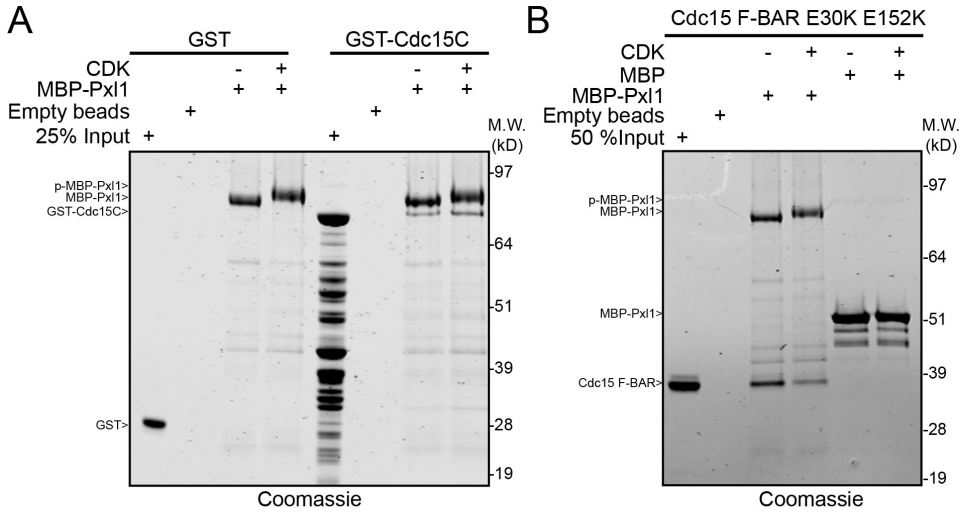

Figure 41. Phosphorylation of MBP-Pxl1 inhibits interaction with Cdc15 F-BAR but not its C-terminus.

A) Coomassie-stained SDS-PAGE of recombinant GST and GST-tagged Cdc15(aa441-927) that was input or pulled-down by empty beads, bead-bound MBP-Pxl1, or bead-bound CDK-phosphorylated MBP-Pxl1. B) Coomassie-stained SDS-PAGE of recombinant Cdc15 F-BAR that was input or pulled-down by empty beads, bead-bound MBP, bead-bound MBP-Pxl1, or bead-bound CDK-phosphorylated MBP-Pxl1.

Consequences of F-BAR protein phosphorylation

In Chapter 4, we studied the phosphorylation of Cdc15 by the DYRK kinase Pom1. The goal of this work was to test two long-standing hypotheses about the mechanism by which Pom1 inhibits tip septation (Huang et al., 2007) and the molecular mechanism by which phosphorylation inhibits Cdc15 (Roberts-Galbraith et al., 2010). We partially accomplished the first, demonstrating that Cdc15 is indeed a key substrate for Pom1-mediated inhibition of tip septation. However, as described in Chapter 4, Pom1 likely regulates a network of proteins to achieve this function.

Instead of proving or disproving the second hypothesis, we generated evidence in support of an alternative hypothesis. We showed for the first time that phosphorylation can directly inhibit Cdc15 interactions, specifically the interaction of Pxl1 with the C-terminus of Cdc15. A C-terminal phosphomimetic also inhibits interaction with Pxl1 *in vitro* (Figure 42). Given that existing literature describes Pxl1 accumulation at the CR through maturation and contraction in a Cdc15 SH3-domain dependent manner (Pinar et al., 2008; Martin-Garcia et al., 2018), we predicted that Cdc15 phosphomimicking mutations would reduce Pxl1 abundance at the CR, but they did not (Figure 42), indicating that the network of Cdc15 SH3-domain scaffolded proteins also participates in Pxl1 recruitment and/or maintenance. Unexpectedly (but perhaps biasedly), these studies converged on a particular interaction: that between Cdc15 and Pxl1. To summarize, Cdc15 has two binding sites for Pxl1: one site in the F-BAR domain that is not inhibited by phosphorylation (Chloe Snider, unpublished data) and a second site consisting of the IDR plus SH3 domain that is inhibited by phosphorylation or phophomimicking mutations. Pxl1 is also phosphorylated and this reduces the interaction with Cdc15 F-BAR but does not affect its ability to bind the C-terminus of Cdc15. Although we do not yet understand the significance of this highly regulated and complex interaction, it demonstrates the importance of zooming into the CR to understand these interactions at the nanoscale.

Other consequences of Cdc15 phosphorylation are still possible. The fact that the interaction between Cdc15 C-terminus and Fic1 is not inhibited by phosphorylation *in vitro*, but is inhibited when Cdc15 is hyper-phosphorylated *in vivo* (Roberts-Galbraith et al., 2010), indicates that multiple consequences of phosphorylation could co-exist. It will be interesting to test whether *in vitro* phosphorylation of full-length, recombinant Cdc15 can inhibit interaction with Fic1. It will also be helpful to determine the structure of full-length Cdc15 and if and how phosphorylation changes the structure. Although our lab can purify full-length, hyper-phosphorylated Cdc15 from bacteria co-producing Pom1 (Chloe Snider, unpublished data), these molecules are too heterogenous for cryo-electron microscopy studies (Mel Ohi lab, personal communication). Although most of the phosphorylation sites are in the highly flexible, IDR of Cdc15, phosphorylation itself does not seem sufficient to impose structural rigidity on the IDR. One strategy that could be used to impose homogeneity on the Cdc15 molecules is to include a binding partner. Indeed, a third possible consequence of phosphorylation is the creation of new phospho-peptide binding sites for 14-3-3 proteins Rad24 and Rad25. 14-3-3 proteins bind phosphorylated RxxS motifs (Reinhardt and Yaffe, 2013), which are exactly the sites created by Pom1 phosphorylation. Large-scale purifications and co-immunoprecipitation experiments demonstrate that Cdc15 and Rad24 interact (Roberts-Galbraith et al., 2010),

although the molecular consequences of 14-3-3 interaction are unknown. We confirmed that Pom1-phosphorylated Cdc15 can bind GST-Rad24 *in vitro* (Rahul Bhattacharjee, unpublished data). Future studies in the lab aim to identify the subset of Pom1 phosphorylation sites that are bound by 14-3-3, to determine how 14-3-3 binding affects Cdc15 *in vitro* and *in vivo*, and to test if binding to 14-3-3 could stabilize a Cdc15 conformation for structural studies.

Also in Chapter 4, although we primarily studied the effect of Pom1 phosphorylation on Cdc15, we also confirmed three other kinases that regulate Cdc15: Kin1, Shk1, and Pck1. Cdc15-22A abolishes most phosphorylation, but to what extent these kinases modify overlapping residues remains to be determined. Once similar phospho-site mapping is performed for these additional kinases, we can study whether they have overlapping or distinct effects. Another potential hypothesis is that even if these kinases modify overlapping sites, they differ in when and/or where they phosphorylate Cdc15. Careful analysis of kinase localization revealed that Shk1 arrives 13.0 +/- 1.6 minutes after SPB separation, just after anaphase B, while Pck1 doesn't arrive until 26.2 +/- 1.1 minutes after SPB separation and after the onset of CR contraction (Figure 43). Keeping in mind that Cdc15 is never completely dephosphorylated (Roberts-Galbraith et al., 2010), the sequential recruitment of kinases to the CR makes it possible that Cdc15 could be regulated by these kinases at different times. For example, Shk1 phosphorylates Rlc1 during CR formation to regulate CR contraction (Loo and Balasubramanian, 2008); Cdc15 could be another substrate of Shk1. The later arrival of Pck1 coincides with the onset of septum formation, consistent with Pck1 being downstream of Rho1 activation (Toda et al., 1993; Kobori et al., 1994; Arellano et al., 1999; Sánchez-Mir et al., 2014). Thus, Pck1 could regulate Cdc15's interaction with cell wall regulators to fine-tune septum synthesis. Considering the multitude and complexity of Cdc15's interactions and its role at multiple stages of cytokinesis, it is certainly within the realm of possibility that it would be so complexly regulated.

Final remark

Taken together, these studies revealed molecular details of cytokinesis in *S. pombe*, assigning previously unappreciated functions to the domain of a well-studied protein and dissecting how known interactions and functions are regulated for efficient cytokinesis. This work not only advances our understanding of Cdc15, Pxl1 and cytokinesis in *S. pombe*, but also serves as a model for how F-BAR proteins function, provides a system for studying how phosphorylation is fine-tuned on proteins through the effort of multiple kinases and phosphatases, and offers insight into cytokinesis generally.

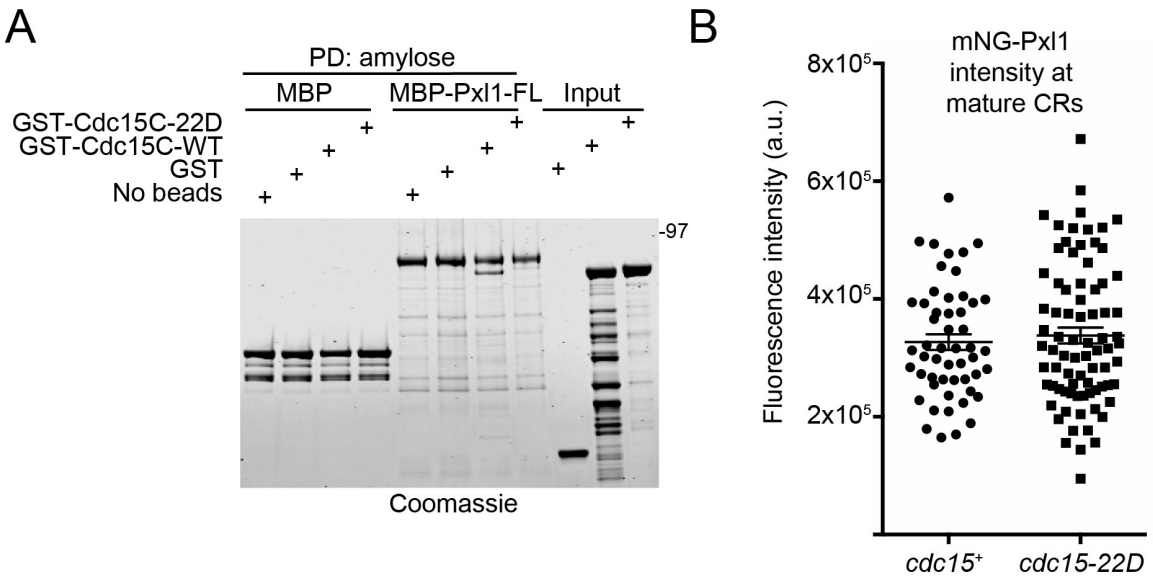

Figure 42. Cdc15 phosphomimicking mutations inhibit interaction with Pxl1 *in vitro* but not *in vivo*.
A) Coomassie-stained SDS-PAGE of recombinant GST and GST-tagged Cdc15C (aa441-927) that was input or pulled-down by empty beads or bead-bound MBP-Pxl1. B) Mean +/- SD of mNG-Pxl1 intensity at CRs in the indicated genetic backgrounds. Individual data points are shown.

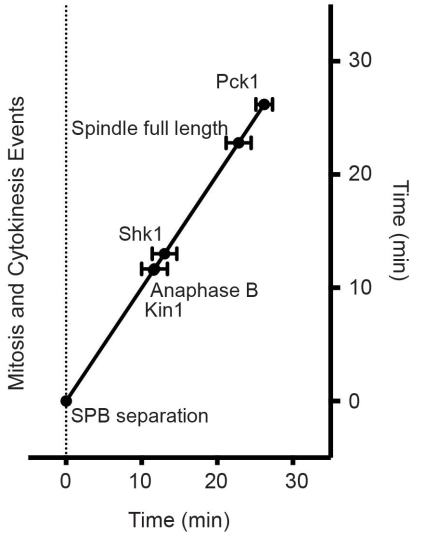

Figure 43. Timing of division site localization of Kin1, Shk1, and Pck1.
Strains expressing mNG-tagged kinase and Sid4-mCherry were imaged at 2-min intervals. Mean +/- SD of each event is plotted relative to SPB separation, which was set to time 0. Anaphase B and full length spindle are observed at 11.7 +/- 1.7 minutes and 22.8 +/- 1.6 min, respectively (30 cells). Kin1, Shk1, and Pck1 arrive at 11.6 +/- 0.7 min (18 cells), 13.0 +/- 1.6 min (12 cells), and 26.1 +/- 1.1 min (11 cells), respectively.

APPENDIX

A. MATERIALS AND METHODS

Yeast methods

S. pombe strains were grown in yeast extract with supplements (YES), YES without additional adenine, or Edinburgh Minimal Media (EMM) plus selective supplements (Moreno et al., 1991; Forsburg and Rhind, 2006). Transformation of yeast with plasmid or linear DNA was accomplished using electroporation (Forsburg and Rhind, 2006) or lithium acetate methods (Keeney and Boeke, 1994; Forsburg and Rhind, 2006), respectively.

For integration of *cdc15* alleles at the endogenous locus, *cdc15*$^+$*/cdc15::ura4*$^+$ was transformed with pIRT2 vector with the desired *cdc15* allele plus *cdc15* 5′ and 3′ noncoding regions (Roberts-Galbraith et al., 2009). Spores were germinated on selective medium to select for *cdc15::ura4*$^+$ haploids that have the vector. Haploid integrants were recovered based on resistance to 5-fluorourotic acid (FOA) and integration and loss of vector was verified by growth on selective media, PCR and/or microscopy, and finally sequencing.

To confirm lethality of *cdc15* mutants, the *ura4*$^+$ cassette in a *cdc15*$^+$*/cdc15::ura4*$^+$ diploid strain was replaced with a cassette consisting of 500 bp 5' *cdc15*$^+$ flanking region, the mutant *cdc15* coding sequence, *kan*^{R}, and 500 bp 3' *cdc15*$^+$ flanking region. Integrants resistant to 5-FOA and G418 were selected and confirmed by whole-cell PCR before sporulation and tetrad dissection.

For integration of *pxl1* alleles at the endogenous locus, *pxl1::ura4*$^+$ was transformed with a cassette consisting of 500 bp 5' *pxl1*$^+$ flanking region, the desired *pxl1* coding sequence, *kan*^{R}, and 500 bp 3' *pxl1*$^+$ flanking region. Spores were germinated on selective medium to select for *cdc15::ura4*$^+$ haploids that have the vector. Integrants were recovered based on resistance to 5-fluorourotic acid and G418.

For integration of the *pxl1(N)-ppb1* fusion at the *ppb1* locus, *ppb1::ura4*$^+$ was transformed with a cassette consisting of 300 bp 5' *ppb1*$^+$ flanking region, *pxl1(nt 1-771)-ppb1*$^+$ coding sequence, *kan*^{R}, and 500 bp 3' *pxl1*$^+$ flanking region. Spores were germinated on selective medium to select for *cdc15::ura4*$^+$ haploids that have the vector. Integrants were recovered based on resistance to 5-fluorourotic acid and G418.

Genes were tagged at *the* 3′ end of their ORFs with mNG:*kan*^{R}, mNG:*hyg*^{R}, or mCherry:*nat*^{R} using pFA6 cassettes as previously described (Wach et al., 1994; Bahler et al., 1998b; Willet et al., 2015a). Integration of tags was verified using whole-cell PCR and/or microscopy.

Introduction of tagged loci or mutants into other genetic backgrounds was accomplished using standard *S. pombe* mating, sporulation, and tetrad dissection techniques.

For growth assays, cells were grown to log phase at 25°C in YES medium. $40x10^6$ cells/ml YES suspension was serially diluted 10-fold and three µl of each dilution were spotted to YES plates for growth at indicated temperatures.

For block-and-release using the *cdc25-22* background, cells were arrested in G2 by shifting to the restrictive temperature (36°C) for 3.5-4 hours and then released back into the cell cycle by shifting to the permissive temperature (25°C). 25 OD Pellets were

collected at the time of release (0 minutes) and at subsequent time points as indicated. Additionally, cells were fixed in ice-cold 70% ethanol for subsequent staining with DAPI and Methyl Blue to visualize nuclei and septa, respectively. To test if calcineurin regulates Pxl1, a cell culture was blocked-and-released as described. After collecting the time 0 pellet, the culture was split into two cultures. One culture was treated with FK506 and the other was treated with DMSO as a vehicle control at time 30 after release.

To inhibit Pom1^{as} *in vivo*, cells were grown in YE at 32°C to mid-log phase and then treated with 4-Amino-1-tert-butyl-3-(3-methylbenzyl)pyrazolo[3,4-3]pyrimidine (3MB-PP1) (Toronto Research Chemical; A602960 or Cayman Chemical; 17860) at a final concentration of 1 µg/ml for 2 hours. Vehicle-treated cells were grown in equal volume of DMSO (Sigma; D2650).

Molecular biology

GST-Pom1 was described previously (Hachet et al., 2011). All other expression and integration vectors were constructed using standard molecular biology techniques. Mutations were made with a QuikChange Multi-lightning mutagenesis kit (Agilent Technolgoies). All constructs were sequenced for verification.

cdc15 plasmids were created by amplifying *cdc15* fragments by PCR from pKG4456 (Roberts-Galbraith et al., 2009) and subsequent cloning into pIRT2 for integration at the endogenous locus (Roberts-Galbraith et al., 2009). Mutations were made in pIRT2 vectors with a QuikChange Multi-lightning mutagenesis kit (Agilent Technolgoies). All constructs were sequenced for verification.

A C-terminal fragment (amino acids 441-stop) was amplified by PCR from an *S. pombe* cDNA library and cloned into pMal-c2 vectors using EcoRI and BamHI sites. An N-terminal fragment (amino acids 1-460) was amplified by PCR from pIRT plasmids containing *cdc15* wildtype (pKG4456) or mutant coding sequences pKG4827) (Roberts-Galbraith et al., 2010). Gibson assembly (Gibson et al., 2009) was used to clone inserts into pMal-c2 digested with BamHI and EcoRI. Vectors were sequenced.

Microscopy methods

Except as noted, images of *S. pombe* cells were acquired using a Personal DeltaVision (GE Healthcare, Issaquah, WA) that includes an Olympus IX71 microscope, 60× NA 1.42 Plan Apochromat and 100× NA 1.40 U Plan S Apochromat objectives, fixed and live-cell filter wheels, a Photometrics CoolSnap HQ2 camera, and softWoRx imaging software (Applied Precision).

For live-cell fluorescence imaging strains were grown overnight to log phase in YES media at 25°C in a shaking water bath. Cells were imaged in YES media at 23–29°C.

Time-lapse imaging was performed using an ONIX microfluidics perfusion system (CellASIC ONIX, EMD Millipore). 50 µl of 40x10^6 cells/ml YES suspension was loaded into Y04C plates for 5 s at 8 psi. YES medium flowed into the chamber at 5 psi throughout imaging. Time-lapse images were obtained at 2-min intervals. Representative fluorescence images are maximum-intensity or sum projections of z sections spaced at 0.2-0.5 µm that have been deconvolved with 10 iterations.

End-on images were acquired with a spinning disk system, which includes a Zeiss Axiovert200m microscope, Yokogawa CSU-22, 63X NA 1.46 planApochromat and 100X numerical aperture (NA) 1.40 PlanApo oil immersion objectives, and Hamamatsu

ImageEM-X2 camera. Cells grown to log-phase in EMM plus adenine, uracil and leucine and loaded to vertical chambers in a 4% MAUL agarose pad and imaged every 2 min. 6 z-slices at 0.5 µm intervals around the middle of the cell were acquired at each time point.

For Figure 14, time-lapse images were acquired with a Nikon spinning disk system, which incorporates a Yokogawa CSU-X1 spinning disk head, Andor DU-897 EMCCD, high-speed piezo [z] stage, a four-line high-power solid state laser launch, and a Plan Apo Lambda (oil) 60x 1.40 NA WD 0.13mm. Cells were mounted on 2% MAUL agarose pads. Images were acquired every 2 min. 15 z-slices at 0.4 µm intervals were acquired at each time point. Sum projections were analyzed and used for representative images. Sum projections were corrected for background fluorescence before quantitation.

To visualize nuclei and septa, cells were grown to log phase at 32°C and fixed with ice-cold 70% ethanol at 4°C for at least 30 min. Approximately 0.5 OD of fixed cells were washed once with PBS pH 7.5 and then incubated in 50 µl 1 mg/ml Methyl Blue (Sigma; M6900) for 30 min at RT. MB-stained cells were concentrated by centrifugation and mixed with 5 µg/ml DAPI (Sigma; D9542) in 1:1 ratio immediately prior to imaging.

For visualizing tip septa, approximately 0.5 OD of fixed cells were washed once with PBS, pH 7.5 and then resuspended in 20 µl of 50 µg/ml Calcofluor White (Sigma; 18909) and incubated at room temperature for 5 minutes. Then, cells were washed once with PBS and imaged immediately.

Image analysis was performed using ImageJ software (Schindelin et al., 2012).

Protein methods

Cell pellets were snap-frozen in dry ice–ethanol baths. Denatured lysates were prepared by bead disruption (Fastprep cell homogenizer; MP Biomedicals) in NP-40 buffer containing SDS as previously described (Gould *et al.*, 1991), except with the addition of 0.5 mM diisopropyl fluorophosphates (Sigma-Aldrich). Additionally, any studies of Pxl1 excluding chelators (e.g. EDTA).

For immunoprecipitation and lambda phosphatase collapse, lysates were incubated with anti-Cdc15 (Roberts-Galbraith et al., 2009) or anti-HA (12CA5) and Protein A magnetic beads or sepharose (GE Healthcare; 17-5280-04) for 2 h at 4°C. Beads were washed three times with NP-40 buffer and two times with phosphatase buffer (150 mM NaCl, 50 mM Hepes pH 7.4) before being split in two and added to either lambda phosphatase reaction or control. Lambda phosphatase collapse was performed according to manufacturer's protocol (New England Biolabs; P0753). Reactions were stopped by the addition of sample buffer.

Protein samples were resolved by SDS-PAGE and transferred to polyvinylidene fluoride (PVDF) membrane (Immobilon P, EMD Millipore). Anti-α-tubulin (B512) mouse monoclonal antibody (Sigma-Aldrich), anti-Cdc2 (PSTAIRE) mouse monoclonal antibody (Sigma-Aldrich; P7962), anti-HA rabbit monoclonal (12CA5), or anti-Cdc15(1-405) rabbit polyclonal antibody (Roberts-Galbraith *et al.*, 2009) were used in immunoprecipitations and/or as primary antibodies in immunoblotting. Secondary antibodies were conjugated to IRDye800 or IRDye680 (LI-COR Biosciences). Blotted proteins were detected via an Odyssey machine (LI-COR Biosciences).

Recombinant protein purification

Glutathione-S-transferase (GST) and maltose binding protein (MBP) fusion proteins were produced in *Escherichia coli* Rosetta2(DE3)pLysS cells. Bacteria were grown in Terrific Broth media (Tartoff and Hobbs, 1987) with antibiotics to log-phase (OD_{595} 1-1.5) at 36°C. Then, induction was initiated by incubating for 15 minutes on ice before adding 0.4 mM IPTG (Fisher Scientific; BP1755). Protein was produced for 16-18 hours at 18°C.

Frozen cell pellets were lysed in either MBP buffer (20 mM Tris-HCl pH 7.4, 150 mM NaCl, 1 mM EDTA, 1 mM DTT) or GST buffer (4.3 mM $NaHPO_4$, 137 mM NaCl, 2.7 mM KCl, 1 mM DTT) with the addition of 200 µg/ml lysozyme (Sigma-Aldrich; L6876), cOmplete™ EDTA-free protease inhibitor cocktail (Roche), and 0.1% NP-40 (US Biologicals; N3500). For purifying Pxl1, all buffers were modified to exclude chelators (i.e. EDTA). Continuous agitation on ice for 20 minutes was used to suspend the cell pellet. Then, lysates were sonicated three times for 30 seconds, with at least 30 seconds pause between sonications (Sonic Dismembrator Model F60, Fisher Scientific; power 15 watts). Lysates were cleared for 15-30 minutes at 10-13K rpm.

Cleared lysate was then used in a batch purification protocol by adding to either amylose (New England Biolabs, Inc.; E8021L) or GST-bind (EMD Millipore; 70541) resin for 2 hours at 4°C. Then, resin was washed three times for 5 minutes at 4°C with the appropriate buffer. To elute proteins from beads, dry beads were resuspended in equal volume of appropriate elution buffer and nutated for 30 minutes at 4°C. MBP fusion proteins were eluted in MBP buffer supplemented with 10 mM maltose (Fisher Scientific; M75-100) and GST proteins were eluted in GST elution buffer (50 mM Tris-HCl pH 8, 10 mM glutathione (Sigma-Aldrich; G4251). The supernatant was separated from the resin to a fresh tube. 100 mM NaCl was added to GST fusion proteins. Eluted fusion proteins were then aliquoted, snap frozen, and stored at -80°C.

Protein concentration was calculated from Coomassie Brilliant Blue G (Sigma-Aldrich; B0770) staining of SDS-PAGE-separated purified proteins and Bovine Serum Albumin (BSA) standards (Sigma-Aldrich).

In vitro kinase assays

Radioactive *in vitro* kinase assays were performed in 30 mM Tris pH 8, 100 mM NaCl, 10 mM MgCl2, 1 mM EGTA, 10% glycerol, 1 mM DTT, 10 µM ATP, and 2 µCi [^{32}P]-ATP (PerkinElmer BLU002250UC) with 0.5 µg GST-Pom1 and 2 µg substrate in a 25 µl reaction. After 30-min at 30°C, reaction was stopped by boiling in sample buffer and analyzed by SDS-PAGE. Inputs were detected by Coomassie Blue (Sigma-Aldrich; B0770) and ^{32}P incorporation was detected by autoradiography.

Cold kinase assays for the identification of phosphorylation sites were performed the same way except without hot ATP, with 40 mM ATP, and in 1 µl final volume. A second dose of GST-Pom1 was added after 45 min and the reaction arrested after 90 min.

Phosphoaminoacid analysis

In vitro kinase assays were performed as described above, except that after SDS-PAGE proteins were transferred to PVDF membranes (Immobilon P; EMD Millipore). Proteins were visualized by staining membrane with REVERT™ Total Protein stain (LI-COR Biosciences). Then, bands corresponding to the substrate were cut from the

membrane. Membrane-bound proteins were subjected to partial acid hydrolysis using boiling 6M HCl for 1 hr. Hydrolyzed amino acids were separated by two-dimensional thin-layer electrophoresis (van der Geer and Hunter, 1994).

Phosphorylation site identification by mass spectrometry

TCA-precipitated proteins were digested and analyzed by two-dimensional liquid chromatography/tandem mass spectrometry as described previously (Chen et al., 2013), except that the following modifications were made. Proteins were digested by trypsin, chymotrypsin, and elastase. The number of salt elution steps was reduced to 6 (i.e., 0, 25, 50, 100, 600, 1000, and 5000 mM ammonium acetate). Peptide identifications were filtered and assembled using Scaffold (version 4.8.4; Proteome Software) and phosphorylation sites were analyzed using Scaffold PTM (version 3.1.0) using the following filters: minimum of 99% protein identification probability, minimum of five unique peptides, minimum of 95% peptide identification probability.

Statistical analysis

Statistical analysis was performed using Prism (GraphPad).

REFERENCES

Aggen, J.B., Nairn, A.C., and Chamberlin, R. (2000). Regulation of protein phosphatase-1. Chemistry & biology 7, R13-R23.

Ahmed, S., Bu, W., Lee, R.T., Maurer-Stroh, S., and Goh, W.I. (2010). F-BAR domain proteins: Families and function. Commun Integr Biol 3, 116-121.

Akamatsu, M., Berro, J., Pu, K.M., Tebbs, I.R., and Pollard, T.D. (2014). Cytokinetic nodes in fission yeast arise from two distinct types of nodes that merge during interphase. J Cell Biol 204, 977-988.

Almonacid, M., Celton-Morizur, S., Jakubowski, J.L., Dingli, F., Loew, D., Mayeux, A., Chen, J.S., Gould, K.L., Clifford, D.M., and Paoletti, A. (2011). Temporal control of contractile ring assembly by Plo1 regulation of myosin II recruitment by Mid1/anillin. Curr Biol 21, 473-479.

Almonacid, M., and Paoletti, A. (2010). Mechanisms controlling division-plane positioning. Seminars in cell & developmental biology 21, 874-880.

Arasada, R., and Pollard, T.D. (2011). Distinct roles for F-BAR proteins Cdc15p and Bzz1p in actin polymerization at sites of endocytosis in fission yeast. Curr Biol 21, 1450-1459.

Arasada, R., and Pollard, T.D. (2014). Contractile ring stability in S. pombe depends on F-BAR protein Cdc15p and Bgs1p transport from the Golgi complex. Cell Rep 8, 1533-1544.

Arellano, M., Duran, A., and Perez, P. (1996). Rho 1 GTPase activates the (1-3)beta-D-glucan synthase and is involved in Schizosaccharomyces pombe morphogenesis. The EMBO journal 15, 4584-4591.

Arellano, M., Valdivieso, M.H., Calonge, T.M., Coll, P.M., Duran, A., and Perez, P. (1999). Schizosaccharomyces pombe protein kinase C homologues, pck1p and pck2p, are targets of rho1p and rho2p and differentially regulate cell integrity. Journal of Cell Science 112, 3569-3578.

Bahler, J., and Pringle, J.R. (1998). Pom1p, a fission yeast protein kinase that provides positional information for both polarized growth and cytokinesis. Genes Dev 12, 1356-1370.

Bahler, J., Steever, A.B., Wheatley, S., Wang, Y., Pringle, J.R., Gould, K.L., and McCollum, D. (1998a). Role of polo kinase and Mid1p in determining the site of cell division in fission yeast. J Cell Biol 143, 1603-1616.

Bahler, J., Wu, J.Q., Longtine, M.S., Shah, N.G., McKenzie, A., 3rd, Steever, A.B., Wach, A., Philippsen, P., and Pringle, J.R. (1998b). Heterologous modules for efficient

and versatile PCR-based gene targeting in Schizosaccharomyces pombe. Yeast 14, 943-951.

Bai, X., Meng, G., Luo, M., and Zheng, X. (2012). Rigidity of wedge loop in PACSIN 3 protein is a key factor in dictating diameters of tubules. J Biol Chem 287, 22387-22396.

Bai, X., and Zheng, X. (2013). Tip-to-tip interaction in the crystal packing of PACSIN 2 is important in regulating tubulation activity. Protein Cell 4, 695-701.

Balasubramanian, M.K. (2016). Exploring the diversity of cytokinesis. Seminars in cell & developmental biology 53, 1.

Balasubramanian, M.K., McCollum, D., Chang, L., Wong, K.C., Naqvi, N.I., He, X., Sazer, S., and Gould, K.L. (1998). Isolation and characterization of new fission yeast cytokinesis mutants. Genetics 149, 1265-1275.

Bathe, M., and Chang, F. (2010). Cytokinesis and the contractile ring in fission yeast: towards a systems-level understanding. Trends Microbiol 18, 38-45.

Beach, Jordan R., Shao, L., Remmert, K., Li, D., Betzig, E., and Hammer, John A. (2014). Nonmuscle Myosin II Isoforms Coassemble in Living Cells. Current Biology 24, 1160-1166.

Begonja, A.J., Pluthero, F.G., Suphamungmee, W., Giannini, S., Christensen, H., Leung, R., Lo, R.W., Nakamura, F., Lehman, W., Plomann, M., Hoffmeister, K.M., Kahr, W.H., Hartwig, J.H., and Falet, H. (2015). FlnA binding to PACSIN2 F-BAR domain regulates membrane tubulation in megakaryocytes and platelets. Blood 126, 80-88.

Betzig, E., Patterson, G.H., Sougrat, R., Lindwasser, O.W., Olenych, S., Bonifacino, J.S., Davidson, M.W., Lippincott-Schwartz, J., and Hess, H.F. (2006). Imaging intracellular fluorescent proteins at nanometer resolution. Science 313, 1642-1645.

Bezanilla, M., Forsburg, S.L., and Pollard, T.D. (1997). Identification of a second myosin-II in Schizosaccharomyces pombe: Myp2p is conditionally required for cytokinesis. Mol Biol Cell 8, 2693-2705.

Bezanilla, M., and Pollard, T.D. (2000). Myosin-II tails confer unique functions in Schizosaccharomyces pombe: characterization of a novel myosin-II tail. Mol Biol Cell 11, 79-91.

Bhatia, P., Hachet, O., Hersch, M., Rincon, S.A., Berthelot-Grosjean, M., Dalessi, S., Basterra, L., Bergmann, S., Paoletti, A., and Martin, S.G. (2014). Distinct levels in Pom1 gradients limit Cdr2 activity and localization to time and position division. Cell Cycle 13, 538-552.

Bhavsar-Jog, Y.P., and Bi, E. (2017). Mechanics and regulation of cytokinesis in budding yeast. Seminars in cell & developmental biology 66, 107-118.

Billington, N., Wang, A., Mao, J., Adelstein, R.S., and Sellers, J.R. (2013). Characterization of three full-length human nonmuscle myosin II paralogs. Journal of Biological Chemistry.

Bloom, J., Cristea, I.M., Procko, A.L., Lubkov, V., Chait, B.T., Snyder, M., and Cross, F.R. (2011). Global analysis of Cdc14 phosphatase reveals diverse roles in mitotic processes. J Biol Chem 286, 5434-5445.

Bohnert, K.A., and Gould, K.L. (2012). Cytokinesis-based constraints on polarized cell growth in fission yeast. PLoS Genet 8, e1003004.

Bohnert, K.A., Grzegorzewska, A.P., Willet, A.H., Vander Kooi, C.W., Kovar, D.R., and Gould, K.L. (2013). SIN-dependent phosphoinhibition of formin multimerization controls fission yeast cytokinesis. Genes Dev 27, 2164-2177.

Bouchoux, C., and Uhlmann, F. (2011). A quantitative model for ordered Cdk substrate dephosphorylation during mitotic exit. Cell 147, 803-814.

Burki, F. (2014). The eukaryotic tree of life from a global phylogenomic perspective. Cold Spring Harbor perspectives in biology 6, a016147.

Carnahan, R.H., and Gould, K.L. (2003). The PCH family protein, Cdc15p, recruits two F-actin nucleation pathways to coordinate cytokinetic actin ring formation in Schizosaccharomyces pombe. J Cell Biol 162, 851-862.

Carpy, A., Krug, K., Graf, S., Koch, A., Popic, S., Hauf, S., and Macek, B. (2014). Absolute proteome and phosphoproteome dynamics during the cell cycle of Schizosaccharomyces pombe (Fission Yeast). Molecular & cellular proteomics : MCP 13, 1925-1936.

Carvalho, A., Desai, A., and Oegema, K. (2009). Structural memory in the contractile ring makes the duration of cytokinesis independent of cell size. Cell 137, 926-937.

Celton-Morizur, S., Racine, V., Sibarita, J.B., and Paoletti, A. (2006). Pom1 kinase links division plane position to cell polarity by regulating Mid1p cortical distribution. J Cell Sci 119, 4710-4718.

Chang, F., Drubin, D., and Nurse, P. (1997). cdc12p, a protein required for cytokinesis in fission yeast, is a component of the cell division ring and interacts with profilin. J Cell Biol 137, 169-182.

Chang, F., Woollard, A., and Nurse, P. (1996). Isolation and characterization of fission yeast mutants defective in the assembly and placement of the contractile actin ring. J Cell Sci 109 (Pt 1), 131-142.

Chen, J.S., Beckley, J.R., McDonald, N.A., Ren, L., Mangione, M., Jang, S.J., Elmore, Z.C., Rachfall, N., Feoktistova, A., Jones, C.M., Willet, A.H., Guillen, R., Bitton, D.A., Bahler, J., Jensen, M.A., Rhind, N., and Gould, K.L. (2015). Identification of new players

in cell division, DNA damage response, and morphogenesis through construction of Schizosaccharomyces pombe deletion strains. G3 (Bethesda) 5, 361-370.

Chen, J.S., Beckley, J.R., Ren, L., Feoktistova, A., Jensen, M.A., Rhind, N., and Gould, K.L. (2016). Discovery of genes involved in mitosis, cell division, cell wall integrity and chromosome segregation through construction of Schizosaccharomyces pombe deletion strains. Yeast 33, 507-517.

Chen, J.S., Broadus, M.R., McLean, J.R., Feoktistova, A., Ren, L., and Gould, K.L. (2013). Comprehensive proteomics analysis reveals new substrates and regulators of the fission yeast clp1/cdc14 phosphatase. Molecular & cellular proteomics : MCP 12, 1074-1086.

Clifford, D.M., Chen, C.T., Roberts, R.H., Feoktistova, A., Wolfe, B.A., Chen, J.S., McCollum, D., and Gould, K.L. (2008a). The role of Cdc14 phosphatases in the control of cell division. Biochemical Society transactions 36, 436-438.

Clifford, D.M., Wolfe, B.A., Roberts-Galbraith, R.H., McDonald, W.H., Yates, J.R., 3rd, and Gould, K.L. (2008b). The Clp1/Cdc14 phosphatase contributes to the robustness of cytokinesis by association with anillin-related Mid1. J Cell Biol 181, 79-88.

Cortes, J.C., Carnero, E., Ishiguro, J., Sanchez, Y., Duran, A., and Ribas, J.C. (2005). The novel fission yeast (1,3)beta-D-glucan synthase catalytic subunit Bgs4p is essential during both cytokinesis and polarized growth. J Cell Sci 118, 157-174.

Cortes, J.C., Pujol, N., Sato, M., Pinar, M., Ramos, M., Moreno, B., Osumi, M., Ribas, J.C., and Perez, P. (2015). Cooperation between Paxillin-like Protein Pxl1 and Glucan Synthase Bgs1 Is Essential for Actomyosin Ring Stability and Septum Formation in Fission Yeast. PLoS Genet 11, e1005358.

Cundell, M.J., Bastos, R.N., Zhang, T., Holder, J., Gruneberg, U., Novak, B., and Barr, F.A. (2013). The BEG (PP2A-B55/ENSA/Greatwall) pathway ensures cytokinesis follows chromosome separation. Mol Cell 52, 393-405.

Daga, R.R., and Chang, F. (2005). Dynamic positioning of the fission yeast cell division plane. Proc Natl Acad Sci U S A 102, 8228-8232.

Daughdrill, G.W., Narayanaswami, P., Gilmore, S.H., Belczyk, A., and Brown, C.J. (2007). Dynamic behavior of an intrinsically unstructured linker domain is conserved in the face of negligible amino acid sequence conservation. J Mol Evol 65, 277-288.

Davidson, R., Pontasch, J.A., and Wu, J.Q. (2016). Sbg1 Is a Novel Regulator for the Localization of the beta-Glucan Synthase Bgs1 in Fission Yeast. PloS one 11, e0167043.

Davies, T., Kim, H.X., Romano Spica, N., Lesea-Pringle, B.J., Dumont, J., Shirasu-Hiza, M., and Canman, J.C. (2018). Cell-intrinsic and -extrinsic mechanisms promote cell-type-specific cytokinetic diversity. Elife 7.

Dawson, J.F., and Holmes, C.F. (1999). Identification of sds21 in fission yeast in an inhibitor-resistant high molecular mass protein phosphatase-1 complex. Biochemistry and cell biology = Biochimie et biologie cellulaire 77, 551-558.

De Wulf, P., Montani, F., and Visintin, R. (2009). Protein phosphatases take the mitotic stage. Curr Opin Cell Biol 21, 806-815.

Dean, S.O., Rogers, S.L., Stuurman, N., Vale, R.D., and Spudich, J.A. (2005). Distinct pathways control recruitment and maintenance of myosin II at the cleavage furrow during cytokinesis. Proc Natl Acad Sci U S A 102, 13473-13478.

Demeter, J., and Sazer, S. (1998). imp2, a new component of the actin ring in the fission yeast Schizosaccharomyces pombe. J Cell Biol 143, 415-427.

Dix, C.L., Matthews, H.K., Uroz, M., McLaren, S., Wolf, L., Heatley, N., Win, Z., Almada, P., Henriques, R., Boutros, M., Trepat, X., and Baum, B. (2018). The Role of Mitotic Cell-Substrate Adhesion Re-modeling in Animal Cell Division. Developmental cell 45, 132-145.e133.

Dosztanyi, Z., Meszaros, B., and Simon, I. (2009). ANCHOR: web server for predicting protein binding regions in disordered proteins. Bioinformatics 25, 2745-2746.

Dunker, A.K., Bondos, S.E., Huang, F., and Oldfield, C.J. (2015). Intrinsically disordered proteins and multicellular organisms. Seminars in cell & developmental biology 37, 44-55.

Eggert, U.S., Mitchison, T.J., and Field, C.M. (2006a). Animal Cytokinesis: From Parts List to Mechanisms. Annual Review of Biochemistry 75, 543-566.

Eggert, U.S., Mitchison, T.J., and Field, C.M. (2006b). Animal cytokinesis: from parts list to mechanisms. Annual review of biochemistry 75, 543-566.

Egloff, M.-P., Johnson, D.F., Moorhead, G., Cohen, P.T.W., Cohen, P., and Barford, D. (1997). Structural basis for the recognition of regulatory subunits by the catalytic subunit of protein phosphatase 1. The EMBO journal 16, 1876-1887.

Eng, K., Naqvi, N.I., Wong, K.C., and Balasubramanian, M.K. (1998). Rng2p, a protein required for cytokinesis in fission yeast, is a component of the actomyosin ring and the spindle pole body. Curr Biol 8, 611-621.

Ennomani, H., Letort, G., Guerin, C., Martiel, J.L., Cao, W., Nedelec, F., De La Cruz, E.M., Thery, M., and Blanchoin, L. (2016). Architecture and Connectivity Govern Actin Network Contractility. Curr Biol 26, 616-626.

Fankhauser, C., Reymond, A., Cerutti, L., Utzig, S., Hofmann, K., and Simanis, V. (1995). The S. pombe cdc15 gene is a key element in the reorganization of F-actin at mitosis. Cell 82, 435-444.

Farr, H., and Gull, K. (2012). Cytokinesis in trypanosomes. Cytoskeleton (Hoboken) 69, 931-941.

Fenix, A.M., Taneja, N., Buttler, C.A., Lewis, J., Van Engelenburg, S.B., Ohi, R., and Burnette, D.T. (2016). Expansion and concatenation of non-muscle myosin IIA filaments drive cellular contractile system formation during interphase and mitosis. Mol Biol Cell.

Fishkind, D.J., and Wang, Y.L. (1993). Orientation and three-dimensional organization of actin filaments in dividing cultured cells. The Journal of Cell Biology 123, 837-848.

Foltman, M., Molist, I., Arcones, I., Sacristan, C., Filali-Mouncef, Y., Roncero, C., and Sanchez-Diaz, A. (2016). Ingression Progression Complexes Control Extracellular Matrix Remodelling during Cytokinesis in Budding Yeast. PLOS Genetics 12, e1005864.

Forsburg, S.L., and Rhind, N. (2006). Basic methods for fission yeast. Yeast 23, 173-183.

Fricke, R., Gohl, C., and Bogdan, S. (2010). The F-BAR protein family Actin' on the membrane. Commun Integr Biol 3, 89-94.

Friend, J.E., Sayyad, W.A., Arasada, R., McCormick, C.D., Heuser, J.E., and Pollard, T.D. (2018). Fission yeast Myo2: Molecular organization and diffusion in the cytoplasm. Cytoskeleton (Hoboken) 75, 164-173.

Frost, A., De Camilli, P., and Unger, V.M. (2007). F-BAR proteins join the BAR family fold. Structure 15, 751-753.

Frost, A., Unger, V.M., and De Camilli, P. (2009). The BAR domain superfamily: membrane-molding macromolecules. Cell 137, 191-196.

Garabedian, M.V., Stanishneva-Konovalova, T., Lou, C., Rands, T.J., Pollard, L.W., Sokolova, O.S., and Goode, B.L. (2018). Integrated control of formin-mediated actin assembly by a stationary inhibitor and a mobile activator. J Cell Biol 217, 3512-3530.

García Cortés, J.C., Ramos, M., Osumi, M., Pérez, P., and Ribas, J.C. (2016). The Cell Biology of Fission Yeast Septation. Microbiol Mol Biol Rev 80, 779-791.

Gawlitta, W., and Stockem, W. (1981). Visualization of actin polymerization and depolymerization cycles during polyamine-induced cytokinesis in living Amoeba proteus. Cell and tissue research 215, 249-261.

Ge, W., and Balasubramanian, M.K. (2008). Pxl1p, a paxillin-related protein, stabilizes the actomyosin ring during cytokinesis in fission yeast. Mol Biol Cell 19, 1680-1692.

Gibson, D.G., Young, L., Chuang, R.-Y., Venter, J.C., Hutchison Iii, C.A., and Smith, H.O. (2009). Enzymatic assembly of DNA molecules up to several hundred kilobases. Nature Methods 6, 343.

Glotzer, M. (2017). Cytokinesis in Metazoa and Fungi. Cold Spring Harb Perspect Biol 9.

Goh, S.L., Wang, Q., Byrnes, L.J., and Sondermann, H. (2012). Versatile membrane deformation potential of activated pacsin. PloS one 7, e51628.

Goss, J.W., Kim, S., Bledsoe, H., and Pollard, T.D. (2014). Characterization of the roles of Blt1p in fission yeast cytokinesis. Mol Biol Cell 25, 1946-1957.

Gouw, M., Michael, S., Samano-Sanchez, H., Kumar, M., Zeke, A., Lang, B., Bely, B., Chemes, L.B., Davey, N.E., Deng, Z., Diella, F., Gurth, C.M., Huber, A.K., Kleinsorg, S., Schlegel, L.S., Palopoli, N., Roey, K.V., Altenberg, B., Remenyi, A., Dinkel, H., and Gibson, T.J. (2018). The eukaryotic linear motif resource - 2018 update. Nucleic acids research 46, D428-d434.

Grallert, A., Boke, E., Hagting, A., Hodgson, B., Connolly, Y., Griffiths, J.R., Smith, D.L., Pines, J., and Hagan, I.M. (2015). A PP1-PP2A phosphatase relay controls mitotic progression. Nature 517, 94-98.

Gu, Y., and Oliferenko, S. (2015). Comparative biology of cell division in the fission yeast clade. Current Opinion in Microbiology 28, 18-25.

Gustafsson, M.G.L., Shao, L., Carlton, P.M., Wang, C.J.R., Golubovskaya, I.N., Cande, W.Z., Agard, D.A., and Sedat, J.W. (2008). Three-Dimensional Resolution Doubling in Wide-Field Fluorescence Microscopy by Structured Illumination. Biophysical Journal 94, 4957-4970.

Guzman-Vendrell, M., Baldissard, S., Almonacid, M., Mayeux, A., Paoletti, A., and Moseley, J.B. (2013). Blt1 and Mid1 provide overlapping membrane anchors to position the division plane in fission yeast. Molecular and cellular biology 33, 418-428.

Hachet, O., Berthelot-Grosjean, M., Kokkoris, K., Vincenzetti, V., Moosbrugger, J., and Martin, S.G. (2011). A phosphorylation cycle shapes gradients of the DYRK family kinase Pom1 at the plasma membrane. Cell 145, 1116-1128.

Hachet, O., and Simanis, V. (2008). Mid1p/anillin and the septation initiation network orchestrate contractile ring assembly for cytokinesis. Genes Dev 22, 3205-3216.

Hansen, C.G., Howard, G., and Nichols, B.J. (2011). Pacsin 2 is recruited to caveolae and functions in caveolar biogenesis. J Cell Sci 124, 2777-2785.

Harasimov, K., and Schuh, M. (2018). Actin Disassembly: How to Contract without Motors? Current Biology 28, R275-R277.

Hardin, W.R., Li, R., Xu, J., Shelton, A.M., Alas, G.C.M., Minin, V.N., and Paredez, A.R. (2017). Myosin-independent cytokinesis in Giardia utilizes flagella to coordinate force generation and direct membrane trafficking. Proc Natl Acad Sci U S A 114, E5854-E5863.

Hayles, J., Wood, V., Jeffery, L., Hoe, K.L., Kim, D.U., Park, H.O., Salas-Pino, S., Heichinger, C., and Nurse, P. (2013). A genome-wide resource of cell cycle and cell shape genes of fission yeast. Open biology 3, 130053.

Henne, W.M., Kent, H.M., Ford, M.G., Hegde, B.G., Daumke, O., Butler, P.J., Mittal, R., Langen, R., Evans, P.R., and McMahon, H.T. (2007). Structure and analysis of FCHo2 F-BAR domain: a dimerizing and membrane recruitment module that effects membrane curvature. Structure 15, 839-852.

Henson, J.H., Ditzler, C.E., Germain, A., Irwin, P.M., Vogt, E.T., Yang, S., Wu, X., and Shuster, C.B. (2017). The ultrastructural organization of actin and myosin II filaments in the contractile ring: new support for an old model of cytokinesis. Mol Biol Cell 28, 613-623.

Hess, S.T., Girirajan, T.P., and Mason, M.D. (2006). Ultra-high resolution imaging by fluorescence photoactivation localization microscopy. Biophys J 91, 4258-4272.

Himpel, S., Tegge, W., Frank, R., Leder, S., Joost, H.G., and Becker, W. (2000). Specificity determinants of substrate recognition by the protein kinase DYRK1A. J Biol Chem 275, 2431-2438.

Hollopeter, G., Lange, J.J., Zhang, Y., Vu, T.N., Gu, M., Ailion, M., Lambie, E.J., Slaughter, B.D., Unruh, J.R., Florens, L., and Jorgensen, E.M. (2014). The membrane-associated proteins FCHo and SGIP are allosteric activators of the AP2 clathrin adaptor complex. eLife 3, e03648.

Holt, L.J., Tuch, B.B., Villen, J., Johnson, A.D., Gygi, S.P., and Morgan, D.O. (2009). Global analysis of Cdk1 substrate phosphorylation sites provides insights into evolution. Science 325, 1682-1686.

Huang, Y., Chew, T.G., Ge, W., and Balasubramanian, M.K. (2007). Polarity determinants Tea1p, Tea4p, and Pom1p inhibit division-septum assembly at cell ends in fission yeast. Dev Cell 12, 987-996.

Huang, Y., Yan, H., and Balasubramanian, M.K. (2008). Assembly of normal actomyosin rings in the absence of Mid1p and cortical nodes in fission yeast. J Cell Biol 183, 979-988.

Itoh, T., and De Camilli, P. (2006). BAR, F-BAR (EFC) and ENTH/ANTH domains in the regulation of membrane-cytosol interfaces and membrane curvature. Biochim Biophys Acta 1761, 897-912.

Itoh, T., Hasegawa, J., Tsujita, K., Kanaho, Y., and Takenawa, T. (2009). The tyrosine kinase Fer is a downstream target of the PLD-PA pathway that regulates cell migration. Sci Signal 2, ra52.

Jahan, M.G.S., and Yumura, S. (2017). Traction force and its regulation during cytokinesis in Dictyostelium cells. European Journal of Cell Biology 96, 515-528.

JC, G.C., Ramos, M., Konomi, M., Barragan, I., Moreno, M.B., Alcaide-Gavilan, M., Moreno, S., Osumi, M., Perez, P., and Ribas, J.C. (2018). Specific detection of fission yeast primary septum reveals septum and cleavage furrow ingression during early anaphase independent of mitosis completion. PLoS Genet 14, e1007388.

Johnson, A.E., McCollum, D., and Gould, K.L. (2012). Polar opposites: Fine-tuning cytokinesis through SIN asymmetry. Cytoskeleton (Hoboken, N.J.) 69, 686-699.

Johnson, B.F., Yoo, B.Y., and Calleja, G.B. (1973). Cell division in yeasts: movement of organelles associated with cell plate growth of Schizosaccharomyces pombe. Journal of bacteriology 115, 358-366.

Jourdain, I., Brzezinska, E.A., and Toda, T. (2013). Fission yeast Nod1 is a component of cortical nodes involved in cell size control and division site placement. PLoS One 8, e54142.

Kamasaki, T., Osumi, M., and Mabuchi, I. (2007). Three-dimensional arrangement of F-actin in the contractile ring of fission yeast. J Cell Biol 178, 765-771.

Kanada, M., Nagasaki, A., and Uyeda, T.Q. (2005). Adhesion-dependent and contractile ring-independent equatorial furrowing during cytokinesis in mammalian cells. Mol Biol Cell 16, 3865-3872.

Kataria, M., Mouilleron, S., Seo, M.H., Corbi-Verge, C., Kim, P.M., and Uhlmann, F. (2018). A PxL motif promotes timely cell cycle substrate dephosphorylation by the Cdc14 phosphatase. Nature structural & molecular biology 25, 1093-1102.

Keeney, J.B., and Boeke, J.D. (1994). Efficient targeted integration at leu1-32 and ura4-294 in Schizosaccharomyces pombe. Genetics 136, 849-856.

Kettenbach, A.N., Deng, L., Wu, Y., Baldissard, S., Adamo, M.E., Gerber, S.A., and Moseley, J.B. (2015). Quantitative phosphoproteomics reveals pathways for coordination of cell growth and division by the conserved fission yeast kinase pom1. Molecular & cellular proteomics : MCP 14, 1275-1287.

Kim, D.U., Hayles, J., Kim, D., Wood, V., Park, H.O., Won, M., Yoo, H.S., Duhig, T., Nam, M., Palmer, G., Han, S., Jeffery, L., Baek, S.T., Lee, H., Shim, Y.S., Lee, M., Kim, L., Heo, K.S., Noh, E.J., Lee, A.R., Jang, Y.J., Chung, K.S., Choi, S.J., Park, J.Y., Park, Y., Kim, H.M., Park, S.K., Park, H.J., Kang, E.J., Kim, H.B., Kang, H.S., Park, H.M., Kim, K., Song, K., Song, K.B., Nurse, P., and Hoe, K.L. (2010). Analysis of a genome-wide set of gene deletions in the fission yeast Schizosaccharomyces pombe. Nat Biotechnol 28, 617-623.

Kitayama, C., Sugimoto, A., and Yamamoto, M. (1997). Type II myosin heavy chain encoded by the myo2 gene composes the contractile ring during cytokinesis in Schizosaccharomyces pombe. J Cell Biol 137, 1309-1319.

Kobori, H., Toda, T., Yaguchi, H., Toya, M., Yanagida, M., and Osumi, M. (1994). Fission yeast protein kinase C gene homologues are required for protoplast regeneration: a functional link between cell wall formation and cell shape control. Journal of Cell Science 107, 1131-1136.

Koch, A., Krug, K., Pengelley, S., Macek, B., and Hauf, S. (2011). Mitotic substrates of the kinase aurora with roles in chromatin regulation identified through quantitative phosphoproteomics of fission yeast. Sci Signal 4, rs6.

Kovar, D.R., Kuhn, J.R., Tichy, A.L., and Pollard, T.D. (2003). The fission yeast cytokinesis formin Cdc12p is a barbed end actin filament capping protein gated by profilin. J Cell Biol 161, 875-887.

Kovar, D.R., Wu, J.Q., and Pollard, T.D. (2005). Profilin-mediated competition between capping protein and formin Cdc12p during cytokinesis in fission yeast. Mol Biol Cell 16, 2313-2324.

Kuilman, T., Maiolica, A., Godfrey, M., Scheidel, N., Aebersold, R., and Uhlmann, F. (2015). Identification of Cdk targets that control cytokinesis. The EMBO journal 34, 81-96.

Laplante, C., Berro, J., Karatekin, E., Hernandez-Leyva, A., Lee, R., and Pollard, T.D. (2015). Three Myosins Contribute Uniquely to the Assembly and Constriction of the Fission Yeast Cytokinetic Contractile Ring. Curr Biol.

Laplante, C., Huang, F., Tebbs, I.R., Bewersdorf, J., and Pollard, T.D. (2016). Molecular organization of cytokinesis nodes and contractile rings by super-resolution fluorescence microscopy of live fission yeast. Proceedings of the National Academy of Sciences 113, E5876-E5885.

Laporte, D., Coffman, V.C., Lee, I.J., and Wu, J.Q. (2011). Assembly and architecture of precursor nodes during fission yeast cytokinesis. J Cell Biol 192, 1005-1021.

Le Goff, X., Motegi, F., Salimova, E., Mabuchi, I., and Simanis, V. (2000). The S. pombe rlc1 gene encodes a putative myosin regulatory light chain that binds the type II myosins myo3p and myo2p. J Cell Sci 113 Pt 23, 4157-4163.

Lee, I.J., Coffman, V.C., and Wu, J.Q. (2012). Contractile-ring assembly in fission yeast cytokinesis: Recent advances and new perspectives. Cytoskeleton (Hoboken, N.J.) 69, 751-763.

Lee, M.E., Rusin, S.F., Jenkins, N., Kettenbach, A.N., and Moseley, J.B. (2018). Mechanisms Connecting the Conserved Protein Kinases Ssp1, Kin1, and Pom1 in Fission Yeast Cell Polarity and Division. Curr Biol 28, 84-92 e84.

Levine, Z.A., Larini, L., LaPointe, N.E., Feinstein, S.C., and Shea, J.E. (2015). Regulation and aggregation of intrinsically disordered peptides. Proc Natl Acad Sci U S A 112, 2758-2763.

Li, Y., Christensen, J.R., Homa, K.E., Hocky, G.M., Fok, A., Sees, J.A., Voth, G.A., and Kovar, D.R. (2016). The F-actin bundler α-actinin Ain1 is tailored for ring assembly and constriction during cytokinesis in fission yeast. Mol Biol Cell.

Linsmeier, I., Banerjee, S., Oakes, P.W., Jung, W., Kim, T., and Murrell, M.P. (2016). Disordered actomyosin networks are sufficient to produce cooperative and telescopic contractility. Nature Communications 7, 12615.

Lippincott, J., and Li, R. (2000). Involvement of PCH family proteins in cytokinesis and actin distribution. Microsc Res Tech 49, 168-172.

Liu, J., Wang, H., and Balasubramanian, M.K. (2000). A checkpoint that monitors cytokinesis in Schizosaccharomyces pombe. J Cell Sci 113 (Pt 7), 1223-1230.

Liu, J., Wang, H., McCollum, D., and Balasubramanian, M.K. (1999). Drc1p/Cps1p, a 1,3-beta-glucan synthase subunit, is essential for division septum assembly in Schizosaccharomyces pombe. Genetics 153, 1193-1203.

Liu, Y., McDonald, N.A., Naegele, S.M., Gould, K.L., and Wu, J.Q. (2019). The F-BAR Domain of Rga7 Relies on a Cooperative Mechanism of Membrane Binding with a Partner Protein during Fission Yeast Cytokinesis. Cell Rep 26, 2540-2548.e2544.

Lock, J.G., Jones, M.C., Askari, J.A., Gong, X., Oddone, A., Olofsson, H., Göransson, S., Lakadamyali, M., Humphries, M.J., and Strömblad, S. (2018). Reticular adhesions are a distinct class of cell-matrix adhesions that mediate attachment during mitosis. Nature cell biology 20, 1290-1302.

Loo, T.H., and Balasubramanian, M. (2008). Schizosaccharomyces pombe Pak-related protein, Pak1p/Orb2p, phosphorylates myosin regulatory light chain to inhibit cytokinesis. J Cell Biol 183, 785-793.

Lord, M., Laves, E., and Pollard, T.D. (2005). Cytokinesis depends on the motor domains of myosin-II in fission yeast but not in budding yeast. Mol Biol Cell 16, 5346-5355.

Ma, X., Kovács, M., Conti, M.A., Wang, A., Zhang, Y., Sellers, J.R., and Adelstein, R.S. (2012). Nonmuscle myosin II exerts tension but does not translocate actin in vertebrate cytokinesis. Proceedings of the National Academy of Sciences 109, 4509-4514.

Mabuchi, I. (1994). Cleavage furrow: timing of emergence of contractile ring actin filaments and establishment of the contractile ring by filament bundling in sea urchin eggs. J Cell Sci 107 (Pt 7), 1853-1862.

Mabuchi, I., Tsukita, S., Tsukita, S., and Sawai, T. (1988). Cleavage furrow isolated from newt eggs: contraction, organization of the actin filaments, and protein components of the furrow. Proc Natl Acad Sci U S A 85, 5966-5970.

Maddox, A.S., Habermann, B., Desai, A., and Oegema, K. (2005). Distinct roles for two C. elegans anillins in the gonad and early embryo. Development 132, 2837.

Mangione, M.C., and Gould, K.L. (2019). Molecular form and function of the cytokinetic ring. J Cell Sci 132.

Mangione, M.C., and Gould, K.L. (In press). Cytokinetic ring: Molecular form and function. J Cell Sci.

Marquardt, J., Chen, X., and Bi, E. (2018). Architecture, remodeling, and functions of the septin cytoskeleton. Cytoskeleton (Hoboken).

Martin, S.G., McDonald, W.H., Yates, J.R., 3rd, and Chang, F. (2005). Tea4p links microtubule plus ends with the formin for3p in the establishment of cell polarity. Dev Cell 8, 479-491.

Martin-Garcia, R., Arribas, V., Coll, P.M., Pinar, M., Viana, R.A., Rincon, S.A., Correa-Bordes, J., Ribas, J.C., and Perez, P. (2018). Paxillin-Mediated Recruitment of Calcineurin to the Contractile Ring Is Required for the Correct Progression of Cytokinesis in Fission Yeast. Cell Rep 25, 772-783.e774.

Martin-Garcia, R., Coll, P.M., and Perez, P. (2014). F-BAR domain protein Rga7 collaborates with Cdc15 and Imp2 to ensure proper cytokinesis in fission yeast. J Cell Sci 127, 4146-4158.

Matsuyama, A., Arai, R., Yashiroda, Y., Shirai, A., Kamata, A., Sekido, S., Kobayashi, Y., Hashimoto, A., Hamamoto, M., Hiraoka, Y., Horinouchi, S., and Yoshida, M. (2006). ORFeome cloning and global analysis of protein localization in the fission yeast Schizosaccharomyces pombe. Nat Biotechnol 24, 841-847.

Maupin, P., and Pollard, T.D. (1986). Arrangement of actin filaments and myosin-like filaments in the contractile ring and of actin-like filaments in the mitotic spindle of dividing HeLa cells. Journal of ultrastructure and molecular structure research 94, 92-103.

Mavrakis, M., Azou-Gros, Y., Tsai, F.C., Alvarado, J., Bertin, A., Iv, F., Kress, A., Brasselet, S., Koenderink, G.H., and Lecuit, T. (2014). Septins promote F-actin ring formation by crosslinking actin filaments into curved bundles. Nature cell biology 16, 322-334.

May, K.M., Watts, F.Z., Jones, N., and Hyams, J.S. (1997). Type II myosin involved in cytokinesis in the fission yeast, Schizosaccharomyces pombe. Cell Motil Cytoskeleton 38, 385-396.

McCollum, D., Balasubramanian, M.K., Pelcher, L.E., Hemmingsen, S.M., and Gould, K.L. (1995). Schizosaccharomyces pombe cdc4+ gene encodes a novel EF-hand protein essential for cytokinesis. J Cell Biol 130, 651-660.

McDonald, N.A., and Gould, K.L. (2016). Linking up at the BAR: Oligomerization and F-BAR protein function. Cell Cycle 15, 1977-1985.

McDonald, N.A., Lind, A.L., Smith, S.E., Li, R., and Gould, K.L. (2017). Nanoscale architecture of the Schizosaccharomyces pombe contractile ring. eLife 6, e28865.

McDonald, N.A., Takizawa, Y., Feoktistova, A., Xu, P., Ohi, M.D., Vander Kooi, C.W., and Gould, K.L. (2016). The Tubulation Activity of a Fission Yeast F-BAR Protein Is Dispensable for Its Function in Cytokinesis. Cell Rep 14, 534-546.

McDonald, N.A., Vander Kooi, C.W., Ohi, M.D., and Gould, K.L. (2015). Oligomerization but Not Membrane Bending Underlies the Function of Certain F-BAR Proteins in Cell Motility and Cytokinesis. Dev Cell 35, 725-736.

Meitinger, F., Boehm, M.E., Hofmann, A., Hub, B., Zentgraf, H., Lehmann, W.D., and Pereira, G. (2011). Phosphorylation-dependent regulation of the F-BAR protein Hof1 during cytokinesis. Genes Dev 25, 875-888.

Meitinger, F., Palani, S., Hub, B., and Pereira, G. (2013). Dual function of the NDR-kinase Dbf2 in the regulation of the F-BAR protein Hof1 during cytokinesis. Mol Biol Cell 24, 1290-1304.

Mendes Pinto, I., Rubinstein, B., Kucharavy, A., Unruh, Jay R., and Li, R. (2012). Actin Depolymerization Drives Actomyosin Ring Contraction during Budding Yeast Cytokinesis. Developmental cell 22, 1247-1260.

Mendes Pinto, I., Rubinstein, B., and Li, R. (2013). Force to divide: structural and mechanical requirements for actomyosin ring contraction. Biophys J 105, 547-554.

Merlini, L., Bolognesi, A., Juanes, M.A., Vandermoere, F., Courtellemont, T., Pascolutti, R., Seveno, M., Barral, Y., and Piatti, S. (2015). Rho1- and Pkc1-dependent phosphorylation of the F-BAR protein Syp1 contributes to septin ring assembly. Mol Biol Cell 26, 3245-3262.

Meszaros, B., Simon, I., and Dosztanyi, Z. (2009). Prediction of protein binding regions in disordered proteins. PLoS Comput Biol 5, e1000376.

Metskas, L.A., and Rhoades, E. (2015). Folding upon phosphorylation: translational regulation by a disorder-to-order transition. Trends Biochem Sci 40, 243-244.

Minet, M., Nurse, P., Thuriaux, P., and Mitchison, J.M. (1979). Uncontrolled septation in a cell division cycle mutant of the fission yeast Schizosaccharomyces pombe. Journal of bacteriology 137, 440-446.

Mitchison, J.M. (1957). The growth of single cells. I. Schizosaccharomyces pombe. Experimental cell research 13, 244-262.

Mitchison, J.M., and Nurse, P. (1985). Growth in cell length in the fission yeast Schizosaccharomyces pombe. J Cell Sci 75, 357-376.

Mitchison, T.J. (1992). Actin based motility on retraction fibers in mitotic PtK2 cells. Cell motility and the cytoskeleton 22, 135-151.

Mocciaro, A., and Schiebel, E. (2010). Cdc14: a highly conserved family of phosphatases with non-conserved functions? J Cell Sci 123, 2867-2876.

Mochida, S., and Hunt, T. (2007). Calcineurin is required to release Xenopus egg extracts from meiotic M phase. Nature 449, 336-340.

Moreno, S., Klar, A., and Nurse, P. (1991). Molecular genetic analysis of fission yeast Schizosaccharomyces pombe. Methods Enzymol 194, 795-823.

Morrell-Falvey, J.L., Ren, L., Feoktistova, A., Haese, G.D., and Gould, K.L. (2005). Cell wall remodeling at the fission yeast cell division site requires the Rho-GEF Rgf3p. J Cell Sci 118, 5563-5573.

Moseley, J.B., Mayeux, A., Paoletti, A., and Nurse, P. (2009). A spatial gradient coordinates cell size and mitotic entry in fission yeast. Nature 459, 857-860.

Motegi, F., Mishra, M., Balasubramanian, M.K., and Mabuchi, I. (2004). Myosin-II reorganization during mitosis is controlled temporally by its dephosphorylation and spatially by Mid1 in fission yeast. J Cell Biol 165, 685-695.

Motegi, F., Nakano, K., Kitayama, C., Yamamoto, M., and Mabuchi, I. (1997). Identification of Myo3, a second type-II myosin heavy chain in the fission yeast Schizosaccharomyces pombe. FEBS Lett 420, 161-166.

Muller, S. (2019). Plant cell division - defining and finding the sweet spot for cell plate insertion. Curr Opin Cell Biol 60, 9-18.

Munoz, J., Cortes, J.C., Sipiczki, M., Ramos, M., Clemente-Ramos, J.A., Moreno, M.B., Martins, I.M., Perez, P., and Ribas, J.C. (2013). Extracellular cell wall beta(1,3)glucan is required to couple septation to actomyosin ring contraction. J Cell Biol 203, 265-282.

Nakano, K., Arai, R., and Mabuchi, I. (1997). The small GTP-binding protein Rho1 is a multifunctional protein that regulates actin localization, cell polarity, and septum formation in the fission yeast Schizosaccharomyces pombe. Genes Cells 2, 679-694.

Nakano, K., and Mabuchi, I. (2006a). Actin-capping protein is involved in controlling organization of actin cytoskeleton together with ADF/cofilin, profilin and F-actin crosslinking proteins in fission yeast. Genes Cells 11, 893-905.

Nakano, K., and Mabuchi, I. (2006b). Actin-depolymerizing protein Adf1 is required for formation and maintenance of the contractile ring during cytokinesis in fission yeast. Mol Biol Cell 17, 1933-1945.

Naqvi, N.I., Wong, K.C., Tang, X., and Balasubramanian, M.K. (2000). Type II myosin regulatory light chain relieves auto-inhibition of myosin-heavy-chain function. Nature cell biology 2, 855-858.

Naylor, S.G., and Morgan, D.O. (2014). Cdk1-dependent phosphorylation of Iqg1 governs actomyosin ring assembly prior to cytokinesis. J Cell Sci 127, 1128-1137.

Nguyen, L.T., Swulius, M.T., Aich, S., Mishra, M., and Jensen, G.J. (2018). Coarse-grained simulations of actomyosin rings point to a nodeless model involving both unipolar and bipolar myosins. Mol Biol Cell 29, 1318-1331.

Nishiyama, T., Yoshizaki, N., Kishimoto, T., and Ohsumi, K. (2007). Transient activation of calcineurin is essential to initiate embryonic development in Xenopus laevis. Nature 449, 341-345.

Noguchi, T., and Mabuchi, I. (2001). Reorganization of actin cytoskeleton at the growing end of the cleavage furrow of Xenopus egg during cytokinesis. J Cell Sci 114, 401-412.

Nurse, P., Thuriaux, P., and Nasmyth, K. (1976). Genetic control of the cell division cycle in the fission yeast Schizosaccharomyces pombe. Mol Gen Genet 146, 167-178.

Oh, Y., Schreiter, J., Nishihama, R., Wloka, C., and Bi, E. (2013). Targeting and functional mechanisms of the cytokinesis-related F-BAR protein Hof1 during the cell cycle. Mol Biol Cell 24, 1305-1320.

Ohkura, H., Kinoshita, N., Miyatani, S., Toda, T., and Yanagida, M. (1989). The fission yeast dis2+ gene required for chromosome disjoining encodes one of two putative type 1 protein phosphatases. Cell 57, 997-1007.

Okada, H., Wloka, C., Wu, J.Q., and Bi, E. (2019). Distinct Roles of Myosin-II Isoforms in Cytokinesis under Normal and Stressed Conditions. iScience 14, 69-87.

Oliferenko, S., Chew, T.G., and Balasubramanian, M.K. (2009). Positioning cytokinesis. Genes Dev 23, 660-674.

Ong, K., Wloka, C., Okada, S., Svitkina, T., and Bi, E. (2014). Architecture and dynamic remodelling of the septin cytoskeleton during the cell cycle. Nature Communications 5, 5698.

Onwubiko, U.N., Mlynarczyk, P.J., Wei, B., Habiyaremye, J., Clack, A., Abel, S.M., and Das, M.E. (2019). A Cdc42 GEF, Gef1, through endocytosis organizes F-BAR Cdc15 along the actomyosin ring and promotes concentric furrowing. J Cell Sci 132.

Orii, M., Kono, K., Wen, H.-I., and Nakanishi, M. (2016). PP1-Dependent Formin Bnr1 Dephosphorylation and Delocalization from a Cell Division Site. PloS one 11, e0146941.

Padmanabhan, A., Bakka, K., Sevugan, M., Naqvi, N.I., D'Souza, V., Tang, X., Mishra, M., and Balasubramanian, M.K. (2011). IQGAP-related Rng2p organizes cortical nodes and ensures position of cell division in fission yeast. Curr Biol 21, 467-472.

Padte, N.N., Martin, S.G., Howard, M., and Chang, F. (2006). The cell-end factor pom1p inhibits mid1p in specification of the cell division plane in fission yeast. Curr Biol 16, 2480-2487.

Palani, S., Chew, T.G., Ramanujam, S., Kamnev, A., Harne, S., Chapa, Y.L.B., Hogg, R., Sevugan, M., Mishra, M., Gayathri, P., and Balasubramanian, M.K. (2017). Motor Activity Dependent and Independent Functions of Myosin II Contribute to Actomyosin Ring Assembly and Contraction in Schizosaccharomyces pombe. Curr Biol 27, 751-757.

Palani, S., Meitinger, F., Boehm, M.E., Lehmann, W.D., and Pereira, G. (2012). Cdc14-dependent dephosphorylation of Inn1 contributes to Inn1-Cyk3 complex formation. J Cell Sci 125, 3091-3096.

Paoletti, A., and Chang, F. (2000). Analysis of mid1p, a protein required for placement of the cell division site, reveals a link between the nucleus and the cell surface in fission yeast. Mol Biol Cell 11, 2757-2773.

Pappu, R.V. (2015). Cell signaling, division, and organization mediated by intrinsically disordered proteins. Seminars in cell & developmental biology 37, 1-2.

Perez, P., Cortes, J.C., Martin-Garcia, R., and Ribas, J.C. (2016). Overview of fission yeast septation. Cell Microbiol 18, 1201-1207.

Pinar, M., Coll, P.M., Rincon, S.A., and Perez, P. (2008). Schizosaccharomyces pombe Pxl1 is a paxillin homologue that modulates Rho1 activity and participates in cytokinesis. Mol Biol Cell 19, 1727-1738.

Pollard, L.W., Bookwalter, C.S., Tang, Q., Krementsova, E.B., Trybus, K.M., and Lowey, S. (2017). Fission yeast myosin Myo2 is down-regulated in actin affinity by light chain phosphorylation. Proc Natl Acad Sci U S A 114, E7236-E7244.

Pollard, L.W., Onishi, M., Pringle, J.R., and Lord, M. (2012). Fission yeast Cyk3p is a transglutaminase-like protein that participates in cytokinesis and cell morphogenesis. Mol Biol Cell 23, 2433-2444.

Pollard, T.D. (2017). Nine unanswered questions about cytokinesis. The Journal of Cell Biology 216, 3007-3016.

Pollard, T.D., and O'Shaughnessy, B. (2019). Molecular Mechanism of Cytokinesis. Annual Review of Biochemistry.

Pollard, T.D., and Wu, J.-Q. (2010a). Understanding cytokinesis: lessons from fission yeast. Nature Reviews Molecular Cell Biology 11, 149.

Pollard, T.D., and Wu, J.Q. (2010b). Understanding cytokinesis: lessons from fission yeast. Nat Rev Mol Cell Biol 11, 149-155.

Proctor, Stephen A., Minc, N., Boudaoud, A., and Chang, F. (2012a). Contributions of Turgor Pressure, the Contractile Ring, and Septum Assembly to Forces in Cytokinesis in Fission Yeast. Current Biology 22, 1601-1608.

Proctor, S.A., Minc, N., Boudaoud, A., and Chang, F. (2012b). Contributions of turgor pressure, the contractile ring, and septum assembly to forces in cytokinesis in fission yeast. Curr Biol 22, 1601-1608.

Pu, K.M., Akamatsu, M., and Pollard, T.D. (2015). The septation initiation network controls the assembly of nodes containing Cdr2p for cytokinesis in fission yeast. J Cell Sci 128, 441-446.

Quan, A., Xue, J., Wielens, J., Smillie, K.J., Anggono, V., Parker, M.W., Cousin, M.A., Graham, M.E., and Robinson, P.J. (2012). Phosphorylation of syndapin I F-BAR domain at two helix-capping motifs regulates membrane tubulation. Proc Natl Acad Sci U S A 109, 3760-3765.

Rachfall, N., Johnson, A.E., Mehta, S., Chen, J.S., and Gould, K.L. (2014). Cdk1 promotes cytokinesis in fission yeast through activation of the septation initiation network. Mol Biol Cell 25, 2250-2259.

Rao, Y., Ma, Q., Vahedi-Faridi, A., Sundborger, A., Pechstein, A., Puchkov, D., Luo, L., Shupliakov, O., Saenger, W., and Haucke, V. (2010). Molecular basis for SH3 domain regulation of F-BAR-mediated membrane deformation. Proc Natl Acad Sci U S A 107, 8213-8218.

Reed, B.J., Locke, M.N., and Gardner, R.G. (2015). A Conserved Deubiquitinating Enzyme Uses Intrinsically Disordered Regions to Scaffold Multiple Protein-Interaction Sites. J Biol Chem.

Reinhardt, H.C., and Yaffe, M.B. (2013). Phospho-Ser/Thr-binding domains: navigating the cell cycle and DNA damage response. Nat Rev Mol Cell Biol 14, 563-580.

Ren, L., Willet, A.H., Roberts-Galbraith, R.H., McDonald, N.A., Feoktistova, A., Chen, J.S., Huang, H., Guillen, R., Boone, C., Sidhu, S.S., Beckley, J.R., and Gould, K.L. (2015). The Cdc15 and Imp2 SH3 domains cooperatively scaffold a network of proteins that redundantly ensure efficient cell division in fission yeast. Mol Biol Cell 26, 256-269.

Ricketson, D., Johnston, C.A., and Prehoda, K.E. (2010). Multiple tail domain interactions stabilize nonmuscle myosin II bipolar filaments. Proceedings of the National Academy of Sciences 107, 20964-20969.

Rincon, S.A., Bhatia, P., Bicho, C., Guzman-Vendrell, M., Fraisier, V., Borek, W.E., Alves Fde, L., Dingli, F., Loew, D., Rappsilber, J., Sawin, K.E., Martin, S.G., and

Paoletti, A. (2014). Pom1 regulates the assembly of Cdr2-Mid1 cortical nodes for robust spatial control of cytokinesis. J Cell Biol 206, 61-77.

Rincon, S.A., and Paoletti, A. (2012). Mid1/anillin and the spatial regulation of cytokinesis in fission yeast. Cytoskeleton (Hoboken, N.J.) 69, 764-777.

Roberts-Galbraith, R.H., Chen, J.S., Wang, J., and Gould, K.L. (2009). The SH3 domains of two PCH family members cooperate in assembly of the Schizosaccharomyces pombe contractile ring. J Cell Biol 184, 113-127.

Roberts-Galbraith, R.H., and Gould, K.L. (2008). Stepping into the ring: the SIN takes on contractile ring assembly. Genes Dev 22, 3082-3088.

Roberts-Galbraith, R.H., and Gould, K.L. (2010). Setting the F-BAR: functions and regulation of the F-BAR protein family. Cell Cycle 9, 4091-4097.

Roberts-Galbraith, R.H., Ohi, M.D., Ballif, B.A., Chen, J.S., McLeod, I., McDonald, W.H., Gygi, S.P., Yates, J.R., 3rd, and Gould, K.L. (2010). Dephosphorylation of F-BAR protein Cdc15 modulates its conformation and stimulates its scaffolding activity at the cell division site. Mol Cell 39, 86-99.

Rust, M.J., Bates, M., and Zhuang, X. (2006). Sub-diffraction-limit imaging by stochastic optical reconstruction microscopy (STORM). Nature methods 3, 793-795.

Saha, S., and Pollard, T.D. (2012). Anillin-related protein Mid1p coordinates the assembly of the cytokinetic contractile ring in fission yeast. Mol Biol Cell 23, 3982-3992.

Sánchez-Mir, L., Soto, T., Franco, A., Madrid, M., Viana, R.A., Vicente, J., Gacto, M., Pérez, P., and Cansado, J. (2014). Rho1 GTPase and PKC Ortholog Pck1 Are Upstream Activators of the Cell Integrity MAPK Pathway in Fission Yeast. PloS one 9, e88020.

Sanger, J.M., and Sanger, J.W. (1980). Banding and polarity of actin filaments in interphase and cleaving cells. J Cell Biol 86, 568-575.

Schindelin, J., Arganda-Carreras, I., Frise, E., Kaynig, V., Longair, M., Pietzsch, T., Preibisch, S., Rueden, C., Saalfeld, S., Schmid, B., Tinevez, J.Y., White, D.J., Hartenstein, V., Eliceiri, K., Tomancak, P., and Cardona, A. (2012). Fiji: an open-source platform for biological-image analysis. Nat Methods 9, 676-682.

Schroeder, T.E. (1972). THE CONTRACTILE RING II. Determining its Brief Existence, Volumetric Changes, and Vital Role in Cleaving. The Journal of Cell Biology 53, 419-434.

Schroeder, T.E. (1990). The contractile ring and furrowing in dividing cells. Annals of the New York Academy of Sciences 582, 78-87.

Senju, Y., Itoh, Y., Takano, K., Hamada, S., and Suetsugu, S. (2011). Essential role of PACSIN2/syndapin-II in caveolae membrane sculpting. J Cell Sci 124, 2032-2040.

Sethi, K., Palani, S., Cortes, J.C., Sato, M., Sevugan, M., Ramos, M., Vijaykumar, S., Osumi, M., Naqvi, N.I., Ribas, J.C., and Balasubramanian, M. (2016). A New Membrane Protein Sbg1 Links the Contractile Ring Apparatus and Septum Synthesis Machinery in Fission Yeast. PLoS Genet 12, e1006383.

Shaner, N.C., Lambert, G.G., Chammas, A., Ni, Y., Cranfill, P.J., Baird, M.A., Sell, B.R., Allen, J.R., Day, R.N., Israelsson, M., Davidson, M.W., and Wang, J. (2013). A bright monomeric green fluorescent protein derived from Branchiostoma lanceolatum. Nat Methods 10, 407-409.

Shimada, A., Takano, K., Shirouzu, M., Hanawa-Suetsugu, K., Terada, T., Toyooka, K., Umehara, T., Yamamoto, M., Yokoyama, S., and Suetsugu, S. (2010). Mapping of the basic amino-acid residues responsible for tubulation and cellular protrusion by the EFC/F-BAR domain of pacsin2/Syndapin II. FEBS Lett 584, 1111-1118.

Shoham, N.G., Centola, M., Mansfield, E., Hull, K.M., Wood, G., Wise, C.A., and Kastner, D.L. (2003). Pyrin binds the PSTPIP1/CD2BP1 protein, defining familial Mediterranean fever and PAPA syndrome as disorders in the same pathway. Proc Natl Acad Sci U S A 100, 13501-13506.

Silva, A.M., Osório, D.S., Pereira, A.J., Maiato, H., Pinto, I.M., Rubinstein, B., Gassmann, R., Telley, I.A., and Carvalho, A.X. (2016). Robust gap repair in the contractile ring ensures timely completion of cytokinesis. The Journal of Cell Biology 215, 789-799.

Simanis, V. (2015). Pombe's thirteen - control of fission yeast cell division by the septation initiation network. J Cell Sci 128, 1465-1474.

Smertenko, A. (2018). Phragmoplast expansion: the four-stroke engine that powers plant cytokinesis. Current opinion in plant biology 46, 130-137.

Snider, C.E., Willet, A.H., Chen, J.S., Arpag, G., Zanic, M., and Gould, K.L. (2017). Phosphoinositide-mediated ring anchoring resists perpendicular forces to promote medial cytokinesis. J Cell Biol 216, 3041-3050.

Sohrmann, M., Fankhauser, C., Brodbeck, C., and Simanis, V. (1996). The dmf1/mid1 gene is essential for correct positioning of the division septum in fission yeast. Genes Dev 10, 2707-2719.

Spira, F., Cuylen-Haering, S., Mehta, S., Samwer, M., Reversat, A., Verma, A., Oldenbourg, R., Sixt, M., and Gerlich, D.W. (2017). Cytokinesis in vertebrate cells initiates by contraction of an equatorial actomyosin network composed of randomly oriented filaments. eLife 6, e30867.

Srivastava, V., Iglesias, P.A., and Robinson, D.N. (2016). Cytokinesis: Robust cell shape regulation. Seminars in cell & developmental biology 53, 39-44.

Stachowiak, M.R., Laplante, C., Chin, H.F., Guirao, B., Karatekin, E., Pollard, T.D., and O'Shaughnessy, B. (2014). Mechanism of cytokinetic contractile ring constriction in fission yeast. Dev Cell 29, 547-561.

Stanishneva-Konovalova, T.B., Kelley, C.F., Eskin, T.L., Messelaar, E.M., Wasserman, S.A., Sokolova, O.S., and Rodal, A.A. (2016). Coordinated autoinhibition of F-BAR domain membrane binding and WASp activation by Nervous Wreck. Proc Natl Acad Sci U S A 113, E5552-5561.

Stegmeier, F., and Amon, A. (2004). Closing mitosis: the functions of the Cdc14 phosphatase and its regulation. Annual review of genetics 38, 203-232.

Sun, S.X., Walcott, S., and Wolgemuth, C.W. (2010). Cytoskeletal cross-linking and bundling in motor-independent contraction. Current biology : CB 20, R649-R654.

Swaffer, M.P., Jones, A.W., Flynn, H.R., Snijders, A.P., and Nurse, P. (2016). CDK Substrate Phosphorylation and Ordering the Cell Cycle. Cell 167, 1750-1761.e1716.

Swaffer, M.P., Jones, A.W., Flynn, H.R., Snijders, A.P., and Nurse, P. (2018). Quantitative Phosphoproteomics Reveals the Signaling Dynamics of Cell-Cycle Kinases in the Fission Yeast Schizosaccharomyces pombe. Cell Rep 24, 503-514.

Swulius, M.T., Nguyen, L.T., Ladinsky, M.S., Ortega, D.R., Aich, S., Mishra, M., and Jensen, G.J. (2018). Structure of the fission yeast actomyosin ring during constriction. Proceedings of the National Academy of Sciences 115, E1455-E1464.

Sydor, A.M., Czymmek, K.J., Puchner, E.M., and Mennella, V. (2015). Super-Resolution Microscopy: From Single Molecules to Supramolecular Assemblies. Trends in Cell Biology 25, 730-748.

Taira, R., and Yumura, S. (2017). A novel mode of cytokinesis without cell-substratum adhesion. Scientific reports 7, 17694.

Tajadura, V., Garcia, B., Garcia, I., Garcia, P., and Sanchez, Y. (2004). Schizosaccharomyces pombe Rgf3p is a specific Rho1 GEF that regulates cell wall beta-glucan biosynthesis through the GTPase Rho1p. J Cell Sci 117, 6163-6174.

Takaine, M., Numata, O., and Nakano, K. (2009). Fission yeast IQGAP arranges actin filaments into the cytokinetic contractile ring. The EMBO journal 28, 3117-3131.

Takaine, M., Numata, O., and Nakano, K. (2014). Fission yeast IQGAP maintains F-actin-independent localization of myosin-II in the contractile ring. Genes Cells 19, 161-176.

Takaine, M., Numata, O., and Nakano, K. (2015). An actin-myosin-II interaction is involved in maintaining the contractile ring in fission yeast. J Cell Sci 128, 2903-2918.

Taneja, N., Fenix, A.M., Rathbun, L., Millis, B.A., Tyska, M.J., Hehnly, H., and Burnette, D.T. (2016). Focal adhesions control cleavage furrow shape and spindle tilt during mitosis. Scientific reports 6, 29846.

Taneja, N., Rathbun, L., Hehnly, H., and Burnette, D.T. (2019). The balance between adhesion and contraction during cell division. Current Opinion in Cell Biology 56, 45-52.

Tao, E.Y., Calvert, M., and Balasubramanian, M.K. (2014a). Rewiring Mid1p-independent medial division in fission yeast. Curr Biol 24, 2181-2188.

Tao, E.Y., Calvert, M., and Balasubramanian, M.K. (2014b). Rewiring Mid1p-independent medial division in fission yeast. Curr Biol 24, 2181-2188.

Tartoff, K.D., and Hobbs, C.A. (1987). Improved media for growing plasmid and cosmid clones. . Bethesda Res Lab Focus 9.

Tebbs, I.R., and Pollard, T.D. (2013). Separate roles of IQGAP Rng2p in forming and constricting the Schizosaccharomyces pombe cytokinetic contractile ring. Mol Biol Cell 24, 1904-1917.

Thiyagarajan, S., Munteanu, E.L., Arasada, R., Pollard, T.D., and O'Shaughnessy, B. (2015). The fission yeast cytokinetic contractile ring regulates septum shape and closure. J Cell Sci 128, 3672-3681.

Thiyagarajan, S., Wang, S., and O'Shaughnessy, B. (2017). A node organization in the actomyosin contractile ring generates tension and aids stability. Mol Biol Cell 28, 3286-3297.

Toda, T., Shimanuki, M., and Yanagida, M. (1993). Two novel protein kinase C-related genes of fission yeast are essential for cell viability and implicated in cell shape control. The EMBO journal 12, 1987-1995.

Tolic-Norrelykke, I.M., Sacconi, L., Stringari, C., Raabe, I., and Pavone, F.S. (2005). Nuclear and division-plane positioning revealed by optical micromanipulation. Curr Biol 15, 1212-1216.

Tolliday, N., Pitcher, M., and Li, R. (2003). Direct Evidence for a Critical Role of Myosin II in Budding Yeast Cytokinesis and the Evolvability of New Cytokinetic Mechanisms in the Absence of Myosin II. Molecular Biology of the Cell 14, 798-809.

Tompa, P. (2002). Intrinsically unstructured proteins. Trends Biochem Sci 27, 527-533.

Tompa, P. (2012). Intrinsically disordered proteins: a 10-year recap. Trends Biochem Sci 37, 509-516.

Tran, P.T., Marsh, L., Doye, V., Inoue, S., and Chang, F. (2001). A mechanism for nuclear positioning in fission yeast based on microtubule pushing. J Cell Biol 153, 397-411.

Tsujita, K., Suetsugu, S., Sasaki, N., Furutani, M., Oikawa, T., and Takenawa, T. (2006). Coordination between the actin cytoskeleton and membrane deformation by a novel membrane tubulation domain of PCH proteins is involved in endocytosis. J Cell Biol 172, 269-279.

Umasankar, P.K., Ma, L., Thieman, J.R., Jha, A., Doray, B., Watkins, S.C., and Traub, L.M. (2014). A clathrin coat assembly role for the muniscin protein central linker revealed by TALEN-mediated gene editing. eLife 3, e04137.

van der Geer, P., and Hunter, T. (1994). Phosphopeptide mapping and phosphoamino acid analysis by electrophoresis and chromatography on thin-layer cellulose plates. Electrophoresis 15, 544-554.

Vavylonis, D., and Horan, B.G. (2017). Cell Biology: Capturing Formin's Mechano-Inhibition. Curr Biol 27, R1078-r1080.

Vavylonis, D., Wu, J.Q., Hao, S., O'Shaughnessy, B., and Pollard, T.D. (2008). Assembly mechanism of the contractile ring for cytokinesis by fission yeast. Science 319, 97-100.

Verkhovsky, A.B., and Borisy, G.G. (1993). Non-sarcomeric mode of myosin II organization in the fibroblast lamellum. The Journal of Cell Biology 123, 637-652.

Vjestica, A., Tang, X.Z., and Oliferenko, S. (2008). The actomyosin ring recruits early secretory compartments to the division site in fission yeast. Mol Biol Cell 19, 1125-1138.

Wach, A., Brachat, A., Pohlmann, R., and Philippsen, P. (1994). New heterologous modules for classical or PCR-based gene disruptions in Saccharomyces cerevisiae. Yeast 10, 1793-1808.

Wachtler, V., Huang, Y., Karagiannis, J., and Balasubramanian, M.K. (2006). Cell cycle-dependent roles for the FCH-domain protein Cdc15p in formation of the actomyosin ring in Schizosaccharomyces pombe. Mol Biol Cell 17, 3254-3266.

Wang, L., and Tran, P.T. (2014). Chapter 15 - Visualizing Single Rod-Shaped Fission Yeast Vertically in Micro-Sized Holes on Agarose Pad Made by Soft Lithography. In: Methods in Cell Biology, vol. 120, eds. M. Piel and M. Théry: Academic Press, 227-234.

Wheatley, S.P., Hinchcliffe, E.H., Glotzer, M., Hyman, A.A., Sluder, G., and Wang, Y. (1997). CDK1 inactivation regulates anaphase spindle dynamics and cytokinesis in vivo. J Cell Biol 138, 385-393.

Willet, A.H., Bohnert, K.A., and Gould, K.L. (2018). Cdk1-dependent phosphoinhibition of a formin-F-BAR interaction opposes cytokinetic contractile ring formation. Mol Biol Cell 29, 713-721.

Willet, A.H., McDonald, N.A., Bohnert, K.A., Baird, M.A., Allen, J.R., Davidson, M.W., and Gould, K.L. (2015a). The F-BAR Cdc15 promotes contractile ring formation through the direct recruitment of the formin Cdc12. J Cell Biol 208, 391-399.

Willet, A.H., McDonald, N.A., and Gould, K.L. (2015b). Regulation of contractile ring formation and septation in Schizosaccharomyces pombe. Curr Opin Microbiol 28, 46-52.

Willet, A.H., McDonald, N.A., and Gould, K.L. (2015c). Regulation of contractile ring formation and septation in Schizosaccharomyces pombe. Current Opinion in Microbiology 28, 46-52.

Wilson-Grady, J.T., Villen, J., and Gygi, S.P. (2008). Phosphoproteome analysis of fission yeast. Journal of proteome research 7, 1088-1097.

Wlodarchak, N., and Xing, Y. (2016). PP2A as a master regulator of the cell cycle. Crit Rev Biochem Mol Biol, 1-23.

Wloka, C., Vallen, E.A., Thé, L., Fang, X., Oh, Y., and Bi, E. (2013). Immobile myosin-II plays a scaffolding role during cytokinesis in budding yeast. The Journal of cell biology 200, 271-286.

Wolf, F., Sigl, R., and Geley, S. (2007). '... The end of the beginning': cdk1 thresholds and exit from mitosis. Cell Cycle 6, 1408-1411.

Wollrab, V., Thiagarajan, R., Wald, A., Kruse, K., and Riveline, D. (2016). Still and rotating myosin clusters determine cytokinetic ring constriction. Nat Commun 7, 11860.

Wu, J.Q., Bahler, J., and Pringle, J.R. (2001). Roles of a fimbrin and an alpha-actinin-like protein in fission yeast cell polarization and cytokinesis. Mol Biol Cell 12, 1061-1077.

Wu, J.Q., Guo, J.Y., Tang, W., Yang, C.S., Freel, C.D., Chen, C., Nairn, A.C., and Kornbluth, S. (2009). PP1-mediated dephosphorylation of phosphoproteins at mitotic exit is controlled by inhibitor-1 and PP1 phosphorylation. Nature cell biology 11, 644-651.

Wu, J.Q., Kuhn, J.R., Kovar, D.R., and Pollard, T.D. (2003). Spatial and temporal pathway for assembly and constriction of the contractile ring in fission yeast cytokinesis. Dev Cell 5, 723-734.

Wu, J.Q., and Pollard, T.D. (2005). Counting cytokinesis proteins globally and locally in fission yeast. Science 310, 310-314.

Wu, J.Q., Sirotkin, V., Kovar, D.R., Lord, M., Beltzner, C.C., Kuhn, J.R., and Pollard, T.D. (2006). Assembly of the cytokinetic contractile ring from a broad band of nodes in fission yeast. J Cell Biol 174, 391-402.

Wurzenberger, C., and Gerlich, D.W. (2011). Phosphatases: providing safe passage through mitotic exit. Nat Rev Mol Cell Biol 12, 469-482.

Xue, Z., and Sokac, A.M. (2016). -Back-to-back mechanisms drive actomyosin ring closure during Drosophila embryo cleavage. J Cell Biol 215, 335-344.

Yamamoto, H., Kondo, A., and Itoh, T. (2018). A curvature-dependent membrane binding by tyrosine kinase Fer involves an intrinsically disordered region. Biochem Biophys Res Commun 495, 1522-1527.

Ye, Y., Lee, I.J., Runge, K.W., and Wu, J.Q. (2012). Roles of putative Rho-GEF Gef2 in division-site positioning and contractile-ring function in fission yeast cytokinesis. Mol Biol Cell 23, 1181-1195.

Yoshida, T., Toda, T., and Yanagida, M. (1994). A calcineurin-like gene ppb1+ in fission yeast: mutant defects in cytokinesis, cell polarity, mating and spindle pole body positioning. J Cell Sci 107, 1725-1735.

Zang, J.-H., Cavet, G., Sabry, J.H., Wagner, P., Moores, S.L., and Spudich, J.A. (1997). On the Role of Myosin-II in Cytokinesis: Division ofDictyostelium Cells under Adhesive and Nonadhesive Conditions. Molecular Biology of the Cell 8, 2617-2629.

Zhou, M., and Wang, Y.L. (2008). Distinct pathways for the early recruitment of myosin II and actin to the cytokinetic furrow. Mol Biol Cell 19, 318-326.

Zhou, Z., Munteanu, E.L., He, J., Ursell, T., Bathe, M., Huang, K.C., and Chang, F. (2015). The contractile ring coordinates curvature-dependent septum assembly during fission yeast cytokinesis. Mol Biol Cell 26, 78-90.

Zhu, Y.H., Ye, Y., Wu, Z., and Wu, J.Q. (2013). Cooperation between Rho-GEF Gef2 and its binding partner Nod1 in the regulation of fission yeast cytokinesis. Mol Biol Cell 24, 3187-3204.

Zimmermann, D., Homa, K.E., Hocky, G.M., Pollard, L.W., De La Cruz, E.M., Voth, G.A., Trybus, K.M., and Kovar, D.R. (2017). Mechanoregulated inhibition of formin facilitates contractile actomyosin ring assembly. Nature communications 8, 703.